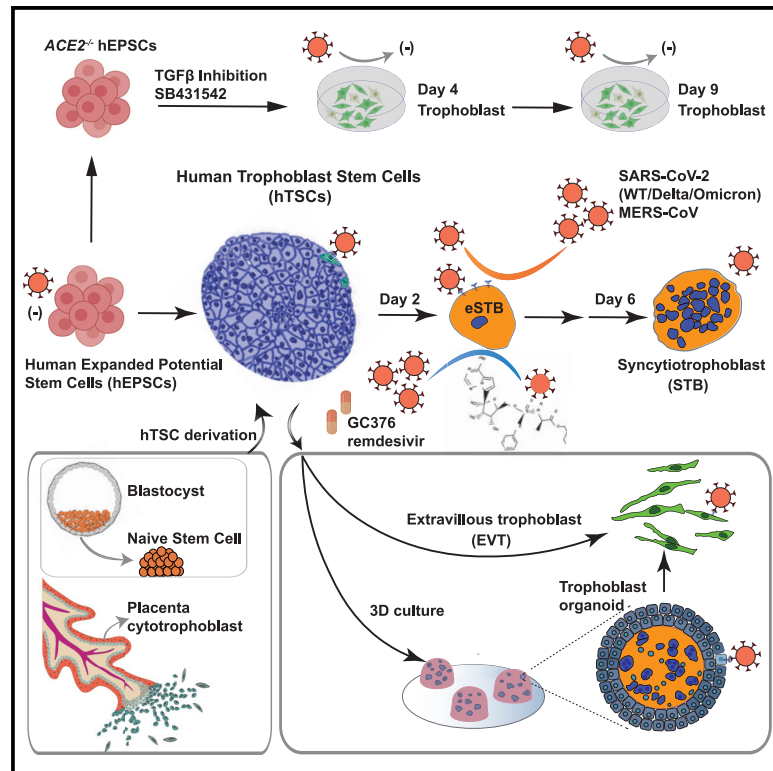**Article**

Human early syncytiotrophoblasts are highly susceptible to SARS-CoV-2 infection

Graphical abstract

Authors

Degong Ruan, Zi-Wei Ye,
Shuofeng Yuan, ..., Fang Liu,
Dong-Yan Jin, Pentao Liu

Correspondence

fang.liu@hkstemcell.hk (F.L.),
dyjin@hku.hk (D.-Y.J.),
pliu88@hku.hk (P.L.)

In brief

Ruan et al. utilize human expanded potential stem cells (hEPSCs) to demonstrate the susceptibility of $ACE2^+$ early syncytiotrophoblasts to SARS-CoV-2 variants. Productive viral infection blocks syncytiotrophoblast maturation, which is rescued by antivirals. Trophoblast organoids are inefficiently infected, reflecting uncommon placental infection *in vivo*.

Highlights

- SARS-CoV-2 infects human trophoblast stem cells (hTSCs) and their derivatives

- $ACE2^+$ early syncytiotrophoblasts (eSTBs) are susceptible to SARS-CoV-2 and MERS-CoV

- eSTB virion production is comparable to that of Vero cells and eliminated by antivirals

- Inefficient infection of trophoblast organoids models rare placental infection

CellPress

Article

Human early syncytiotrophoblasts are highly susceptible to SARS-CoV-2 infection

Degong Ruan,[1,2,9] Zi-Wei Ye,[4,9] Shuofeng Yuan,[4,9] Zhuoxuan Li,[3,9] Weiyu Zhang,[1,2,9] Chon Phin Ong,[4] Kaiming Tang,[4] Timothy Theodore Ka Ki Tam,[3] Jilong Guo,[3] Yiyi Xuan,[3] Yunying Huang,[3] Qingqing Zhang,[6] Cheuk-Lun Lee,[6] Liming Lu,[7] Philip C.N. Chiu,[6] William S.B. Yeung,[1,2,6] Fang Liu,[1,8,*] Dong-Yan Jin,[4,*] and Pentao Liu[1,2,3,5,10,*]

[1]Centre for Translational Stem Cell Biology, The University of Hong Kong, Hong Kong Special Administrative Region, China
[2]Shenzhen Key Laboratory of Fertility Regulation, The University of Hong Kong-Shenzhen Hospital, Shenzhen, China
[3]Stem Cell & Regenerative Medicine Consortium, School of Biomedical Sciences, Li Ka Shing Faculty of Medicine, The University of Hong Kong, Hong Kong Special Administrative Region, China
[4]Department of Microbiology, Li Ka Shing Faculty of Medicine, The University of Hong Kong, Hong Kong Special Administrative Region, China
[5]School of Biomedical Sciences, Li Ka Shing Faculty of Medicine, The University of Hong Kong, Hong Kong Special Administrative Region, China
[6]Department of Obstetrics and Gynaecology, School of Clinical Medicine, The University of Hong Kong, Hong Kong Special Administrative Region, China
[7]Shanghai Institute of Immunology, Shanghai Jiao Tong University, School of Medicine, Shanghai, China
[8]Foshan Stomatology Hospital, School of Medicine, Foshan University, No. 5 Hebing Road, Foshan, Guangdong Province, China
[9]These authors contributed equally
[10]Lead contact
*Correspondence: fang.liu@hkstemcell.hk (F.L.), dyjin@hku.hk (D.-Y.J.), pliu88@hku.hk (P.L.)
https://doi.org/10.1016/j.xcrm.2022.100849

SUMMARY

Direct *in vivo* investigation of human placenta trophoblast's susceptibility to SARS-CoV-2 is challenging. Here we report that human trophoblast stem cells (hTSCs) and their derivatives are susceptible to SARS-CoV-2 infection, which reveals heterogeneity in hTSC cultures. Early syncytiotrophoblasts (eSTBs) generated from hTSCs have enriched transcriptomic features of peri-implantation trophoblasts, express high levels of angiotensin-converting enzyme 2 (*ACE2*), and are productively infected by SARS-CoV-2 and its Delta and Omicron variants to produce virions. Antiviral drugs suppress SARS-CoV-2 replication in eSTBs and antagonize the virus-induced blockage of STB maturation. Although less susceptible to SARS-CoV-2 infection, trophoblast organoids originating from hTSCs show detectable viral replication reminiscent of the uncommon placental infection. These findings implicate possible risk of COVID-19 infection in peri-implantation embryos, which may go unnoticed. Stem cell-derived human trophoblasts such as eSTBs can potentially provide unlimited amounts of normal and genome-edited cells and facilitate coronavirus research and antiviral discovery.

INTRODUCTION

The human placenta protects the fetus by using multiple cellular and molecular defense mechanisms at the maternal-fetal interface to safeguard against infection during pregnancy, but certain viruses still replicate in the placenta and infect the fetus.[1] SARS-CoV-2 infection of the human placenta and resultant damage, although relatively uncommon, have been reported.[2–9] In rare cases, vertical transmission from mother to fetus has been reported.[4,10,11]

The human placenta consists of both maternal and fetal tissues.[12] The extraembryonic ectoderm generates the proliferative mononucleated trophoblast progenitors known as villous cytotrophoblasts (vCTBs), which can differentiate into invasive extravillous trophoblasts (EVTs) in the anchoring villi that grow out into the maternal decidua and, by cell fusion, into non-proliferative multinucleated syncytiotrophoblasts (STBs) that form a physical barrier against pathogens.[13]

SARS-CoV-2 infects cells via its spike (S) protein binding to the host entry receptor ACE2[14,15] and being primed by the transmembrane serine protease 2 (TMPRSS2).[16] Molecular assays and single-cell RNA sequencing (scRNA-seq) studies have identified *ACE2* and *TMPRSS2* co-expression in only a small number of first-trimester STBs and second-trimester EVTs,[17–19] which are gradually decreased during pregnancy.[17,20] ACE2 shedding may also help prevent SARS-CoV-2 infection from continuing to spread in the placenta.[21] These molecular studies are in line with the overall low risk of COVID-19 to pregnant women. However, little is known about COVID-19's risk to early pregnancy, since the impacts could be unnoticed and it is technically and ethically challenging to study normal trophoblasts of early pregnancy stages. Laboratory model organisms for SARS-CoV-2 have substantial differences from humans in trophoblast biology and placenta development. Therefore, 2D and 3D cellular models of normal human
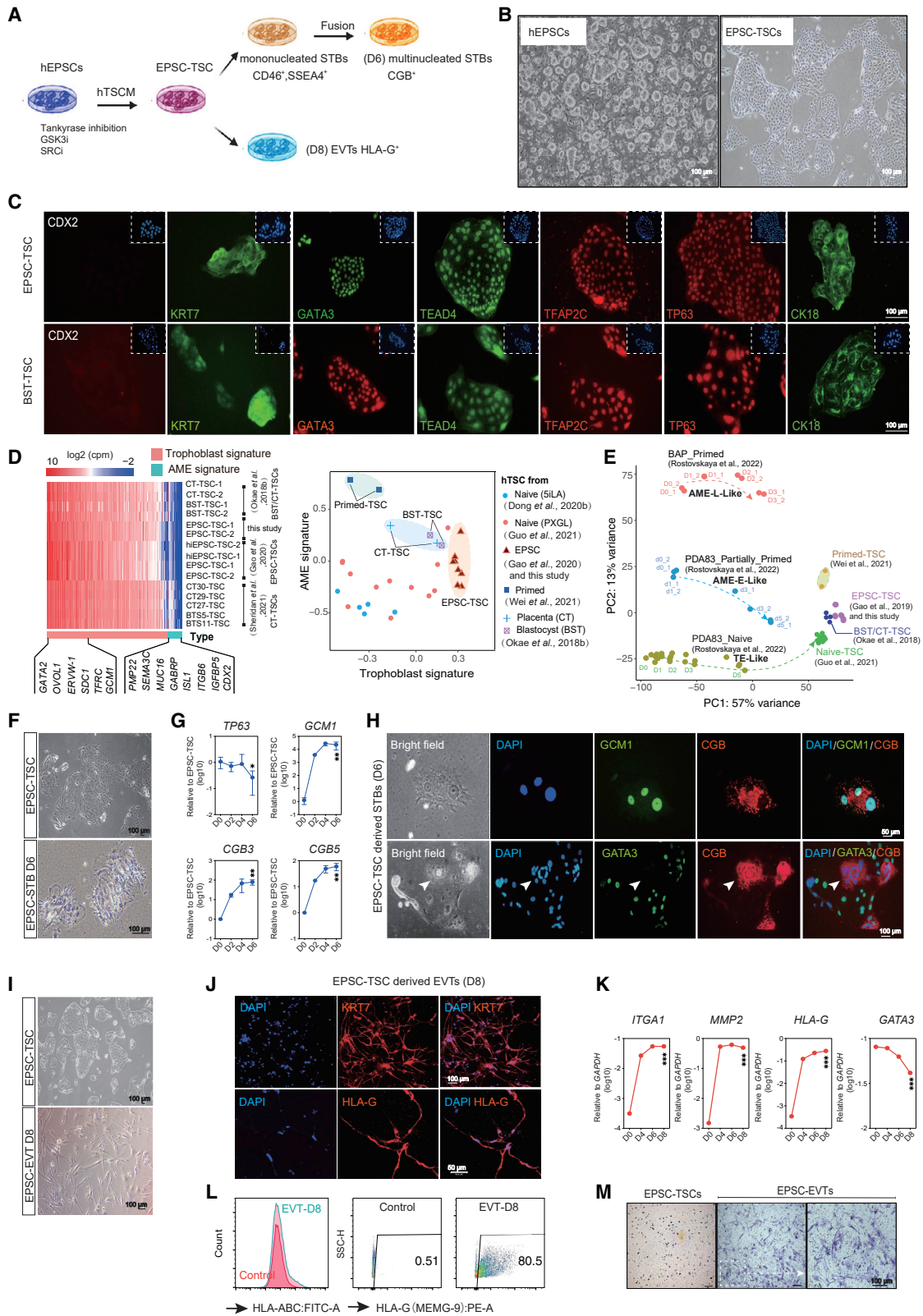
(legend on next page)

trophoblasts are needed to decipher SARS-CoV-2 infection in trophoblasts and in early pregnancy.

Expanded potential stem cells (EPSCs) derived from cleavage-stage preimplantation embryos retain developmental potential for both extraembryonic and embryonic cell lineages.[22–25] In particular, human (h) EPSCs directly generated human trophoblast stem cells (hTSCs) *in vitro*.[24,26] Standard human embryonic stem cells (hESCs) could also generate trophoblast-like cells[27–29] and derive hTSC-like lines.[30] hTSCs were recently established from human naive ESCs,[26,31–34] which may reflect the property of human naive epiblast to regenerate trophoblasts.[32]

In the present study, we establish and validate a stem cell-based system to interrogate trophoblast susceptibility to SARS-CoV-2 infection by generating hTSCs from EPSCs and naive stem cells and hTSC derivatives. SARS-CoV-2 infected a small number of hTSCs expressing ACE2. In stark contrast, early STBs (eSTBs) generated from hTSCs expressed high levels of ACE2 and were highly efficient in supporting SARS-CoV-2 infection and virion production. Knockout of *ACE2* abolished SARS-CoV-2 infection. eSTBs also expressed the *DPP4* gene, which encodes the receptor for Middle East respiratory syndrome coronavirus (MERS-CoV), and were susceptible to the virus infection. Low concentrations (nanomolar) of the antiviral drugs remdesivir and GC376 effectively suppressed viral replication and rescued the developmental defects caused by the infection. In line with relatively uncommon placental infection, hTSC-derived trophoblast organoids expressed low *ACE2* and *TMPRSS2* and were inefficiently infected by SARS-CoV-2. Taken together, our stem cell-based 2D and 3D trophoblast infection results and the *in vivo* peri-implantation embryo gene expression profiles implicate a possible risk of COVID-19 infection in early pregnancy, but a relatively lower risk in late pregnancy. Importantly, human stem cells can provide normal and genome-edited cells such as eSTBs to advance coronavirus isolation, propagation, and production, which may help address some of the challenging technical issues of the currently used mammalian cells in virus research.

RESULTS

Establishment of EPSC-TSCs and generation of STBs and EVTs for infection

Based on the published culture conditions,[35] we established several hTSC lines from M1 hEPSCs, which were converted from the primed human ESC line M1[24] (Figures 1A and 1B).

EPSC-TSCs formed cobblestone-shaped colonies and expressed typical hTSC markers (Figures 1B, 1C, and S1A) and trophoblast-specific C19MC miRNAs (*has-miR-517c-3p*, *517-5p*, *525-3p*, and *526b-3p*)[38] (Figure S1B) highly resembling human blastocyst-derived TSCs (BST-TSCs).[35] They were low or negative for the classical human leukocyte antigen (HLA) class I molecules HLA-A and -B, like BST-TSCs (Figures S1C and S1D). EPSC-TSCs did not highly express putative amniotic epithelium (AME) signature genes such as *CDX2*, *MUC16*, *GABRP*, *ITGB6*, or *VTCN1*[39–43] (Figures 1D, S1E, and S1F; Table S1), similar to those derived from human blastocyst and placenta cytotrophoblasts (BST-TSCs, CT-TSCs, CT27-TSCs, CT29-TSCs, CT30-TSCs, BTS5-TSCs, and BTS-11-TSCs).[35,36] We further transcriptomically compared hTSCs derived from EPSCs, primed, and naive stem cells with those of *in vivo* origins and AME-like cells[24,30–32,35–37] (Table S2). EPSC-TSCs and naive-TSCs were more similar to each other than to "primed"-TSCs in the expression of putative AME signature genes (Figures 1D, 1E, and S1G).

EPSC-TSCs were induced to generate STBs (Figures 1F and S1H). The trophoblast progenitor marker *TP63* was reduced, while STB genes such as *GCM1*, β-chorionic gonadotrophin 3 gene (*CGB3*), and *CGB5* were quickly increased (Figure 1G). Immunofluorescence staining of day 6 differentiated cells (STB-D6) detected GCM1+ and CGB+ and multinucleated STBs (Figures 1H and S1I), some of which seemingly lost GATA3 expression (Figure 1H). Functionally, in the supernatant of STB-D6 cells, ELISA detected properly folded and secreted β-hCG hormone (Figure S1J). Under TGF-β inhibition, EPSC-TSCs efficiently generated EVTs with mesenchymal morphologies and were stained positively for KRT7, HLA-G, ITGA1, and IGTA5 (Figures 1I, 1J, and S1K), with *ITGA1*, *MMP2*, and *HLA-G* rapidly increased and *GATA3* decreased or absent

---

Figure 1. Generation of human trophoblast stem cells (TSCs) and trophoblast subtypes from hEPSCs

(A) Schematic diagram of sequential generation of hTSCs, STBs, and EVTs from hEPSCs.

(B) Bright-field images of hEPSCs and EPSC-TSCs. Scale bars: 100 μm.

(C) Immunofluorescence-stained EPSC-TSCs and human blastocyst-derived hTSCs (BST-TSC).[35] Scale bars, 100 μm.

(D) Left: RNA-seq analysis of human trophoblast and putative AME signature gene (Table S1) expression in EPSC- and BST/CT-TSC and five human placenta-derived CT-TSCs.[36] Right: Scatterplot for gene set scores for human trophoblast and putative AME signature genes (Table S1) in hTSCs of various origins.

(E) PCA for comparison of hTSCs of *in vivo* (BST/CT) and *in vitro* origins (naive, primed, and EPSC). Datasets include *in vitro* differentiation of naive hPSCs to TSCs (D0–D5), primed hPSCs to AME-L (late)-like cells (D0–D3), and partially primed hPSCs to AME-E (early)-like (D0–D5).[37] The dashed lines and arrows indicate the differentiation trajectories.

(F) Bright-field images of EPSC-TSCs differentiating toward STBs (STB-D6). Scale bars, 100 μm.

(G) Gene expression (qRT-PCR) during EPSC-TSC differentiation toward STBs. Data are mean ± SD; n = 3 biological replicates. Student's t test, *p < 0.05, **p < 0.01.

(H) Immunostaining of STBs-D6 for GCM1 and CGB (top) and GATA3 (bottom). Arrows indicate the lack of GATA3 in a multinucleated CGB+ mature STB. Scale bars, 50 or 100 μm as indicated.

(I) Bright-field images of EPSC-TSCs differentiating toward EVT-D8. Scale bars, 100 μm.

(J) Immunostaining of EVT-D8 for KRT7 and HLA-G. Scale bars, 50 or 100 μm as indicated.

(K) Gene expression (qRT-PCR) during EPSC-TSC differentiation toward EVTs. Data are mean ± SD; n = 3 biological replicates. Student's t test, ***p < 0.001.

(L) Flow cytometric analysis of HLA-A, -B, -C and HLA-G on EVT-D8. EPSC-TSCs were used as the control.

(M) Invasiveness of EVT-D8 in the transwell assay. The invading/migrating cells on the lower surface were stained with crystal violet. Scale bar, 100 μm.
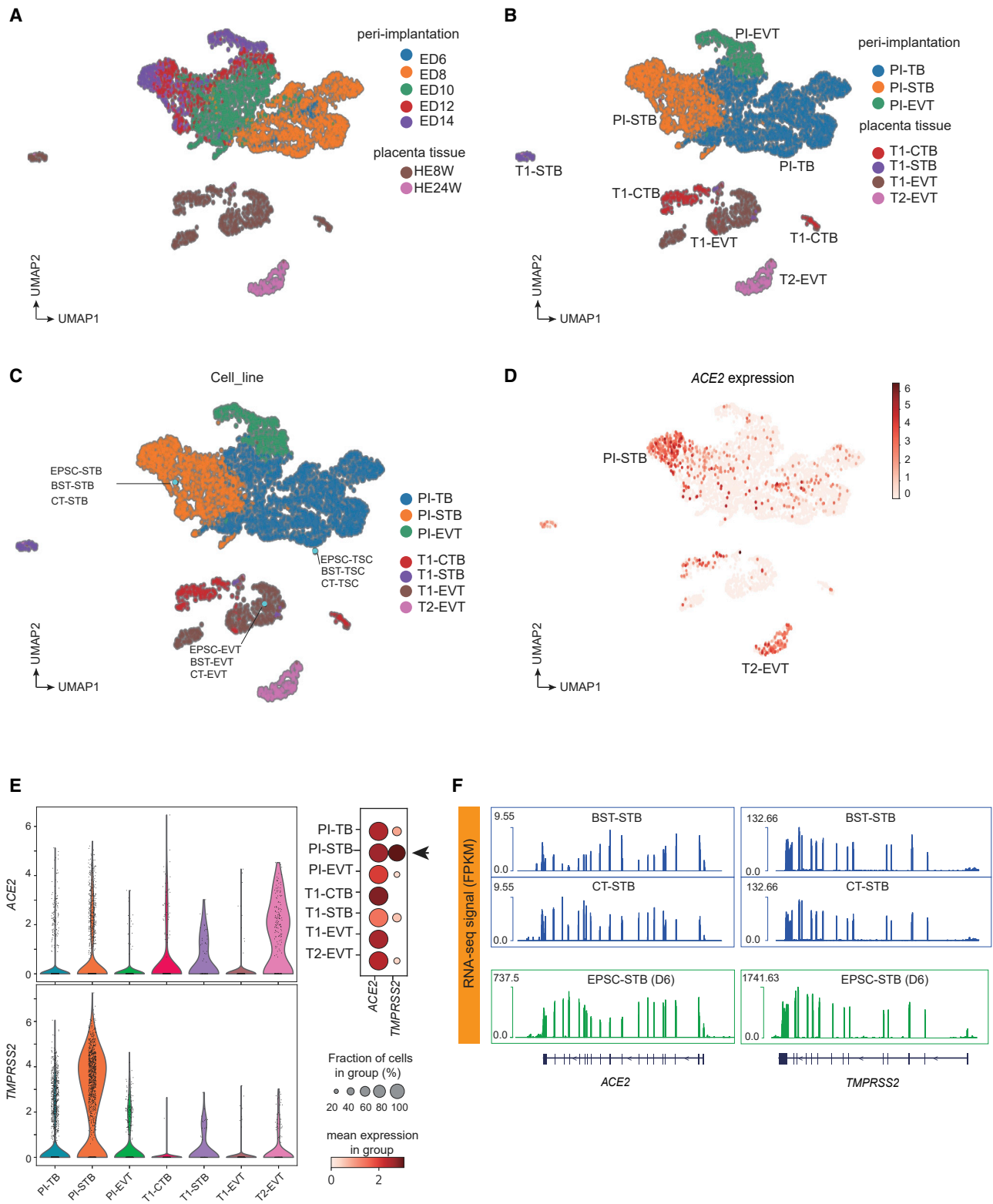
Figure 2. Trophoblasts derived from hEPSCs resemble those in human peri-implantation embryos and placenta

(A and B) UMAP analysis of scRNA-seq data of cells from *in vitro*-cultured peri-implantation (PI) embryo stages (top) and of cells from first (T1)- and second (T2)-trimester placenta (bottom). Cells are colored by developmental time points (ED6–14, embryonic day 6–14; HE8W/HE24W, placenta trophoblasts at 8 or 24 weeks of gestation, corresponding to first or second trimester) in (A) and trophoblast subtypes at each stage in (B).

(legend continued on next page)

(Figures 1K and S1L). On day 8, most cells were positive for HLA-G, ITGA1, and ITGA5, but negative for the classical HLA class I molecules HLA-A and -B (Figures 1L and S1M). Functionally, EPSC-TSC-derived EVTs possessed potent invasiveness capability (Figure 1M).

We next performed RNA-seq analysis of EPSC-TSCs and their derivative STBs (D2, D4, and D6) and EVTs (D4, D6, and D8) and compared them with human primary trophoblast-derived hTSCs (CT-TSC, BTS-TSC) and their derivatives.[36] Principal-component analysis (PCA) showed that EPSC-TSCs again clustered closely to both CT-TSCs and BTS-TSCs, while EPSC-EVTs and EPSC-STBs clustered closely to CT-EVTs/BTS-EVTs and CT-STBs/BTS-STBs, respectively (Figure S1N). RNA-seq further confirmed low classical HLA class I molecules HLA-A and -B (Figure S1O) in all TSCs.[36]

Trophoblasts derived from hEPSCs molecularly resemble those in human peri-implantation embryos and placenta

We next computationally compared EPSC-derived trophoblasts with those in human peri-implantation embryos and the placenta to validate the lineage identity of the *in vitro*-generated trophoblasts. We extracted scRNA-seq data of 4,041 peri-implantation extraembryonic cells (embryonic days 6–14) in a prolonged culture of human embryos *in vitro*[44] and 952 placental cells from first- and second-trimester pregnancies[45] and subsequently combined these scRNA-seq datasets to compute the joint uniform manifold approximation and projection (UMAP), with their developmental times highlighted (in embryonic day, or ED, or gestational week, or W) (Figure 2A) and developmental stages and subtypes annotated (Figure 2B). The peri-implantation sector contained the trophoblast cells (PI-TBs), which possessed stemness and potency to differentiate into EVTs (PI-EVTs) and STBs (PI-STBs) as shown in the same sector (Figure 2B). Correspondingly, the placenta cells were identified as first-trimester cytotrophoblast cells (T1-CTBs), T1-EVTs, and T1-STB or second-trimester placenta EVTs (T2-EVTs) (Figure 2B). The trophoblast markers were examined in each stage-specific subtype, which validated their trophoblast identities (Figure S2A). Notably, these human *in vivo* trophoblasts did not appear to highly express the reported putative amnion marker genes *MUC16*, *GABRP*, or *CDX2*, whereas some did express *VTCN1*, *ITGB6*, and *ISL1* (Figure S2B), whose identity warrants further investigation.

We then projected and mapped EPSC-TSCs and blastocyst- or cytotrophoblast-derived TSCs (BST-TSCs, CT-TSCs) and their STBs/EVTs[35] against the *in vivo* trophoblast clusters categorized by stage and lineage as described in Figures 2A and 2B. All hTSCs (EPSC-TSCs, BST-TSCs, CT-TSCs) were pro-

jected proximal to PI-TBs,[33] whereas STBs were projected proximal to PI-STBs, and EVTs to T1-EVTs, regardless of cell line origin (Figure 2C). The resemblance between *in vitro*-generated trophoblasts and *in vivo* counterparts was supported by whole-transcriptome Pearson correlation (Figure S2C). Notably, none of the hTSCs or their STBs/EVTs expressed the putative AME genes at high levels (Figure S2D).

To explore the potential trophoblast susceptibility to SARS-CoV-2, we examined *ACE2* in the *in vivo* trophoblasts and detected its high expression in the PI-STB cluster (Figures 2D and 2E). *ACE2* and trophoblast subtype markers exhibit significant positive correlations with STB markers such as *CD46*, *CGB5*, *ENG*, and *CSH2* (r = 0.245, 0.200, 0.207, and 0.248, respectively, p < 0.0001) (Figure S2E), but not EVT genes (Table S3). The PI-STB cluster also co-expressed the highest levels of *ACE2* and *TMPRSS2*, whereas some co-expression was detected in PI-TBs, T1-STBs, and T2-EVTs (Figures 2E and S2F), in line with previous studies.[17,19] Other reported SARS-CoV-2 receptors, like *BSG*[46] and *AXL*,[47] however, did not appear to be expressed in any specific cell cluster (Figure S2F).

In the *in vitro*-cultured trophoblasts, EPSC-TSCs, BST-TSCs, CT-TSCs, and their STBs and EVT derivatives, all expressed *ACE2* and *TMPRSS2*, with STBs having the highest levels (Figures 2F, S2G, and S2H), whereas hEPSCs had barely detectable *ACE2* or *TMPRSS2* (Figure S2H). The host factor expression profiles in both *in vivo* and *in vitro* trophoblasts highlighted STBs' potential susceptibility to SARS-CoV-2 infection.

hTSCs are susceptible to SARS-CoV-2 infection

We next experimentally compared the viral replication kinetics among hEPSCs, EPSC-TSCs, STBs, and EVTs. Briefly, cells were infected with SARS-CoV-2 (SARS-CoV-2 HKU-001a strain; GenBank accession no. MT230940) for 2 h, followed by incubation in fresh medium for another 24, 48, or 72 h or hpi (hours post infection) (Figure 3A). The supernatant and cell lysates were collected for viral genome and antigen detection. hEPSCs did not express *ACE2* (Figure S2H) and thus were poorly infected by SARS-CoV-2, as evidenced by viral genome detection in the supernatant or cell lysate and negative immunofluorescence staining of the viral N protein (Figures 3B, S3A, and S3B). In line with the relatively low *ACE2* and *TMPRSS2* expression levels (Figure S2H), SARS-CoV-2 infected EPSC-TSCs, but only about 3%–4% of the cells stained positive for the viral N protein (Figures 3B and 3C). Infected EPSC-TSCs were positively stained for ACE2 and the pan-trophoblast marker KRT7 (Figure 3D). Intriguingly, infected EPSC-TSCs expressed the blastocyst trophectoderm (TE) marker ENPEP[34] (Figure 3E), which is a candidate co-receptor

(C) Mapping of *in vitro* human trophoblast cell bulk RNA-seq data to the peri-implantation and placental trophoblast clusters in (B). The *in vitro* cells are highlighted in light blue filled circles.

(D) Expression of *ACE2* in peri-implantation and placenta trophoblast scRNA-seq clusters.

(E) Left: violin plots of *ACE2* and *TMPRSS2* expression (log-transformed transcripts per million [TPM]). Right: dot plot of *ACE2* and *TMPRSS2* expression levels in *ACE2*-positive cells, categorized according to stage and cell lineage. Dots are colored according to the mean expression value in each category and dot size indicates the percentage of *ACE2*- or *TMPRSS2*-positive cells from each category that expresses *ACE2*.

(F) RNA-seq signals of *ACE2* and *TMPRSS2* in BST/CT-STBs and EPSC-STBs. The *ACE2* and *TMPRSS2* genomic loci are plotted at the bottom, where each vertical bar represents an exon, and the transcription direction is from right to left.
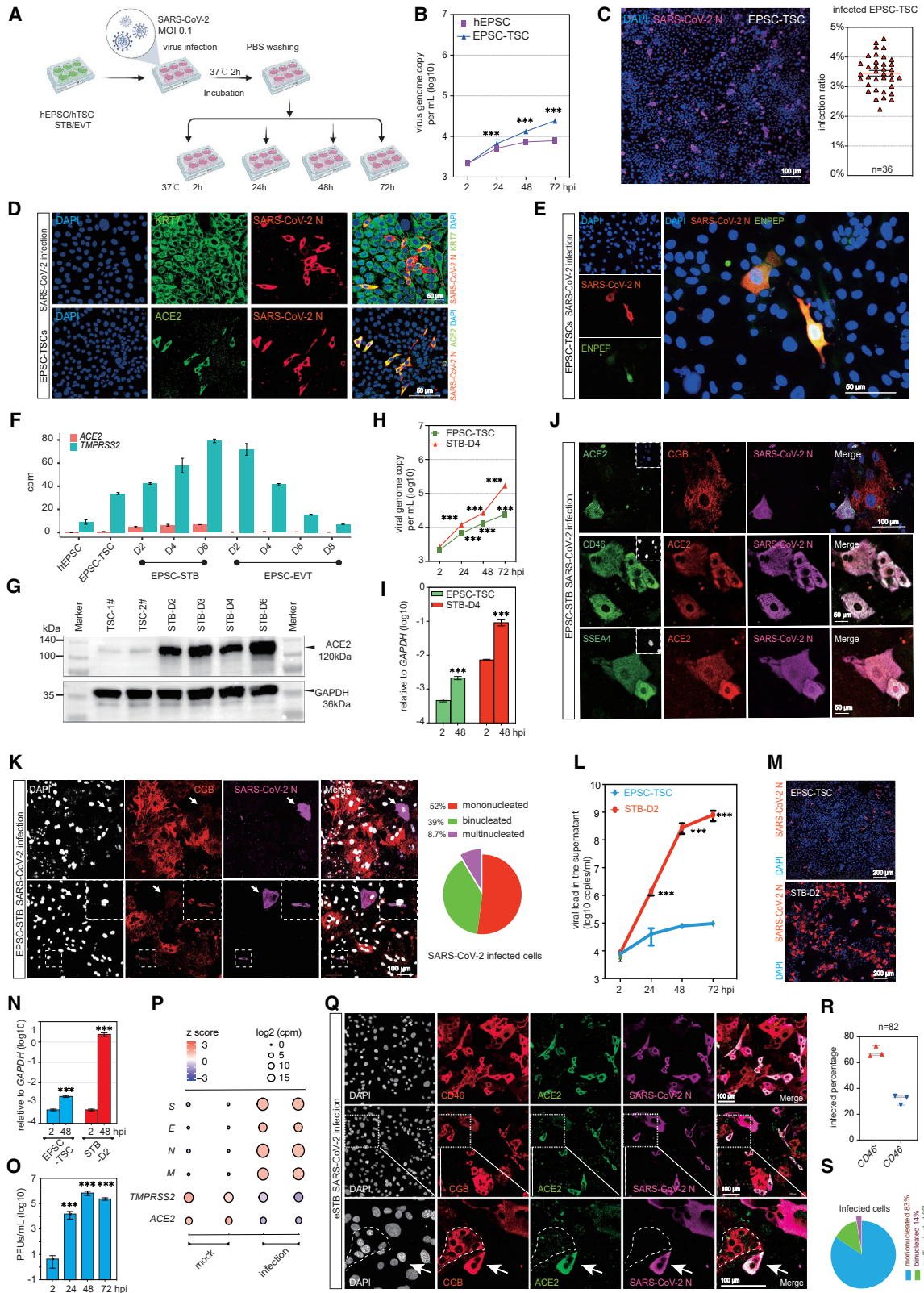
(legend on next page)

for SARS-CoV-2.[48] Similar to EPSC-TSCs, about 0.5%–1% of BST-TSCs derived from human blastocysts[35] were infected by SARS-CoV-2 and stained positive for KRT7, ACE2, and ENPEP (Figures S3C and S3D).

We next converted human primed ESCs (H1) into naive stem cells in the PXGL condition[32] (Figures S3E-S3K) for deriving naive TSCs. Consistently, 2%–3% of the naive TSCs were infected by SARS-CoV-2 (Figure S3L) while expressing ACE2 (Figure S3M) and ENPEP (Figure S3M). The presence of a small number of ACE2+ and SARS-CoV-2-susceptible hTSCs revealed the heterogeneity of the current hTSC cultures, which warrants future investigation. The observation that hTSCs are transcriptionally similar to PI-TBs[33] (Figure 2C) and that ACE2+ hTSCs were susceptible to SARS-CoV-2 indicates that human peri-implantation embryos are potentially at risk of SARS-CoV-2 infection.

eSTBs are highly susceptible to SARS-CoV-2 infection

STBs in peri-implantation embryos and those generated from hTSCs co-expressed ACE2 and TMPRSS2 (Figures 2D, 2E, 2F, and S2F). In hTSC differentiation toward STBs, expression of both ACE2 and TMPRSS2 was substantially increased starting from day 2 (STB-D2) (Figures 3F and 3G), in line with more efficient infection by SARS-CoV-2 in STBs than in hTSCs (Figures 3H and 3I). We noticed that the virus-infected cells were generally positive for early STB markers (SSEA4 and CD46)[49,50] (Figure 3J). Indeed, multinucleated and CGB+ mature STBs did not express ACE2 highly and accounted for only a minor population of infected cells (Figure 3K). These results indicate that SARS-CoV-2 appears to preferentially infect immature or early STBs.

In STB-D2, most cells were mononucleated and negative for CGB, and only 3% of cells were multinucleated (Figures S3N and S3O). The early STB gene CD46 was transiently upregulated in STB-D2, whereas the mature STB gene CGB markedly increased after D2 (Figure S3P). Notably, ACE2 and TMPRSS2 expression was rapidly upregulated in STB-D2 (Figures 3F and 3G). We thus used STB-D2 cells for subsequent infection experiments and empirically named these cells as eSTBs.

Following infection of eSTBs with SARS-CoV-2 (MOI 0.1), supernatants were collected at 2, 24, 48, and 72 hpi and quantified for viral RNA load, which revealed that eSTBs produced high amounts of supernatant viral RNA at 48 and 72 hpi (Figure 3L). Immunofluorescence staining at 24 hpi showed substantially higher rates of infection than that of EPSC-TSCs (Figure 3M). In line with this observation, >3 $\log_{10}$ viral genome copies in the cell lyses was documented comparing eSTBs with hTSCs (Figure 3N). A continuous release of infectious virus particles from the infected eSTBs was detectable in plaque assays (Figure 3O). The robust production of SARS-CoV-2 was further revealed in RNA-seq, where abundant transcripts of viral Envelope (E), Membrane glycoprotein (M), Nucleocapsid (N), and S genes were detected (Figure 3P).[51] Immunostaining for SARS-CoV-2 N protein revealed that the virus-infected cells were primarily CD46+, whereas those multinucleated cells were infrequently infected (Figures 3Q, 3R, and 3S). Similar results were obtained in eSTBs generated from naive TSCs (Figures S3Q and S3R).

EPSC-EVTs expressed low levels of ACE2 and TMPRSS2 (Figure S2H). Consistently, only 1%–2% of EVTs were infected by SARS-CoV-2 (Figures S3S, S3T, S3U, and S3V).

Figure 3. eSTBs are highly susceptible to SARS-CoV-2 infection among trophoblasts

(A) Schematic diagram of SARS-CoV-2 infection of in vitro trophoblasts.

(B) qRT-PCR detection of SARS-CoV-2 genome copy numbers (per mL) in the supernatants of virus-co-cultured cells at different time points. Data are mean ± SD; n = 3 biological replicates. Student's t test, ***p < 0.001.

(C) Immunofluorescence image of 24 hpi EPSC-TSCs stained for SARS-CoV-2 N protein. Scale bar, 100 μm. Right: percentages of N-protein-positive cells. Data are mean ± SEM; n = 36, quantification of 36 random images.

(D) Immunofluorescence detection of KRT7, ACE2, and N protein in the infected EPSC-TSCs. Scale bars, 50 μm.

(E) Representative immunofluorescence images of N protein and ENPEP at 24 hpi in EPSC-TSCs. Scale bar, 50 μm.

(F) Bar plot for expression (cpm) of ACE2 and TMPRSS2 in hEPSCs, EPSC-TSCs, and STBs and EVTs differentiated from EPSC-TSCs at indicated time points.

(G) Detection of ACE2 protein in EPSC-TSCs and during their differentiation toward STBs.

(H) qRT-PCR detection of SARS-CoV-2 genome copy numbers (per mL) in the supernatants of virus-co-cultured EPSC-TSCs and (day 4) STBs. Data are mean ± SD; n = 3. Student's t test, ***p < 0.001.

(I) qRT-PCR analysis of SARS-CoV-2 genome copy number in cell lysates of 48 hpi EPSC-TSCs and STB-D4. Data are mean ± SD; n = 3. Student's t test, ***p < 0.001.

(J) Immunofluorescence staining of 48 hpi STB-D6 for ACE2, CGB, and N protein and for early STB markers CD46 and SSEA4. Scale bars, 50 or 100 μm as specified.

(K) Immunofluorescence staining of 48 hpi STB-D6 for ACE2, CGB, and N protein, and percentages of mono-, bi-, and multinucleated CGB+ cells in the infected STB-D6. Arrowheads indicate that some CGB-low or mono- or binucleated cells were infected by SARS-CoV-2. DAPI stains the nucleus. Scale bars, 100 μm.

(L) qRT-PCR detection of SARS-CoV-2 genome copy number (per mL) in the supernatants of virus-co-cultured EPSC-TSCs and eSTBs (STB-D2). Data are mean ± SD; n = 3. Student's t test, ***p < 0.001.

(M) Representative immunofluorescence images of 24 hpi EPSC-TSCs and eSTBs (STB-D2) stained for N protein. Scale bars, 200 μm.

(N) qRT-PCR detection of SARS-CoV-2 gene expression in cell lysates of the infected cells at 48 hpi. Data are mean ± SD; n = 3. Student's t test, ***p < 0.001.

(O) Plaque formation assay to detect SARS-CoV-2 virus in supernatants from the infected eSTBs (48 hpi). Data are mean ± SD; n = 3 three independent experiments; ***p < 0.001 (Student's t test). PFUs, plaque-forming units.

(P) Bubble plot for RNA-seq analysis of SARS-CoV-2 genes (E, M, N, S) in the cell lysates of 48 hpi eSTBs.

(Q) Representative immunofluorescence images of 24 hpi eSTBs stained for ACE2 and N protein and for STB markers CD46 and CGB. The dotted area shows an uninfected multinucleated CGB+ cell. Arrows indicate an infected binucleated STB. Scale bars, 100 μm.

(R) Quantification of the percentages of eSTB marker CD46 in 24 hpi eSTBs. Data are mean ± SEM.

(S) Quantification of the percentages of mono-, bi-, and multinucleated cells in 24 hpi eSTBs. SARS-CoV-2 preferentially infects mononucleated cells.
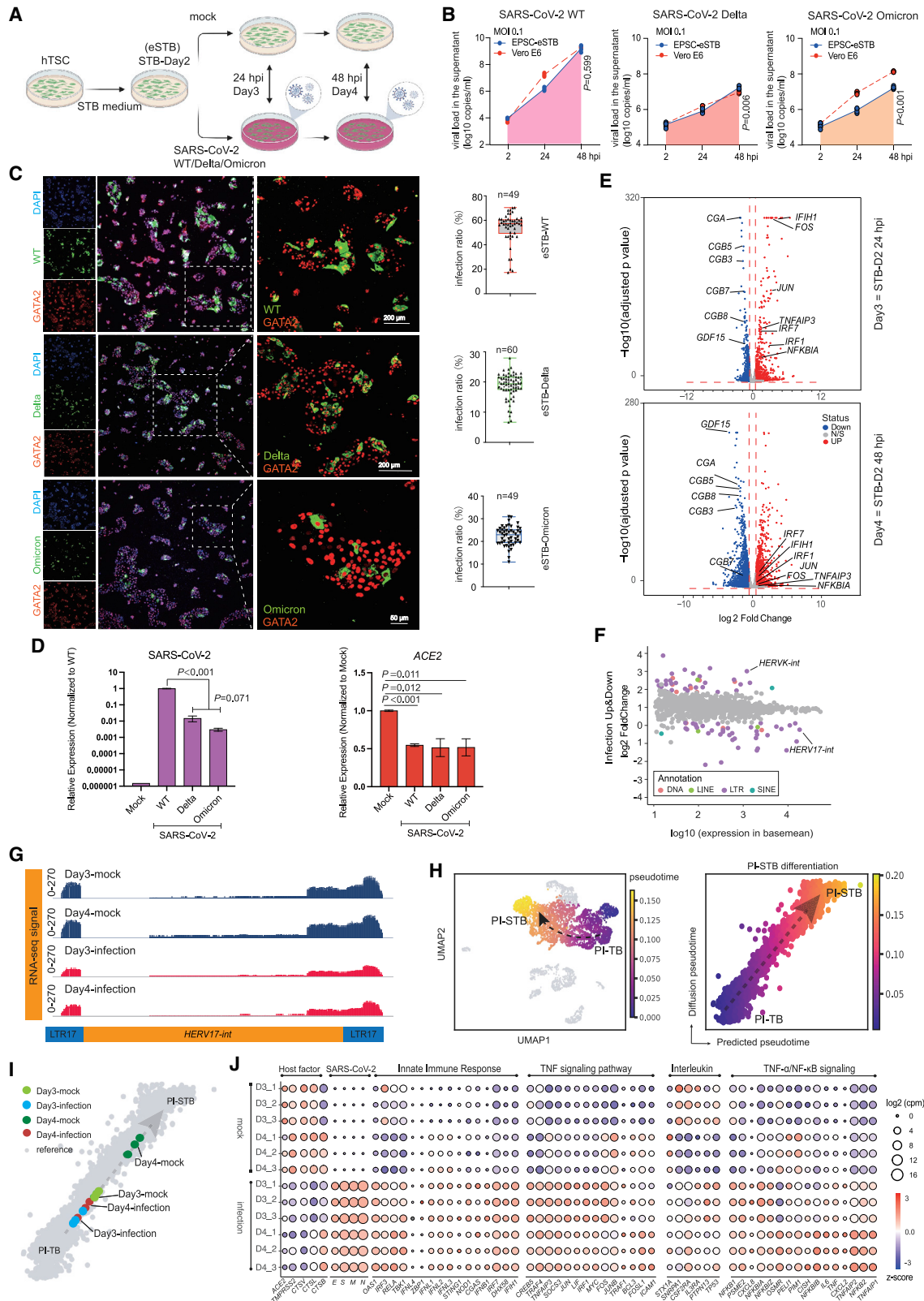
(legend on next page)

Susceptibility of human trophoblasts to SARS-CoV-2 variants of concern

SARS-CoV-2 variants carrying various mutations have been found to influence virus replication, infectivity, transmission, and infection- and vaccine-induced immunity.[52] The Delta variant was the previous predominant circulating SARS-CoV-2 strain, but was overtaken by the Omicron variants in late November 2021. Quantification of viral RNA genome copies generated over a period of 48 h demonstrated that both the Delta (B.1.617.2) and the Omicron (B.1.1.529) variants replicated robustly in EPSC-eSTBs and appeared to be as good as in Vero E6 cells (Figures 4A and 4B).

Among the three lineages of SARS-CoV-2, less viral NP antigen in EPSC-eSTBs was found in Delta- (~18.8%) and Omicron-infected cells (~22%) compared with the wild-type (WT) SARS-CoV-2 (~54%) (Figure 4C), as confirmed by viral genome quantification (Figure 4D). In line with a previous *in vivo* study,[51] *ACE2* expression was significantly downregulated in EPSC-eSTBs following either Delta or Omicron infection (Figure 4D). Similar phenotypes were observed in eSTBs generated from additional EPSC-TSC lines (EPSC-TSC 3# and hiEPSC-TSC[24]) and from naive-TSCs and BST-TSCs for their susceptibility to the WT, Delta, and Omicron variants (Figures S4A and S4B). Thus, eSTBs' susceptibility to SARS-CoV-2 infection is independent of cell origin and genetic background.

SARS-CoV-2 infection impairs hTSC differentiation to STBs and induces a potent innate immune response

We next investigated global transcriptomic changes in infected EPSC-eSTBs (Figure 4E). Pearson correlation and cluster analysis revealed that the SARS-CoV-2-infected cells (24 hpi or STB-D3; 48 hpi or STB-D4) were clustered together and separated from the mock infection controls (Figure S4C). Comparative transcriptomic analysis identified 654 upregulated and 736 downregulated differentially expressed genes (DEGs) in the infected cells (Figure S4C).

Among the DEGs significantly decreased in SARS-CoV-2-infected cells were *CGA*, *CGBs* (*CGB3, 5, 7, 8*), *GCM1*, *SDC1*, and *ENDOU* and others that are highly expressed in mature and multinucleated STBs (Figures 4E and S4D), indicating that the infection caused a possible developmental blockage. Gene set enrichment analysis (GSEA) revealed a significant enrichment of cell-cycle, in particular, G2-M, related genes in the infected cells compared with the mock control (Figure S4E). The lack of mature STB signature and higher cell-cycle genes in infected cells are consistent, since mature and multinucleated STBs are known to have inactive cell cycles.

Interestingly, GSEA revealed that SARS-CoV-2 infection did not substantially affect the infected cells' viability, as apoptosis-related genes were not significantly changed (Figure S4E). In contrast, infected Vero E6 cells had enriched expression of apoptosis-related genes[53] (Figure S4E). Experimentally, Vero E6 cells mostly detached by 72 hpi due to cell death, whereas eSTBs did not show an obvious cytopathogenic effect (CPE) (Figure S4F). Furthermore, TUNEL cell apoptosis assay confirmed that, distinct from Vero E6 cells, eSTBs did not undergo appreciable apoptosis by 72 hpi (Figure S4F). Therefore, the lack of mature STBs in the infected cells is more likely caused by developmental block.

The multinucleate STB formation requires the endogenous retrovirus (HERV) proteins Syncytin-1, an envelope gene of HERV-W, and Syncytin-2, produced by HERV-FRD.[54,55] SARS-CoV-2 infection of eSTBs resulted in lower levels of both *HERV-W* (*HERV17-int*, *Syncytin-1*) and *HERV-FRD* (*Syncytin-2*), but substantially increased HERV-K expression (Figures 4G and S4G). *HERV-K* is known to be exclusively expressed in cytotrophoblast cells (progenitors) in the human placenta.[56]

To further investigate eSTB development following the infection, we extracted the PI-TB and PI-STB differentiation process from the *in vivo* trophoblast scRNA-seq data[44] to generate a pseudotime trajectory, which increased from immature PI-TB to relatively mature PI-STB (Figure 4H). Using machine learning, we mapped the mock- and virus-infected STB cells (STB-D3 and STB-D4) to this pseudotime trajectory and discovered that the infected cells were closer to PI-TB along the pseudotime trajectory compared with the mock cells (Figure 4I). SARS-CoV-2 infection thus impaired eSTB differentiation and maturation, implicating a potential COVID-19 risk in early pregnancy, which may be asymptomatic and unnoticed.[57]

Figure 4. SARS-CoV-2 variants robustly replicate in eSTBs

(A) Schematic diagram of eSTBs for SARS-CoV-2 wild-type (WT) and Delta or Omicron variant infection.

(B) Comparison of SARS-CoV-2 replication kinetics in EPSC-eSTBs and Vero E6 cells.

(C) Left: representative immunofluorescence images of N protein and GATA2 in EPSC-eSTBs infected by SARS-CoV-2 WT, Delta, and Omicron at 24 hpi. Right: percentages of N protein-positive EPSC-eSTBs. Error bars: mean and SEM; n = 49, 60, and 49 for quantification of random immunofluorescence images in WT-, Delta-, and Omicron-infected eSTBs, respectively.

(D) qRT-PCR analysis of *ACE2* and virus gene expression levels in 48 hpi EPSC-eSTBs. Data are mean ± SD; n = 3. Student's t test, exact p values are presented.

(E) Volcano plots of gene expression in infected STB-D3 and STB-D4. The horizontal red dashed line marks the adjusted p value (Wald test) 0.05, while the vertical red dashed lines marks expression fold change of 1.5.

(F) A scatter diagram of the transcriptomic analysis of TEs after virus infection. Differentially expressed TEs (p < 0.05) are in colors, while non-differentially expressed TEs are in gray. Expression levels of TEs used for the x axis are from DESeq2 results. Data from STB-D3 and STB-D4 are combined in this analysis.

(G) RNA-seq signal of HERV-W in infected STB-3 and STB-4 and the mock-infection control cells. Library size was used to normalize the read counts.

(H) Pseudotime analysis depicting PI-TB to PI-STB development trajectory. The black dashed arrow indicates the imputed direction of differentiation. PI-TB to PI-STB subpopulations are colored by machine learning predicted pseudotime. The x axis is the predicted pseudotime, and the y axis is the diffusion pseudotime computed using SCANPY. Gray dashed arrow describes the linear regression relationship between the predicted pseudotime and the diffusion pseudotime.

(I) Infected vs. normal (mock) STB-D3 and STB-D4 mapped against the PI-TB to PI-STB pseudotime trajectory (see STAR Methods).

(J) Bubble plot for host factors *ACE2*, *TMPRSS2*, *CTSL*, *CTSV*, and *CTSB*; infection-related signaling pathways; and virus genes in infected eSTBs. Bubble colors are in accordance with *Z* score and bubble sizes are proportional to expression levels.
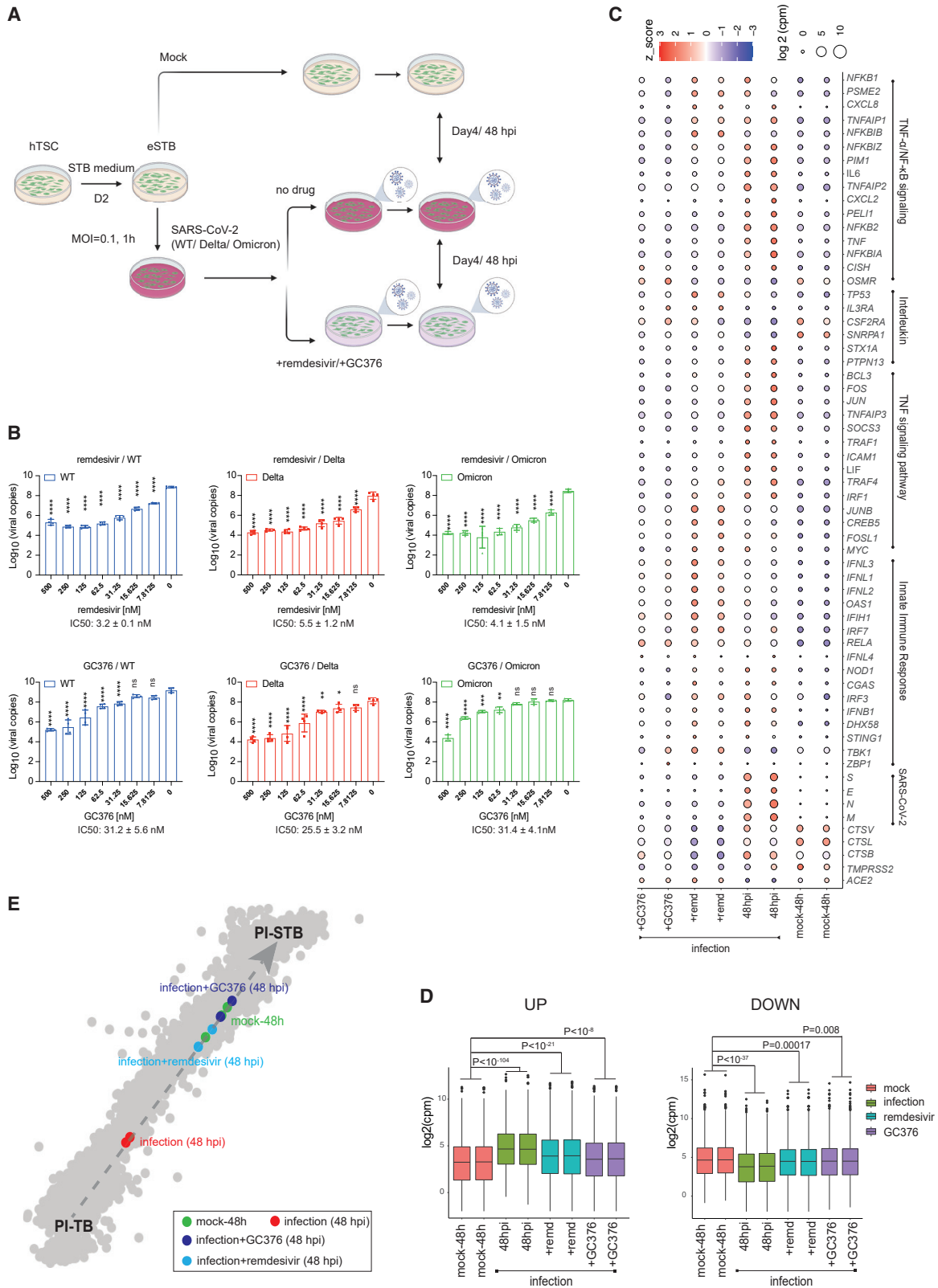
(legend on next page)

SARS-CoV-2 infection caused a strong innate immunity response. Genes encoding interferon signaling components (*IFNL1*, *IFIH1*) and genes associated with TNF-α signaling via NF-κB, such as *TNFAIP3* and *NFKBIA*, were upregulated in infected cells (Figures 4E and S4D). Gene ontology (GO) term analysis found enriched terms related to virus cellular response and immune response pathways in SARS-CoV-2-infected STBs (Figure S4H). As expected, KEGG pathway analysis revealed that the coronavirus disease COVID-19 pathway was among the overrepresented ones (Figure S4H). Bubble plot analysis further demonstrated an enrichment of pathways associated with innate immune response and interleukin and TNF signaling pathways in the upregulated genes (Figure 4J).

The double-stranded RNA (dsRNA) generated during coronavirus genome replication and transcription could be recognized by melanoma differentiation gene 5 (MDA5/IFIH1) in the cytoplasm to trigger innate immune activation upon coronavirus infection.[58–60] *IFIH1* was highly upregulated in the infected cells (Figure 4J). Meanwhile, DNA is not known to be involved in the SARS-CoV-2 life cycle. Consistently, genes encoding *cGAS* and *STING1*, both being components of the cGAS-STING pathway of the innate immune system detecting cytosolic DNA, were not substantially altered (Figure 4J).

In response to viral infections, interferons (IFNs) initiate signaling cascades that stimulate the expression of many genes and create an intracellular antiviral defense. Type III IFNs are important antiviral factors.[61] Particularly, IFN-λ1 is known to be constitutively released from human placental trophoblasts to protect the fetus from viral infections.[62,63] Type III IFNs have also been shown to restrict SARS-CoV-2 infection in airway and intestinal epithelia.[64,65] Infected cells expressed high levels of genes encoding type III IFNs, including IFN-λ1 (IL-29 or IFNL1), IFN-λ2 (IL-28A or IFNL2), IFN-λ3 (IL-28B or IFNL3), and IFN-λ4 (IFNL4) (Figure 4J). *2′-5′-oligoadenylate synthetase 1* (*OAS1*) is a recently identified IFN-signaling downstream gene that stimulates RNase L and specifically inhibits the virus.[66] It was highly expressed in the infected eSTBs (Figure 4J).

In line with Vero E6 cells being genetically defective in IFN signaling and TMPRSS2,[67,68] they expressed *ACE2* but not *TMPRSS2* (Figure S4I).[53] In the infected Vero E6 cells, the IFN genes *IFNb1*, *IRF3*, and *TBK1* showed no changes and the antiviral effector *OAS1* showed only mild upregulation (Figure S4I).

The relatively high Omicron replication in *TMPRSS2*-deficient Vero E6 cells, as presented in Figures 4B, S4A, and S4B, is possibly due to Omicron infection being more dependent on cathepsins or other endosomal proteases than other variants of concern.[69–72] Vero E6 expressed *Cathepsin L* (*CTSL*) and *Cathepsin L2* (*CTSV*), which were downregulated following the infection (Figure S4I). Similarly, eSTBs expressed both Cathepsin genes, and the infected cells showed decreased expression (Figure 4J), which may be a mechanism for Omicron replication in eSTBs.

Remdesivir and GC376 effectively eliminate eSTB SARS-CoV-2 and variant infection

The eSTBs permitted robust SARS-CoV-2 infection and thus provide normal and physiologically relevant cells for evaluating antiviral drugs. To this end, we tested the FDA-approved antiviral drug remdesivir[73] and a veterinary drug, GC376,[74] in our cell models (Figure 5A). Remdesivir effectively eliminated SARS-CoV-2 infection in Vero E6 cells at around 5 μM with an IC_{50} of 0.77 μM.[75] In eSTBs, remarkably, remdesivir demonstrated an IC_{50} of 3.2 ± 0.1 nM for SARS-CoV-2 and 5.5 ± 1.2 nM for Delta and 4.1 ± 1.5 nM for Omicron variants (Figures 5B, S5A, and S5B).

GC376 is a repurposed SARS-CoV-2 main protease inhibitor that increases survival of mice with a fatal SARS-CoV-2 infection.[76] GC376 suppressed the virus infection in eSTBs with an IC_{50} of 31.2 ± 5.6 nM against WT, 25.5 ± 3.2 nM against Delta variant, and 31.4 ± 4.1 nM against Omicron variant (Figures 5B and S5B), which were much lower than in Vero E6 cells (0.70 μM).[77] The effectiveness of these two drugs against SARS-CoV-2 in eSTBs was further confirmed by the substantially reduced viral N antigen expression in immunofluorescence staining (Figure S5C). Similar results were obtained in naive eSTBs (Figure S5D).

Expression of the *DPP4* gene, the host entry receptor of MERS-CoV, another highly pathogenic human coronavirus, is highly correlated with *ACE2* and *ENPEP* in human preimplantation embryos[48] and was detected in eSTBs (Figure S5E). MERS-CoV infected eSTBs derived from hEPSC-TSCs at an efficiency comparable to that in Vero E6 cells,[78] and both remdesivir and GC376 could effectively block MERS-CoV replication in eSTBs with efficiencies comparable to those in Vero E6 cells (Figure S5F). These results indicate the potential of eSTBs for antiviral evaluation against SARS-CoV-2, MERS-CoV, and other coronaviruses.

We next examined the global transcriptome of infected and drug-treated cells. Both drug treatments drastically reduced expression of SARS-CoV-2 genes (E, M, N, and S) (Figure 5C). Neither drug appeared to cause substantial changes in host innate immune response genes such as *MDA5*, *IFNL1-4*, *IFNB1*, and *OAS*, but proinflammatory cytokine genes such as *TNF*, *IL-6*, and *IL-8* were all downregulated in the drug-treated cells (Figures 5C and S5G).

Figure 5. Antiviral drugs remdesivir and GC376 effectively inhibit replication of SARS-CoV-2 and its variants in eSTBs

(A) Schematic diagram of SARS-CoV-2 infection in an eSTB cell model.

(B) Dose-dependent inhibition of SARS-CoV-2 WT/Delta/Omicron by remdesivir/GC376 in EPSC-derived eSTBs. Viral copies in the supernatant were quantified by qRT-PCR. Data are mean ± SEM; n = 3. Two-way ANOVA; ns, not significant; *p < 0.05, **p < 0.01, ***p < 0.001, ****p < 0.0001.

(C) Bubble plot for genes of host factors, infection-related signaling pathways, and virus genes in infected eSTBs. Bubble color is in accordance with expression Z score and bubble size is expression level.

(D) Boxplots for upregulated and downregulated genes in 48 hpi EPSC-eSTBs, with or without SARS-CoV-2 infection, and in the presence or absence of remdesivir or GC376. Statistical significance was calculated by Wilcoxon test using mean of expression values.

(E) Mapping of 48 hpi EPSC-eSTBs in the presence or absence of remdesivir (10 μM) or GC376 (10 μM) against *in vivo* pseudotime trajectory.
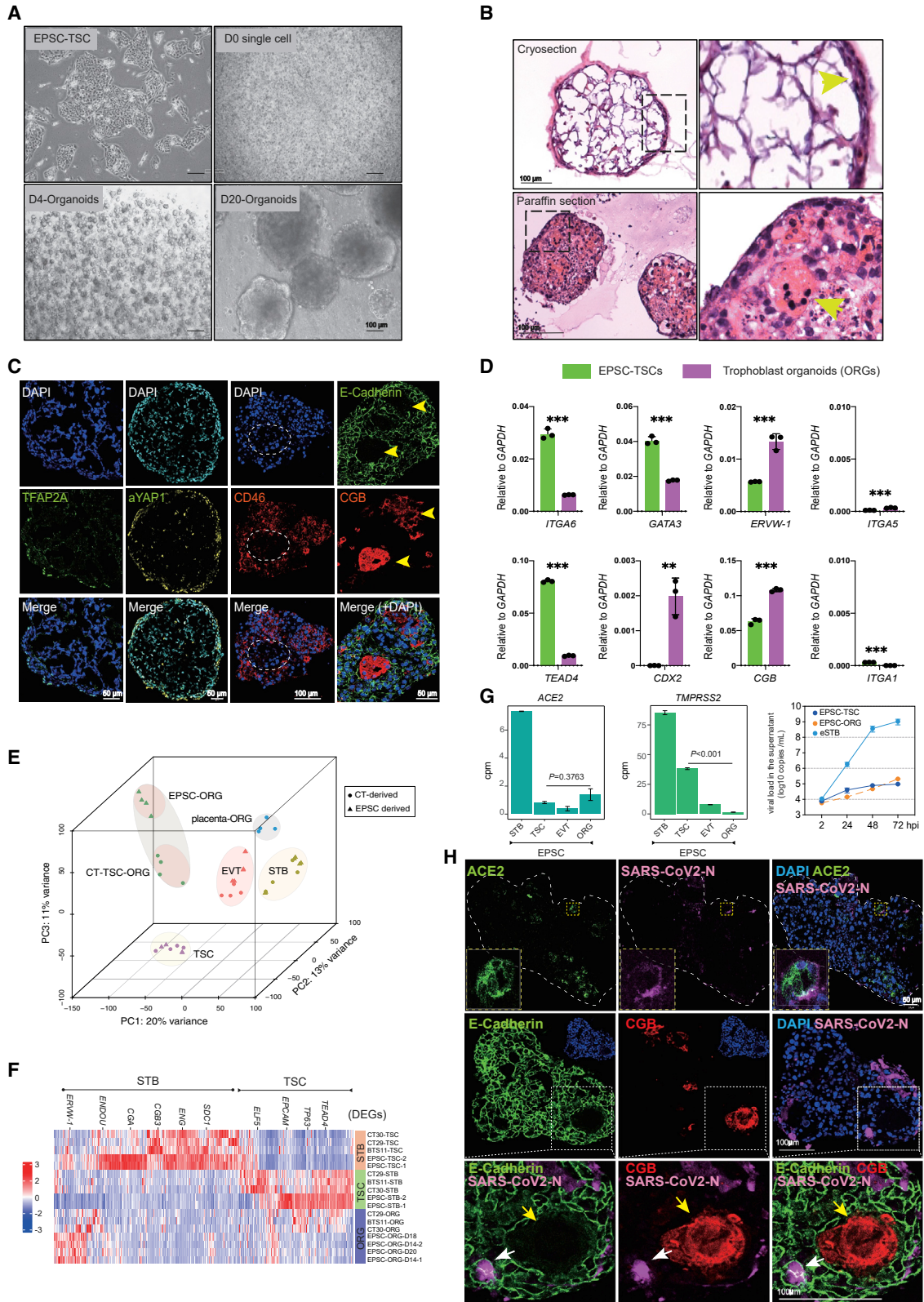
(legend on next page)

We next asked whether remdesivir and GC376 treatment could mitigate the infection-caused developmental defect. Hierarchical clustering analysis confirmed a shift of the drug-treated cells toward the mock infection control STBs (Figure S5H), with substantially reduced upregulated and downregulated genes (Figure 5D). Furthermore, machine learning analysis based on global expression decomposition revealed that, along the PI-TB to PI-STB pseudotime trajectory, drug treatment induced a shift away from PI-TB and toward PI-STB, indicating a partial rescue of eSTB development defects (Figure 5E).

Direct derivation of 3D trophoblast organoids from EPSC-TSCs for SARS-CoV-2 infection

Human organoids, particularly of respiratory cells, have been extensively investigated for SARS-CoV-2 infection.[79] Long-term and genetically stable trophoblast organoids are derived from first-trimester placenta tissues or blastocysts, which grow as complex structures closely recapitulating the organization of *in vivo* placental villi.[80,81] It was recently reported that 3D or organoid culture of hTSCs more closely resembled the *in vivo* counterparts than 2D hTSCs.[36] We thus investigated 3D trophoblast organoids in SARS-CoV-2 infection. From EPSC-TSCs, we directly established trophoblast organoids,[82] where individual hTSCs self-aggregated and developed into 3D organoids (Figure 6A). The organoids were reminiscent of those derived from the placenta,[80,81] where the basement membrane was on the outside in contact with the Matrigel substratum, whereas syncytial masses lined the central cavity (Figure 6B). Multinucleated mature STBs expressing CGB and ENDON were found at the organoids' center and most of them did not highly express the stemness transcription factors GATA3, TFAP2A, and TFAP2C or the eSTB marker CD46 (Figures 6C, S6A, and S6B). Trophoblast organoids harbored both stem cells and STBs.[80,81] They expressed genes of both hTSCs and STBs, although the levels were lower than those in hTSC or STB cultures (Figures 6D and S6C), and secreted full-length and properly folded β-hCG hormone (Figure S6D). Consistent with a recent study,[36] hTSC-trophoblast organoids expressed higher levels of trophoblast-specific miRNAs (*has-miR-517a* and *525-3p*) compared with

the 2D TSCs (Figure S6E). These trophoblast organoids did not express appreciable levels of EVT genes but could be induced to robustly generate migrating HLA-G⁺ and ITGA5⁺ EVT cells (Figures S6F and S6G), confirming the presence of bipotential stem cells.

RNA-seq analysis further unraveled the global gene expression similarities between trophoblast organoids derived from EPSC-TSCs (EPSC-ORGs) and from placental CT-TSCs (CT-TSC-ORGs) (Figure 6E).[36] Both co-expressed markers for TSCs and STBs, similar to trophoblast organoids derived from primary villous placenta[80,81] (Figure 6F and Table S4).

In EPSC-ORGs, *ACE2* was expressed at levels comparable to those in EPSC-TSCs, but *TMPRSS2* expression was much lower (Figure 6G), resembling that in the placenta.[17–19] EPSC-ORGs were next infected with SARS-CoV-2 at an MOI of 10 based on the published condition for SARS-CoV-2 infection in organoids.[83] SARS-CoV-2 RNA copy number in the supernatants from infected EPSC-ORGs was at levels comparable to those of EPSC-TSC infection (Figure 6G). Immunofluorescence staining revealed a small number of cells located along the periphery of the EPSC-ORGs positive for SARS-CoV-2 N, which varied substantially among organoids, possibly due to cellular heterogeneity. The infected cells tended to co-express ACE2, CD46, and E-cadherin but not CGB (Figures 6H and S6H), although the co-expression was much more clearly demonstrated in 2D-cultured eSTBs (Figure 3Q). The low SARS-CoV-2 infection in the trophoblast organoids *in vitro* supports clinical observations that opportunistic SARS-CoV-2 infection of the human placenta are uncommon.[5,6]

ACE2 is essential for SARS-CoV-2 infection in trophoblasts

To genetically validate the role of ACE2 in SARS-CoV-2 infection in human trophoblasts, we made homozygous deletions in *ACE2* coding exon 2 in hEPSCs using CRISPR-Cas9 (Figures S7A–S7D). The *ACE2* knockout hEPSCs (*ACE2*-KO) had normal morphology and expressed high levels of key pluripotency genes (*OCT4* and *NANOG*) and markers (SSEA3 and TRA-1-60) but low levels of lineage genes (Figures 7A, S7E, and S7F), comparable to the normal parental hEPSCs.

Figure 6. Infection of EPSC-TSC trophoblast organoids (EPSC-ORG) by SARS-CoV-2

(A) Bright-field images of EPSC-ORGs derived from EPSC-TSCs. Scale bars, 100 μm.

(B) H&E staining of cryosections (top) and paraffin sections (bottom) of EPSC-ORGs. Arrowhead in the cryosection (top right) indicates densely packed cell clusters in the outer layer of EPSC-ORGs. Arrowhead in the paraffin section (bottom right) indicates the multinucleated STBs inside EPSC-ORG. Scale bars, 100 μm.

(C) Immunofluorescence staining of EPSC-ORG sections for cytotrophoblast markers TFAP2A and YAP1 and for STB markers CD46 and CGB. Yellow arrows point to the multinucleated STBs that express high CGB but are negatively stained for E-cadherin. The dashed line box areas are shown for the multinucleated STBs that are negatively stained for CD46. Scale bars, 100 or 50 μm as indicated.

(D) Changes in gene expression (qRT-PCR) in EPSC-TSCs and EPSC-ORGs. Data are mean ± SD; n = 3 independent replicates; **p < 0.01, ***p < 0.001 (Student's t test).

(E) 3D PCA for placenta-derived trophoblasts (CT-TSC/-STB/-EVT) and trophoblast organoids (CT-TSC-generated trophoblast organoids, CT-TSC-ORG; placenta-tissue-generated trophoblast organoids, placenta-ORG) and EPSC-derived trophoblasts (EPSC-TSC/STB/EVT) and EPSC-ORG. Cell sources are indicated by shape.

(F) Heatmap showing EPSC-ORG expression of both TSC and STB trophoblast genes, similar to trophoblast organoids generated from CT-TSCs (CT29, CT30, and BTS11). Z score of cpm was used and shown as heatmap signatures.

(G) Bar plots of expression (cpm) of *ACE2* and *TMPRSS2* in EPSC-TSC/STB/EVT and EPSC-ORG. Right: qRT-PCR detection of SARS-CoV-2 genome copy numbers (per mL) in the supernatants of virus-co-cultured EPSC-TSCs, eSTBs (STB-D2), and EPSC-ORGs. Data are mean ± SD; n = 3.

(H) Immunofluorescence images of paraffin sections of SARS-CoV-2-infected EPSC-ORG stained for N, ACE2, E-Cadherin, and CGB. White arrows indicate the mononucleated infected cells, whereas yellow arrows point to a large multinucleated STB that expresses high CGB. The dashed line box areas are shown in higher resolution. Scale bars, 50 or 100 μm as indicated.
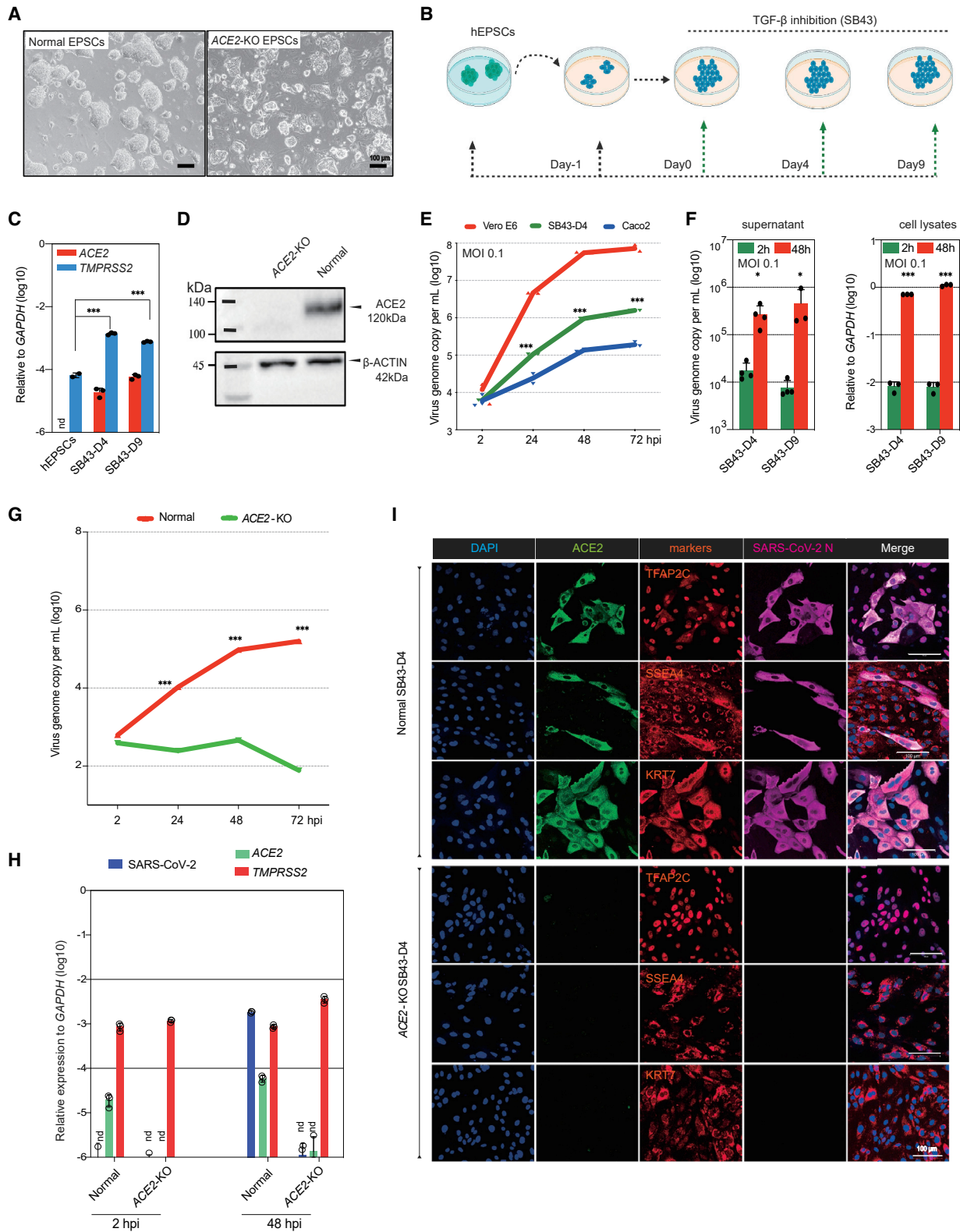
Figure 7. ACE2 is required for SARS-CoV-2 infection of trophoblasts differentiated from hEPSCs

(A) Normal and *ACE2*-KO hEPSCs. Scale bars, 100 μm.

(B) Experimental flow of hEPSC differentiation toward trophoblasts via TGF-β inhibitor SB-431542 (SB43) treatment.

(legend continued on next page)

We induced normal and *ACE2*-KO hEPSCs to trophoblasts using a simple and efficient protocol via the TGF-β inhibitor SB431542 (Figures 7B and S7G).[24] Normal hEPSCs did not express *ACE2* (Figures 7C and S2H) and were not infected by SARS-CoV-2. The differentiated cells expressed *ACE2*, *TMPRSS2*s, and typical STB markers (Figures 7C, S7H, and S7I). In contrast, no ACE2 protein was detected in cells differentiated from the *ACE2*-KO hEPSCs (Figure 7D).

We next selected cells of days 4 and 9 differentiation for infection, as they expressed *ACE2* and *TMPRSS2* (Figure 7C), which produced substantial amounts of viral genome in the supernatant and cell lysates (Figures 7E and 7F). The infected cells, detected as SARS-CoV-2 nucleocapsid (N) protein positive, all expressed ACE2 and trophoblast markers TFAP2C, SSEA4, and KRT7 and were mostly mononucleated (Figure S7J). Loss of *ACE2* abolished the infection, as indicated by the drastic decrease in viral genome in supernatants and cell lysates (Figures 7G and 7H). In immunofluorescence staining, no cells were stained positive for either SARS-CoV-2 N protein or ACE2 in the *ACE2*-KO cells (Figure 7I). Therefore, in trophoblasts, ACE2 is essential for SARS-CoV-2 infection.

DISCUSSION

We report a stem cell-based system to study human trophoblasts' susceptibility to SARS-CoV-2 and its variants. Specifically, eSTBs that were differentiated from hTSCs originating from EPSCs, naive stem cells, and human blastocysts were found to be highly susceptible to SARS-CoV-2.

An important issue about hTSCs is that they may possess AME gene signatures. We examined the transcriptome of hTSCs originating from human EPSCs and naive stem cells by comparing them with those of *in vivo* origins and found that these hTSCs were highly similar and expressed low or no putative AME cell genes.

hTSCs are thought to represent *in vivo* post-implantation cells.[33] SARS-CoV-2 infected 0.5%–4% of hTSCs that were *ACE2*+ and co-expressed high levels of the TE marker ENPEP. These *ACE2*+ hTSCs warrant further investigation for their molecular properties and developmental potential.

eSTBs expressed high levels of *ACE2* and *TMPRSS2* and supported the replication of SARS-CoV-2 and the Delta and Omicron variants and MERS-CoV. The infection was effectively suppressed, and the infection-induced developmental delay was partially rescued by two known antivirals, remdesivir and GC376. hTSCs and eSTBs have enriched transcriptomic features of peri-implantation trophoblasts. Their susceptibility to coronaviruses and the resultant developmental defects imply that these early embryos may be at risk of the virus infection.

The syncytialized trophoblasts generated from human ESCs (primed) by BAP treatment (BMP4, TGF-β inhibitor A83-01, and FGF2 signaling inhibitor PD173074) were found to co-express *ACE2* and *TMPRSS2* and supported replicative and persistent infection by SARS-CoV-2 [57]. These results differ from our observation that eSTBs derived from hTSCs expressed *ACE2* and were highly susceptible to SARS-CoV-2 infection, whereas the syncytialized or more mature STBs were much less susceptible. The discrepancy could be due to either technical reasons, as eSTBs are expected to be transiently present in hTSC differentiation, or the difference between BAP cells (putative trophoblasts) and hTSCs/eSTBs. Indeed, our discovery of eSTBs was made possible by the stem cell-based *in vitro* system, since eSTB-like cells likely exist only transiently along placental trophoblast development before they differentiate to the nonproliferative multinucleated STBs. Neither trophoblastic cell lines nor primary trophoblasts are representative of these eSTBs.

Several human cell lines have been used in coronavirus research. However, they suffer from genetic and/or innate immune defects and have some long-standing technical challenges such as cell transfection and genetic manipulation. Vero E6 cells, which originated from African green monkey, are commonly used for isolation and propagation of SARS-CoV-2[15] and have been approved for use in vaccine manufacturing. They have genetic defects, including large genomic deletions encompassing the IFN gene clusters (IFN-a and -b) and the *CDKN2A/B* loci, and are thus deficient in IFN response,[67] which has prevented their application in the study of antiviral response. Furthermore, the lack of TMPRSS2 in Vero E6 cells results in the selection of SARS-CoV-2 variants that have lost the polybasic Furin cleavage site at the S1-S2 junction.[68] Meanwhile, the current dominant SARS-CoV-2 Omicron variant, which relies more on Cathepsins and other endosomal proteases, replicates well in Vero E6 cells and the upper airway, in which ACE2 and Cathepsins are more abundant, but not in Calu3 and Caco2 cells or in lung cells.[71,72]

eSTBs are normal human cells with an intact innate immune system and no major known genetic or epigenetic defects and support highly productive propagation of SARS-CoV-2 and its variants. SARS-CoV-2 infection causes massive cell death in

---

(C) qRT-PCR analysis of *ACE2* and *TMPRSS2* in hEPSCs and the differentiated cells on days 4 and 9. nd, undetectable. Data are mean ± SD; n = 3; ***p < 0.001 (Student's t test).

(D) Western blotting confirms loss of ACE2 protein in the SB43-treated hEPSCs on day 9 (SB43D9) of differentiation.

(E) SARS-CoV-2 replication kinetics in cells differentiated from hEPSCs compared with Vero E6 and Caco2 cells. Data are mean ± SD; n = 3 biological replicates; ***p < 0.001 (Student's t test).

(F) Left: qRT-PCR of supernatant viral load in SB43-treated hEPSCs at 2 and 48 hpi. Right: qRT-PCR quantification of SARS-CoV-2 genome in cell lysates of SB43-treated hEPSCs on days 4 and 9. Data are mean ± SD; n = 3 biological replicates; *p < 0.05, ***p < 0.001 (Student's t test).

(G) Quantification of supernatant viral RNA loads of SB43-treated (day 4) normal and *ACE2*-KO EPSCs. Data are mean ± SD; n = 3 biological replicates; ***p < 0.001 (Student's t test).

(H) SARS-CoV-2 viral genome quantitation and expression of *ACE2* and *TMPRSS2* in normal vs. SB43-treated *ACE2*-KO EPSCs at day 4. Data are mean ± SD; n = 3 biological replicates; nd, not detectable.

(I) Representative immunofluorescence staining images for ACE2, trophoblast factors and markers, and SARS-CoV-2 N protein in normal (top) and *ACE2*-KO cells (bottom) (day 4 of SB43 treatment) at 48 hpi. Scale bars, 100 μm.

Vero E6 cells but not in eSTBs. The lack of cell death in infected eSTBs is different from recent reports that primitive human trophoblasts generated from human ESCs were susceptible to and lysed by an African lineage strain Zika virus,[84,85] but may provide a practical advantage for viral production.

The hTSC-derived trophoblast organoids expressed low levels of *ACE2* and *TMPRSS2* and were much less susceptible to the virus infection, reminiscent of the placenta. Similar findings on stem cell-derived trophoblast organoids and their use in SARS-CoV-2 study were recently reported.[86]

Human EPSCs and naive stem cells permit efficient genome editing and possess differentiation potential for all embryonic and extraembryonic lineages.[24,32] In addition to trophoblasts, these stem cells can be explored to derive diverse cell types and to functionally assess their susceptibility to SARS-CoV-2 and variants, like airway epithelium, gastrointestinal epithelium, and neurons. These qualities grant them potential in overcoming the long-standing challenges in cell transfection and genetic manipulation of various target cells. Cells generated from these stem cells, in particular eSTBs, may thus represent a genetically normal human cell source for investigating host-virus interactions in current and future pandemics, performing genetic screens to identify biological determinants of infections, and evaluating and discovering antivirals.

Limitations of this study

The current study lacks experimental and clinical data on SARS-CoV-2 infection in human peri-implantation pregnancy, particularly regarding any *in vivo* counterparts of eSTBs. The eSTB model *in vitro* also requires further characterization at the single-cell level to delineate culture heterogeneity and compare their identity with *in vivo* counterparts. The current *in vitro* eSTBs are transient in culture and thus require enrichment for performing high-throughput antiviral drug screens and large-scale viral production. Meanwhile, the scRNA-seq finding of some peri-implantation embryonic trophoblasts expressing *ACE2* and *TMPRSS2* requires proteomic validation in human embryos. The mechanistic role of *ACE2* in trophoblast development also remains to be dissected.

STAR★METHODS

Detailed methods are provided in the online version of this paper and include the following:

- KEY RESOURCES TABLE
- RESOURCE AVAILABILITY
  - Lead contact
  - Materials availability
  - Data and code availability
- EXPERIMENTAL MODEL AND SUBJECT DETAILS
  - Human expanded potential stem cells (hEPSCs)
  - Culture of human trophoblast stem cells (hTSCs)
  - Cell lines
  - Culturing hEPSC-TSC derived trophoblast organoids
  - Virus
- METHOD DETAILS
  - Culture of hEPSCs and naive stem cells

- Differentiation of hEPSCs to trophoblast lineages by TGF-β inhibitor SB431542 treatment
- Derivation of human trophoblast stem cells (hTSCs) from hEPSCs and naive stem cells
- Differentiation of EPSC-TSCs to STBs
- Differentiation of EPSC-TSCs to EVTs
- Generation of trophoblast organoids from EPSC-TSCs
- SARS-CoV-2 infection and viral copy detection
- Plaque assay
- Antiviral evaluation in eSTBs
- Guide RNA design and plasmid DNA preparation
- Electroporation and selection
- Genotyping and sanger sequencing
- Reverse transcription- quantitative polymerase chain reaction (RT-qPCR)
- Immunofluorescence staining
- Western blotting
- Flow cytometry
- Transwell invasion assay
- QUANTIFICATION AND STATISTICAL ANALYSIS
  - Statistical analysis and reproducibility
  - RNA-seq analysis
  - scRNA preprocessing
  - Integration of *in vitro* and *in vivo* extra-embryonic datasets
  - Whole-transcriptome correlation analysis between *in vitro* cell line bulk RNA-seq and *in vivo* scRNA-seq
  - Integrative pseudotime analysis

SUPPLEMENTAL INFORMATION

Supplemental information can be found online at https://doi.org/10.1016/j.xcrm.2022.100849.

AUTHOR CONTRIBUTIONS

P.L., D.J., F.L., and D.R. conceived the project and designed the experiments. The co-first authors, P.L. and D.J., wrote the manuscript together. F.L. and T.T.K.K.T. performed the SB43 differentiation-related experiments and *ACE2*-KO to establish mutant hEPSCs. J.G., Y.H., and Y.X. contributed to the CRISPR technology and western blotting. Z.Y. and C.P.O. performed all infection studies, including viral load analysis. S.Y. and K.T. helped with viral infection and antiviral drug evaluation. D.R. performed the hTSC generation

and differentiation, immunofluorescence staining, and FACS assays. D.R., Q.Z., and C.L. contributed to trophoblast organoid generation and characterization. W.Z. and Z.L. performed RNA-seq data analysis. P.C.N.C. and W.S.B.Y. provided advice.

REFERENCES

1. Pereira, L. (2018). Congenital viral infection: traversing the uterine-placental interface. Annu. Rev. Virol. 5, 273–299. https://doi.org/10.1146/annurev-virology-092917-043236.

2. Algarroba, G.N., Rekawek, P., Vahanian, S.A., Khullar, P., Palaia, T., Peltier, M.R., Chavez, M.R., and Vintzileos, A.M. (2020). Visualization of severe acute respiratory syndrome coronavirus 2 invading the human placenta using electron microscopy. Am. J. Obstet. Gynecol. 223, 275–278.

3. Hosier, H., Farhadian, S.F., Morotti, R.A., Deshmukh, U., Lu-Culligan, A., Campbell, K.H., Yasumoto, Y., Vogels, C.B., Casanovas-Massana, A., Vijayakumar, P., et al. (2020). SARS-CoV-2 infection of the placenta. J. Clin. Invest. 130, 4947–4953. https://doi.org/10.1172/JCI139569.

4. Vivanti, A.J., Vauloup-Fellous, C., Prevot, S., Zupan, V., Suffee, C., Do Cao, J., Benachi, A., and De Luca, D. (2020). Transplacental transmission of SARS-CoV-2 infection. Nat. Commun. 11, 3572. https://doi.org/10.1038/s41467-020-17436-6.

5. Roberts, D.J., Edlow, A.G., Romero, R.J., Coyne, C.B., Ting, D.T., Hornick, J.L., Zaki, S.R., Das Adhikari, U., Serghides, L., Gaw, S.L., et al. (2021). A standardized definition of placental infection by SARS-CoV-2, a consensus statement from the national institutes of health/eunice Kennedy Shriver national Institute of child Health and human development SARS-CoV-2 placental infection workshop. Am. J. Obstet. Gynecol. 225, 593.e1–593.e9. https://doi.org/10.1016/j.ajog.2021.07.029.

6. Male, V. (2022). SARS-CoV-2 infection and COVID-19 vaccination in pregnancy. Nat. Rev. Immunol. 22, 277–282. https://doi.org/10.1038/s41577-022-00703-6.

7. Schwartz, D.A., Avvad-Portari, E., Babál, P., Baldewijns, M., Blomberg, M., Bouachba, A., Camacho, J., Collardeau-Frachon, S., Colson, A., Dehaene, I., et al. (2022). Placental tissue destruction and insufficiency from COVID-19 causes stillbirth and neonatal death from hypoxic-ischemic injury: a study of 68 cases with SARS-CoV-2 placentitis from 12 countries. Arch. Pathol. Lab. Med. https://doi.org/10.5858/arpa.2022-0029-SA.

8. Valdespino-Vázquez, M.Y., Helguera-Repetto, C.A., León-Juárez, M., Villavicencio-Carrisoza, O., Flores-Pliego, A., Moreno-Verduzco, E.R., Díaz-Pérez, D.L., Villegas-Mota, I., Carrasco-Ramírez, E., López-Martínez, I.E., et al. (2021). Fetal and placental infection with SARS-CoV-2 in early pregnancy. J. Med. Virol. 93, 4480–4487. https://doi.org/10.1002/jmv.26965.

9. Baud, D., Greub, G., Favre, G., Gengler, C., Jaton, K., Dubruc, E., and Pomar, L. (2020). Second-trimester miscarriage in a pregnant woman with SARS-CoV-2 infection. JAMA 323, 2198–2200. https://doi.org/10.1001/jama.2020.7233.

10. Allotey, J., Chatterjee, S., Kew, T., Gaetano, A., Stallings, E., Fernández-García, S., Yap, M., Sheikh, J., Lawson, H., Coomar, D., et al. (2022). SARS-CoV-2 positivity in offspring and timing of mother-to-child transmission: living systematic review and meta-analysis. BMJ 376, e067696. https://doi.org/10.1136/bmj-2021-067696.

11. Dong, L., Tian, J., He, S., Zhu, C., Wang, J., Liu, C., and Yang, J. (2020). Possible vertical transmission of SARS-CoV-2 from an infected mother to her newborn. JAMA 323, 1846–1848.

12. Burton, G.J., and Fowden, A.L. (2015). The placenta: a multifaceted, transient organ. Philos. Trans. R. Soc. Lond. B Biol. Sci. 370, 20140066. https://doi.org/10.1098/rstb.2014.0066.

13. Zeldovich, V.B., Clausen, C.H., Bradford, E., Fletcher, D.A., Maltepe, E., Robbins, J.R., and Bakardjiev, A.I. (2013). Placental syncytium forms a biophysical barrier against pathogen invasion. PLoS Pathog. 9, e1003821. https://doi.org/10.1371/journal.ppat.1003821.

14. Letko, M., Marzi, A., and Munster, V. (2020). Functional assessment of cell entry and receptor usage for SARS-CoV-2 and other lineage B betacoronaviruses. Nat. Microbiol. 5, 562–569. https://doi.org/10.1038/s41564-020-0688-y.

15. Zhou, P., Yang, X.L., Wang, X.G., Hu, B., Zhang, L., Zhang, W., Si, H.R., Zhu, Y., Li, B., Huang, C.L., et al. (2020). A pneumonia outbreak associated with a new coronavirus of probable bat origin. Nature 579, 270–273. https://doi.org/10.1038/s41586-020-2012-7.

16. Hoffmann, M., Kleine-Weber, H., Schroeder, S., Krüger, N., Herrler, T., Erichsen, S., Schiergens, T.S., Herrler, G., Wu, N.-H., Nitsche, A., et al. (2020). SARS-CoV-2 cell entry depends on ACE2 and TMPRSS2 and is blocked by a clinically proven protease inhibitor. Cell 181, 271–280.e8.

17. Ashary, N., Bhide, A., Chakraborty, P., Colaco, S., Mishra, A., Chhabria, K., Jolly, M.K., and Modi, D. (2020). Single-cell RNA-seq identifies cell subsets in human placenta that highly expresses factors driving pathogenesis of SARS-CoV-2. Front. Cell Dev. Biol. 8, 783. https://doi.org/10.3389/fcell.2020.00783.

18. Pique-Regi, R., Romero, R., Tarca, A.L., Luca, F., Xu, Y., Alazizi, A., Leng, Y., Hsu, C.D., and Gomez-Lopez, N. (2020). Does the human placenta express the canonical cell entry mediators for SARS-CoV-2? Elife 9, e58716. https://doi.org/10.7554/eLife.58716.

19. Chen, W., Yuan, P., Yang, M., Yan, Z., Kong, S., Yan, J., Liu, X., Chen, Y., Qiao, J., and Yan, L. (2020). SARS-CoV-2 entry factors: ACE2 and TMPRSS2 are expressed in peri-implantation embryos and the maternal–fetal interface. Engineering 6, 1162–1169.

20. Colson, A., Depoix, C.L., Dessilly, G., Baldin, P., Danhaive, O., Hubinont, C., Sonveaux, P., and Debiève, F. (2021). Clinical and in vitro evidence against placenta infection at term by severe acute respiratory syndrome coronavirus 2. Am. J. Pathol. 191, 1610–1623. https://doi.org/10.1016/j.ajpath.2021.05.009.

21. Taglauer, E.S., Wachman, E.M., Juttukonda, L., Klouda, T., Kim, J., Wang, Q., Ishiyama, A., Hackam, D.J., Yuan, K., and Jia, H. (2022). Acute severe acute respiratory syndrome coronavirus 2 infection in pregnancy is associated with placental angiotensin-converting enzyme 2 shedding. Am. J. Pathol. 192, 595–603. https://doi.org/10.1016/j.ajpath.2021.12.011.

22. Yang, Y., Liu, B., Xu, J., Wang, J., Wu, J., Shi, C., Xu, Y., Dong, J., Wang, C., Lai, W., et al. (2017). Derivation of pluripotent stem cells with in vivo embryonic and extraembryonic potency. Cell 169, 243–257.e25. https://doi.org/10.1016/j.cell.2017.02.005.

23. Yang, J., Ryan, D.J., Wang, W., Tsang, J.C.H., Lan, G., Masaki, H., Gao, X., Antunes, L., Yu, Y., Zhu, Z., et al. (2017). Establishment of mouse expanded potential stem cells. Nature 550, 393–397. https://doi.org/10.1038/nature24052.

24. Gao, X., Nowak-Imialek, M., Chen, X., Chen, D., Herrmann, D., Ruan, D., Chen, A.C.H., Eckersley-Maslin, M.A., Ahmad, S., Lee, Y.L., et al. (2019). Establishment of porcine and human expanded potential stem cells. Nat. Cell Biol. 21, 687–699.

25. Zhao, L., Gao, X., Zheng, Y., Wang, Z., Zhao, G., Ren, J., Zhang, J., Wu, J., Wu, B., Chen, Y., et al. (2021). Establishment of bovine expanded potential stem cells. Proc. Natl. Acad. Sci. USA 118, e2018505118. https://doi.org/10.1073/pnas.2018505118.

26. Cinkornpumin, J.K., Kwon, S.Y., Guo, Y., Hossain, I., Sirois, J., Russett, C.S., Tseng, H.-W., Okae, H., Arima, T., Duchaine, T.F., et al. (2020). Naive human embryonic stem cells can give rise to cells with a trophoblast-like transcriptome and methylome. Stem Cell Rep. *15*, 198–213.

27. Amita, M., Adachi, K., Alexenko, A.P., Sinha, S., Schust, D.J., Schulz, L.C., Roberts, R.M., and Ezashi, T. (2013). Complete and unidirectional conversion of human embryonic stem cells to trophoblast by BMP4. Proc. Natl. Acad. Sci. USA *110*, E1212–E1221.

28. Xu, R.-H., Chen, X., Li, D.S., Li, R., Addicks, G.C., Glennon, C., Zwaka, T.P., and Thomson, J.A. (2002). BMP4 initiates human embryonic stem cell differentiation to trophoblast. Nat. Biotechnol. *20*, 1261–1264.

29. Horii, M., Li, Y., Wakeland, A.K., Pizzo, D.P., Nelson, K.K., Sabatini, K., Laurent, L.C., Liu, Y., and Parast, M.M. (2016). Human pluripotent stem cells as a model of trophoblast differentiation in both normal development and disease. Proc. Natl. Acad. Sci. USA *113*, E3882–E3891. https://doi.org/10.1073/pnas.1604747113.

30. Wei, Y., Wang, T., Ma, L., Zhang, Y., Zhao, Y., Lye, K., Xiao, L., Chen, C., Wang, Z., Ma, Y., et al. (2021). Efficient derivation of human trophoblast stem cells from primed pluripotent stem cells. Sci. Adv. *7*, eabf4416. https://doi.org/10.1126/sciadv.abf4416.

31. Dong, C., Beltcheva, M., Gontarz, P., Zhang, B., Popli, P., Fischer, L.A., Khan, S.A., Park, K.-m., Yoon, E.-J., Xing, X., et al. (2020). Derivation of trophoblast stem cells from naïve human pluripotent stem cells. Elife *9*, e52504.

32. Guo, G., Stirparo, G.G., Strawbridge, S.E., Spindlow, D., Yang, J., Clarke, J., Dattani, A., Yanagida, A., Li, M.A., Myers, S., et al. (2021). Human naive epiblast cells possess unrestricted lineage potential. Cell Stem Cell *28*, 1040–1056.e6. https://doi.org/10.1016/j.stem.2021.02.025.

33. Castel, G., Meistermann, D., Bretin, B., Firmin, J., Blin, J., Loubersac, S., Bruneau, A., Chevolleau, S., Kilens, S., Chariau, C., et al. (2020). Induction of human trophoblast stem cells from somatic cells and pluripotent stem cells. Cell Rep. *33*, 108419. https://doi.org/10.1016/j.celrep.2020.108419.

34. Io, S., Kabata, M., Iemura, Y., Semi, K., Morone, N., Minagawa, A., Wang, B., Okamoto, I., Nakamura, T., Kojima, Y., et al. (2021). Capturing human trophoblast development with naive pluripotent stem cells in vitro. Cell Stem Cell *28*, 1023–1039.e13. https://doi.org/10.1016/j.stem.2021.03.013.

35. Okae, H., Toh, H., Sato, T., Hiura, H., Takahashi, S., Shirane, K., Kabayama, Y., Suyama, M., Sasaki, H., and Arima, T. (2018). Derivation of human trophoblast stem cells. Cell Stem Cell *22*, 50–63.e6.

36. Sheridan, M.A., Zhao, X., Fernando, R.C., Gardner, L., Perez-Garcia, V., Li, Q., Marsh, S.G.E., Hamilton, R., Moffett, A., and Turco, M.Y. (2021). Characterization of primary models of human trophoblast. Development *148*. https://doi.org/10.1242/dev.199749.

37. Rostovskaya, M., Andrews, S., Reik, W., and Rugg-Gunn, P.J. (2022). Amniogenesis occurs in two independent waves in primates. Cell Stem Cell *29*, 744–759.e6. https://doi.org/10.1016/j.stem.2022.03.014.

38. Lee, C.Q.E., Gardner, L., Turco, M., Zhao, N., Murray, M.J., Coleman, N., Rossant, J., Hemberger, M., and Moffett, A. (2016). What is trophoblast? A combination of criteria define human first-trimester trophoblast. Stem Cell Rep. *6*, 257–272.

39. Zheng, Y., Xue, X., Shao, Y., Wang, S., Esfahani, S.N., Li, Z., Muncie, J.M., Lakins, J.N., Weaver, V.M., Gumucio, D.L., and Fu, J. (2019). Controlled modelling of human epiblast and amnion development using stem cells. Nature *573*, 421–425. https://doi.org/10.1038/s41586-019-1535-2.

40. Xiang, L., Yin, Y., Zheng, Y., Ma, Y., Li, Y., Zhao, Z., Guo, J., Ai, Z., Niu, Y., Duan, K., et al. (2020). A developmental landscape of 3D-cultured human pre-gastrulation embryos. Nature *577*, 537–542. https://doi.org/10.1038/s41586-019-1875-y.

41. Zhao, C., Reyes, A.P., Schell, J.P., Weltner, J., Ortega, N.M., Zheng, Y., Björklund, Å.K., Rossant, J., Fu, J., Petropoulos, S., and Lanner, F. (2021). Reprogrammed blastoids contain amnion-like cells but not tro-

42. Chhabra, S., and Warmflash, A. (2021). BMP-treated human embryonic stem cells transcriptionally resemble amnion cells in the monkey embryo. Biol. Open *10*, bio058617. https://doi.org/10.1242/bio.058617.

43. Tyser, R.C.V., Mahammadov, E., Nakanoh, S., Vallier, L., Scialdone, A., and Srinivas, S. (2021). Single-cell transcriptomic characterization of a gastrulating human embryo. Nature *600*, 285–289. https://doi.org/10.1038/s41586-021-04158-y.

44. Zhou, F., Wang, R., Yuan, P., Ren, Y., Mao, Y., Li, R., Lian, Y., Li, J., Wen, L., Yan, L., et al. (2019). Reconstituting the transcriptome and DNA methylome landscapes of human implantation. Nature *572*, 660–664. https://doi.org/10.1038/s41586-019-1500-0.

45. Liu, Y., Fan, X., Wang, R., Lu, X., Dang, Y.L., Wang, H., Lin, H.Y., Zhu, C., Ge, H., Cross, J.C., and Wang, H. (2018). Single-cell RNA-seq reveals the diversity of trophoblast subtypes and patterns of differentiation in the human placenta. Cell Res. *28*, 819–832. https://doi.org/10.1038/s41422-018-0066-y.

46. Wang, K., Chen, W., Zhang, Z., Deng, Y., Lian, J.-Q., Du, P., Wei, D., Zhang, Y., Sun, X.-X., Gong, L., et al. (2020). CD147-spike protein is a novel route for SARS-CoV-2 infection to host cells. Signal. Transduct. Target. Ther. *5*, 283. https://doi.org/10.1038/s41392-020-00426-x.

47. Wang, S., Qiu, Z., Hou, Y., Deng, X., Xu, W., Zheng, T., Wu, P., Xie, S., Bian, W., Zhang, C., et al. (2021). AXL is a candidate receptor for SARS-CoV-2 that promotes infection of pulmonary and bronchial epithelial cells. Cell Res. *31*, 126–140. https://doi.org/10.1038/s41422-020-00460-y.

48. Qi, F., Qian, S., Zhang, S., and Zhang, Z. (2020). Single cell RNA sequencing of 13 human tissues identify cell types and receptors of human coronaviruses. Biochem. Biophys. Res. Commun. *526*, 135–140. https://doi.org/10.1016/j.bbrc.2020.03.044.

49. Gamage, T.K., Chamley, L.W., and James, J.L. (2016). Stem cell insights into human trophoblast lineage differentiation. Hum. Reprod. Update *23*, 77–103. https://doi.org/10.1093/humupd/dmw026.

50. Holmes, C.H., Simpson, K.L., Okada, H., Okada, N., Wainwright, S.D., Purcell, D.F., and Houlihan, J.M. (1992). Complement regulatory proteins at the feto-maternal interface during human placental development: distribution of CD59 by comparison with membrane cofactor protein (CD46) and decay accelerating factor (CD55). Eur. J. Immunol. *22*, 1579–1585. https://doi.org/10.1002/eji.1830220635.

51. Banu, N., Panikar, S.S., Leal, L.R., and Leal, A.R. (2020). Protective role of ACE2 and its downregulation in SARS-CoV-2 infection leading to Macrophage Activation Syndrome: therapeutic implications. Life Sci. *256*, 117905. https://doi.org/10.1016/j.lfs.2020.117905.

52. DeGrace, M.M., Ghedin, E., Frieman, M.B., Krammer, F., Grifoni, A., Alisoltani, A., Alter, G., Amara, R.R., Baric, R.S., Barouch, D.H., et al. (2022). Defining the risk of SARS-CoV-2 variants on immune protection. Nature *605*, 640–652. https://doi.org/10.1038/s41586-022-04690-5.

53. Riva, L., Yuan, S., Yin, X., Martin-Sancho, L., Matsunaga, N., Pache, L., Burgstaller-Muehlbacher, S., De Jesus, P.D., Teriete, P., Hull, M.V., et al. (2020). Discovery of SARS-CoV-2 antiviral drugs through large-scale compound repurposing. Nature *586*, 113–119. https://doi.org/10.1038/s41586-020-2577-1.

54. Mi, S., Lee, X., Li, X., Veldman, G.M., Finnerty, H., Racie, L., LaVallie, E., Tang, X.Y., Edouard, P., Howes, S., et al. (2000). Syncytin is a captive retroviral envelope protein involved in human placental morphogenesis. Nature *403*, 785–789. https://doi.org/10.1038/35001608.

55. Dupressoir, A., Marceau, G., Vernochet, C., Bénit, L., Kanellopoulos, C., Sapin, V., and Heidmann, T. (2005). Syncytin-A and syncytin-B, two fusogenic placenta-specific murine envelope genes of retroviral origin conserved in Muridae. Proc. Natl. Acad. Sci. USA *102*, 725–730. https://doi.org/10.1073/pnas.0406509102.

56. Kämmerer, U., Germeyer, A., Stengel, S., Kapp, M., and Denner, J. (2011). Human endogenous retrovirus K (HERV-K) is expressed in villous and

phectoderm. Preprint at bioRxiv. https://doi.org/10.1101/2021.05.07.442980.

extravillous cytotrophoblast cells of the human placenta. J. Reprod. Immunol. *91*, 1–8. https://doi.org/10.1016/j.jri.2011.06.102.

57. Zhou, J., Choi, S., Liu, H., Zhang, J., Tian, Y., Edlow, A.G., Ezashi, T., Roberts, R.M., Ma, W., and Schust, D.J. (2021). Is SARS-CoV-2 infection a risk factor for early pregnancy loss? ACE2 and TMPRSS2 coexpression and persistent replicative infection in primitive trophoblast. J. Infect. Dis. *224*, S660–S669. https://doi.org/10.1093/infdis/jiab309.

58. Kindler, E., Thiel, V., and Weber, F. (2016). Interaction of SARS and MERS coronaviruses with the antiviral interferon response. Adv. Virus Res. *96*, 219–243.

59. Li, J., Liu, Y., and Zhang, X. (2010). Murine coronavirus induces type I interferon in oligodendrocytes through recognition by RIG-I and MDA5. J. Virol. *84*, 6472–6482.

60. Yin, X., Riva, L., Pu, Y., Martin-Sancho, L., Kanamune, J., Yamamoto, Y., Sakai, K., Gotoh, S., Miorin, L., De Jesus, P.D., et al. (2021). MDA5 governs the innate immune response to SARS-CoV-2 in lung epithelial cells. Cell Rep. *34*, 108628. https://doi.org/10.1016/j.celrep.2020.108628.

61. Ye, L., Schnepf, D., and Staeheli, P. (2019). Interferon-λ orchestrates innate and adaptive mucosal immune responses. Nat. Rev. Immunol. *19*, 614–625. https://doi.org/10.1038/s41577-019-0182-z.

62. Chen, J., Liang, Y., Yi, P., Xu, L., Hawkins, H.K., Rossi, S.L., Soong, L., Cai, J., Menon, R., and Sun, J. (2017). Outcomes of congenital Zika disease depend on timing of infection and maternal-fetal interferon action. Cell Rep. *21*, 1588–1599. https://doi.org/10.1016/j.celrep.2017.10.059.

63. Bayer, A., Lennemann, N.J., Ouyang, Y., Bramley, J.C., Morosky, S., Marques, E.T.D.A., Jr., Cherry, S., Sadovsky, Y., and Coyne, C.B. (2016). Type III interferons produced by human placental trophoblasts confer protection against Zika virus infection. Cell Host Microbe *19*, 705–712. https://doi.org/10.1016/j.chom.2016.03.008.

64. Vanderheiden, A., Ralfs, P., Chirkova, T., Upadhyay, A.A., Zimmerman, M.G., Bedoya, S., Aoued, H., Tharp, G.M., Pellegrini, K.L., Manfredi, C., et al. (2020). Type I and type III interferons restrict SARS-CoV-2 infection of human airway epithelial cultures. J. Virol. *94*, e009855–e01020. https://doi.org/10.1128/jvi.00985-20.

65. Stanifer, M.L., Kee, C., Cortese, M., Zumaran, C.M., Triana, S., Mukenhirn, M., Kraeusslich, H.G., Alexandrov, T., Bartenschlager, R., and Boulant, S. (2020). Critical role of type III interferon in controlling SARS-CoV-2 infection in human intestinal epithelial cells. Cell Rep. *32*, 107863. https://doi.org/10.1016/j.celrep.2020.107863.

66. Wickenhagen, A., Sugrue, E., Lytras, S., Kuchi, S., Noerenberg, M., Turnbull, M.L., Loney, C., Herder, V., Allan, J., Jarmson, I., et al. (2021). A prenylated dsRNA sensor protects against severe COVID-19. Science *374*, eabj3624. https://doi.org/10.1126/science.abj3624.

67. Osada, N., Kohara, A., Yamaji, T., Hirayama, N., Kasai, F., Sekizuka, T., Kuroda, M., and Hanada, K. (2014). The genome landscape of the african green monkey kidney-derived vero cell line. DNA Res. *21*, 673–683. https://doi.org/10.1093/dnares/dsu029.

68. Sasaki, M., Uemura, K., Sato, A., Toba, S., Sanaki, T., Maenaka, K., Hall, W.W., Orba, Y., and Sawa, H. (2021). SARS-CoV-2 variants with mutations at the S1/S2 cleavage site are generated in vitro during propagation in TMPRSS2-deficient cells. PLoS Pathog. *17*, e1009233. https://doi.org/10.1371/journal.ppat.1009233.

69. Koch, J., Uckeley, Z.M., Doldan, P., Stanifer, M., Boulant, S., and Lozach, P.-Y. (2021). TMPRSS2 expression dictates the entry route used by SARS-CoV-2 to infect host cells. EMBO J. *40*, e107821.

70. Beumer, J., Geurts, M.H., Lamers, M.M., Puschhof, J., Zhang, J., van der Vaart, J., Mykytyn, A.Z., Breugem, T.I., Riesebosch, S., Schipper, D., et al. (2021). A CRISPR/Cas9 genetically engineered organoid biobank reveals essential host factors for coronaviruses. Nat. Commun. *12*, 5498. https://doi.org/10.1038/s41467-021-25729-7.

71. Shuai, H., Chan, J.F.-W., Hu, B., Chai, Y., Yuen, T.T.-T., Yin, F., Huang, X., Yoon, C., Hu, J.-C., Liu, H., et al. (2022). Attenuated replication and path-

72. ogenicity of SARS-CoV-2 B.1.1.529 Omicron. Nature. https://doi.org/10.1038/s41586-022-04442-5.

72. Hui, K.P.Y., Ho, J.C.W., Cheung, M.-c., Ng, K.-c., Ching, R.H.H., Lai, K.-l., Kam, T.T., Gu, H., Sit, K.-Y., Hsin, M.K.Y., et al. (2022). SARS-CoV-2 Omicron variant replication in human bronchus and lung ex vivo. Nature *603*, 715–720. https://doi.org/10.1038/s41586-022-04479-6.

73. Rubin, D., Chan-Tack, K., Farley, J., and Sherwat, A. (2020). FDA approval of remdesivir - a step in the right direction. N. Engl. J. Med. *383*, 2598–2600. https://doi.org/10.1056/NEJMp2032369.

74. Ma, C., Sacco, M.D., Hurst, B., Townsend, J.A., Hu, Y., Szeto, T., Zhang, X., Tarbet, B., Marty, M.T., Chen, Y., and Wang, J. (2020). Boceprevir, GC-376, and calpain inhibitors II, XII inhibit SARS-CoV-2 viral replication by targeting the viral main protease. Cell Res. *30*, 678–692. https://doi.org/10.1038/s41422-020-0356-z.

75. Wang, M., Cao, R., Zhang, L., Yang, X., Liu, J., Xu, M., Shi, Z., Hu, Z., Zhong, W., and Xiao, G. (2020). Remdesivir and chloroquine effectively inhibit the recently emerged novel coronavirus (2019-nCoV) in vitro. Cell Res. *30*, 269–271. https://doi.org/10.1038/s41422-020-0282-0.

76. Dampalla, C.S., Zheng, J., Perera, K.D., Wong, L.-Y.R., Meyerholz, D.K., Nguyen, H.N., Kashipathy, M.M., Battaile, K.P., Lovell, S., Kim, Y., et al. (2021). Postinfection treatment with a protease inhibitor increases survival of mice with a fatal SARS-CoV-2 infection. Proc. Natl. Acad. Sci. USA *118*, e2101555118. https://doi.org/10.1073/pnas.2101555118.

77. Fu, L., Ye, F., Feng, Y., Yu, F., Wang, Q., Wu, Y., Zhao, C., Sun, H., Huang, B., Niu, P., et al. (2020). Both Boceprevir and GC376 efficaciously inhibit SARS-CoV-2 by targeting its main protease. Nat. Commun. *11*, 4417. https://doi.org/10.1038/s41467-020-18233-x.

78. de Wilde, A.H., Raj, V.S., Oudshoorn, D., Bestebroer, T.M., van Nieuwkoop, S., Limpens, R.W.A.L., Posthuma, C.C., van der Meer, Y., Bárcena, M., Haagmans, B.L., et al. (2013). MERS-coronavirus replication induces severe in vitro cytopathology and is strongly inhibited by cyclosporin A or interferon-α treatment. J. Gen. Virol. *94*, 1749–1760. https://doi.org/10.1099/vir.0.052910-0.

79. Han, Y., Yang, L., Lacko, L.A., and Chen, S. (2022). Human organoid models to study SARS-CoV-2 infection. Nat. Methods *19*, 418–428. https://doi.org/10.1038/s41592-022-01453-y.

80. Turco, M.Y., Gardner, L., Kay, R.G., Hamilton, R.S., Prater, M., Hollinshead, M.S., McWhinnie, A., Esposito, L., Fernando, R., Skelton, H., et al. (2018). Trophoblast organoids as a model for maternal-fetal interactions during human placentation. Nature *564*, 263–267. https://doi.org/10.1038/s41586-018-0753-3.

81. Haider, S., Meinhardt, G., Saleh, L., Kunihs, V., Gamperl, M., Kaindl, U., Ellinger, A., Burkard, T.R., Fiala, C., Pollheimer, J., et al. (2018). Self-renewing trophoblast organoids recapitulate the developmental Program of the early human placenta. Stem Cell Rep. *11*, 537–551. https://doi.org/10.1016/j.stemcr.2018.07.004.

82. Sheridan, M.A., Fernando, R.C., Gardner, L., Hollinshead, M.S., Burton, G.J., Moffett, A., and Turco, M.Y. (2020). Establishment and differentiation of long-term trophoblast organoid cultures from the human placenta. Nat. Protoc. *15*, 3441–3463. https://doi.org/10.1038/s41596-020-0381-x.

83. Zhang, B.-Z., Chu, H., Han, S., Shuai, H., Deng, J., Hu, Y.-f., Gong, H.-r., Lee, A.C.-Y., Zou, Z., Yau, T., et al. (2020). SARS-CoV-2 infects human neural progenitor cells and brain organoids. Cell Res. *30*, 928–931. https://doi.org/10.1038/s41422-020-0390-x.

84. Sheridan, M.A., Yunusov, D., Balaraman, V., Alexenko, A.P., Yabe, S., Verjovski-Almeida, S., Schust, D.J., Franz, A.W., Sadovsky, Y., Ezashi, T., and Roberts, R.M. (2017). Vulnerability of primitive human placental trophoblast to Zika virus. Proc. Natl. Acad. Sci. USA *114*, E1587–E1596. https://doi.org/10.1073/pnas.1616097114.

85. Sheridan, M.A., Balaraman, V., Schust, D.J., Ezashi, T., Roberts, R.M., and Franz, A.W.E. (2018). African and Asian strains of Zika virus differ in their ability to infect and lyse primitive human placental trophoblast. PLoS One *13*, e0200086. https://doi.org/10.1371/journal.pone.0200086.

86. Karvas, R.M., Khan, S.A., Verma, S., Yin, Y., Kulkarni, D., Dong, C., Park, K.M., Chew, B., Sane, E., Fischer, L.A., et al. (2022). Stem-cell-derived trophoblast organoids model human placental development and susceptibility to emerging pathogens. Cell Stem Cell 29, 810–825.e8. https://doi.org/10.1016/j.stem.2022.04.004.

87. Wilkinson, A.C., Ryan, D.J., Kucinski, I., Wang, W., Yang, J., Nestorowa, S., Diamanti, E., Tsang, J.C.-H., Wang, J., and Campos, L.S. (2019). Expanded potential stem cell media as a tool to study human developmental hematopoiesis in vitro. Exp. Hematol. 76, 1–12.e5.

88. Zhao, H., Lu, L., Peng, Z., Chen, L.L., Meng, X., Zhang, C., Ip, J.D., Chan, W.M., Chu, A.W.H., Chan, K.H., et al. (2022). SARS-CoV-2 Omicron variant shows less efficient replication and fusion activity when compared with Delta variant in TMPRSS2-expressed cells. Emerg. Microbes Infect. 11, 277–283. https://doi.org/10.1080/22221751.2021.2023329.

89. Yuan, S., Chu, H., Huang, J., Zhao, X., Ye, Z.-W., Lai, P.-M., Wen, L., Cai, J.-P., Mo, Y., Cao, J., et al. (2020). Viruses harness YxxØ motif to interact with host AP2M1 for replication: a vulnerable broad-spectrum antiviral target. Sci. Adv. 6, eaba7910. https://doi.org/10.1126/sciadv.aba7910.

90. Yuan, S., Wang, R., Chan, J.F.-W., Zhang, A.J., Cheng, T., Chik, K.K.-H., Ye, Z.-W., Wang, S., Lee, A.C.-Y., Jin, L., et al. (2020). Metallodrug ranitidine bismuth citrate suppresses SARS-CoV-2 replication and relieves virus-associated pneumonia in Syrian hamsters. Nat. Microbiol. 5, 1439–1448. https://doi.org/10.1038/s41564-020-00802-x.

91. Yuan, S., Yin, X., Meng, X., Chan, J.F.-W., Ye, Z.-W., Riva, L., Pache, L., Chan, C.C.-Y., Lai, P.-M., Chan, C.C.-S., et al. (2021). Clofazimine broadly inhibits coronaviruses including SARS-CoV-2. Nature 593, 418–423. https://doi.org/10.1038/s41586-021-03431-4.

92. Rostovskaya, M., Andrews, S., Reik, W., and Rugg-Gunn, P.J. (2022). Amniogenesis occurs in two independent waves in primates. Cell Stem Cell 29, 744–759.e6.

93. Wolf, F.A., Angerer, P., and Theis, F.J. (2018). SCANPY: large-scale single-cell gene expression data analysis. Genome Biol. 19, 15. https://doi.org/10.1186/s13059-017-1382-0.

94. Haghverdi, L., Büttner, M., Wolf, F.A., Buettner, F., and Theis, F.J. (2016). Diffusion pseudotime robustly reconstructs lineage branching. Nat. Methods 13, 845–848. https://doi.org/10.1038/nmeth.3971.

95. Halko, N., Martinsson, P.-G., and Tropp, J.A. (2009). Finding structure with randomness: probabilistic algorithms for constructing approximate matrix decompositions. Preprint at arXiv, 0909.4061. https://doi.org/10.48550/arXiv.0909.4061.

96. Pedregosa, F., Varoquaux, G., Gramfort, A., Michel, V., Thirion, B., Grisel, O., Blondel, M., Prettenhofer, P., Weiss, R., and Dubourg, V. (2011). Scikit-learn: machine learning in Python. J.Mach. Learn. Res. 12, 2825–2830.

STAR★METHODS

KEY RESOURCES TABLE

REAGENT or RESOURCE	SOURCE	IDENTIFIER
Antibodies		
Anti-Oct-3/4	R and D Systems	Cat#AF1759; RRID:AB_354975
Anti-TEAD4	Abcam	Cat#ab58310; RRID:AB_945789
ENPEP	Abcam	Cat#ab155991; RRID:AB_2916048
Purified anti-human CD75 Antibody	BioLegend	Cat#326901; RRID:AB_2194435
Anti-KLF17 antibody	Sigma-Aldrich	Cat#HPA024629; RRID:AB_1668927
Recombinant Anti-active YAP1 antibody	Abcam	Cat#ab205270; RRID:AB_2813833
Anti-CDX2 antibody [EPR2764Y]	Abcam	Cat#ab76541; RRID:AB_1523334
GCM1 Antibody	Novus	Cat#NBP2-48520; RRID:AB_2916049
PE anti-human CD49e Antibody	BioLegend	Cat#328009; RRID:AB_893368
Purified anti-human/mouse CD49f Antibody	BioLegend	Cat#313602; RRID:AB_345296
FITC anti-human CD49a Antibody	BioLegend	Cat#328307; RRID:AB_1236430
Alexa Fluor® 488 anti-human HLA-A,B,C Antibody	BioLegend	Cat#311413; RRID:AB_493133
ENDOU Antibody	Novus biologicals	Cat#NBP2-55877; RRID:AB_2916050
Anti-E Cadherin [EP700Y]	Abcam	Cat#ab40772; RRID:AB_731493
Anti-Transcription factor AP-2-alpha [EPR2688(2)]	Abcam	Cat#ab108311; RRID:AB_10861200
Purified anti-human CD49e Antibody	BioLegend	Cat#328002; RRID:AB_8933
Anti-GATA-3	R and D Systems	Cat#MAB6330; RRID:AB_10640512
Anti-TRA-1-60	STEMCELL Technologies	Cat#60064; RRID:AB_2686905
Anti-ACE2	Thermo Fisher Scientific	Cat# MA5-32307; RRID:AB_2809589
ACE2 Rabbit mAb	ABclonal	Cat#A4612; RRID:AB_2863309
Anti-SSEA-4	STEMCELL Technologies	Cat#60062; RRID:AB_2721031
Anti-hCGB	Thermo Fisher Scientific	Cat#14-6508-82; RRID:AB_10853505
Anti-KRT7	Santa Cruz Biotechnology	Cat# sc-70936; RRID:AB_2234501
Anti-AP-2 gamma	R and D Systems	Cat#AF5059; RRID:AB_2255891
Anti-HLA-G	Abcam	Cat#ab7759; RRID:AB_306053
Anti-CD46	BioLegend	Cat#352403; RRID:AB_10897448
Anti-ZO-1	ABclonal	Cat#A0659; RRID:AB_2757321
Anti-KRT18	R and D Systems	Cat#MAB7619; RRID:AB_2893116
Alexa Fluor® 488 anti-human/mouse SSEA-3 Antibody	BioLegend	Cat#330305; RRID:AB_1279441
Alexa Fluor® 488 anti-human/mouse TRA-1-60 Antibody	BioLegend	Cat#330613; RRID:AB_2295395
Anti-p63/TP73L	R and D Systems	Cat#AF1916; RRID:AB_2207174
Donkey anti-Mouse 555	Thermo Fisher Scientific	Cat#A-31570; RRID:AB_2536180
Donkey anti-Mouse 488	Thermo Fisher Scientific	Cat#A-21202; RRID:AB_141607
Donkey anti-Goat 555	Thermo Fisher Scientific	Cat#A-21432; RRID:AB_2535853
Donkey anti-Goat 488	Thermo Fisher Scientific	Cat#A-11055; RRID:AB_2534102
Donkey anti-Rabbit 594	Thermo Fisher Scientific	Cat#A-21207; RRID:AB_141637
Donkey anti-Rabbit 488	Thermo Fisher Scientific	Cat#A-21206; RRID:AB_2535792
Goat anti-Guinea Pig 647	Thermo Fisher Scientific	Cat#A-21450; RRID:AB_141882

(Continued on next page)

Continued

REAGENT or RESOURCE	SOURCE	IDENTIFIER
Bacterial and virus strains		
SARS-CoV-2 (HKU-001a)	In house	GenBank: MT230904
SARS-CoV-2 Omicron	hCoV-19/Hong Kong/HKU-344/2021	GISAID: EPI_ISL_7357684
SARS-CoV-2 Delta	hCoV-19/Hong Kong/HKU-210804-001/2021	GISAID: EPI_ISL_3221329
MERS-CoV (EMC/2012)	Erasmus Medical Center, Netherlands	GenBank:JX869059.2
Top10 Competent Cell	TIANGEN	CB104-02
Chemicals, peptides, and recombinant proteins		
GC376	MedChemExpress	HY-100721
CTS™ (Cell Therapy Systems) N-2 Supplement	Thermo Fisher Scientific	A1370701
B-27™ Supplement (50X), serum free	Thermo Fisher Scientific	17504044
XAV939	MedChemExpress	HY-15147
PD0325901	MedChemExpress	HY-10254
Gö 6983	MedChemExpress	HY-13689
Neurobasal Medium	Thermo Fisher Scientific	21103049
remdesivir	MedChemExpress	HY-104077
DMEM/F-12, no glutamine	Thermo Fisher Scientific	21331020
Y-27632 dihydrochloride	Tocris	1254/10
FBS	Thermo Fisher Scientific	10270
LIF Recombinant Human Protein	Thermo Fisher Scientific	PHC9484
DPBS, powder, no calcium, no magnesium	Thermo Fisher Scientific	21600010
FastQuant RT Super Mix	TIANGEN	KR108-01
PowerUp™ SYBR™ Green Master Mix	Thermo Fisher Scientific	A25776
SB-431542	Tocris	1614
A83-01	Tocris	2939
CHIR-99021	Tocris	4423
A 419259 trihydrochloride	MedChemExpress	HY-15764A
Geltrex™ LDEV-Free Reduced Growth Factor Basement Membrane Matrix	Thermo Fisher Scientific	A1413201
MicroAmp™ Fast Optical 96-Well Reaction Plate with Barcode, 0.1 mL	Thermo Fisher Scientific	4346906
MicroAmp™ Optical Adhesive Film	Thermo Fisher Scientific	4360954
Forskolin	Sigma-Aldrich	F3917
Matrigel Matrix. GFR	Corning	354230
EGF Recombinant Human Protein	Thermo Fisher Scientific	PHG0311
Prostaglandin E2	MedChemExpress	HY-101952
HGF Protein, Human, Recombinant	Sino biological	Cat: 10463-HNAS
RSPO1 Protein, Human, Recombinant	Sino biological	Cat: 11083-HNAS
DMSO, Anhydrous	Thermo Fisher Scientific	D12345
BSA solution	Sigma-Aldrich	A7979
Recombinant Human NRG1-beta 1/HRG1-beta 1 EGF Domain Protein	R and D Systems	396-HB-050
Normal Donkey Serum	Abcam	ab7475
Knockout serum replacement	Thermo Fisher Scientific	10828010
Valproic Acid (Sodium Salt)	Stem cell technology	72292
Cell Recovery Solution	Corning	354253
Recombinant Human FGF basic/FGF2/bFGF (146 aa) Protein	R and D Systems	233-FB-500/CF
μ-Slide 8 Well high Glass Bottom	ibidi	80807
b-Mercaptoethanol	Thermo Fisher Scientific	31350010
TryPLE-Express	Thermo Fisher Scientific	12605036

(Continued on next page)

Continued

REAGENT or RESOURCE	SOURCE	IDENTIFIER
Trypsin/EDTA	Thermo Fisher Scientific	25200072
Penicillin-Streptomycin-Glutamine (100X)	Thermo Fisher Scientific	10378016
Minimum Essential Medium (MEM) Vitamin Solution	Thermo Fisher Scientific	11120052
Insulin-Transferrin-Selenium-Ethanolamine (ITS-X) (100X)	Thermo Fisher Scientific	51500056
Triton X-100	Sigma-Aldrich	T9284
4% Paraformaldehyde	Sigma-Aldrich	P6148
2-phospho-L-ascorbic-acid	Sigma-Aldrich	A8960-5G
Critical commercial assays		
CellTiter-Glo® Luminescent Cell Viability Assay	Promega	G7570
miRcute Plus miRNA cDNA First-Strand cDNA Kit	TIANGEN	KR211-01
miRcute Plus miRNA qPCR Kit (SYBR Green)	TIANGEN	FP411-01
QuantiNova Probe RT-PCR kit	QIAGEN	208354
Transwell invasion assay	Corning	354480
TUNEL cell apoptosis detection kit	Servicebio	G1501
Deposited data		
RNA-seq data	(Okae et al., 2018)[35]	DDBJ: JGA00000000074
RNA-seq data	(Okae et al., 2018)[35]	DDBJ: JGA00000000117
RNA-seq data	(Okae et al., 2018)[35]	DDBJ: JGA00000000122
RNA-seq data	(Gao, ,2019)[24]	ARRAYEXPRESS: E-MTAB-7253
RNA-seq data	(Sheridan, 2021)	ARRAYEXPRESS: E-MTAB-10429
scRNA-seq data	(Zhou, et al., 2019)[44]	GEO: GSE109555
scRNA-seq data	(Liu, et al., 2018)[45]	GEO: GSE89497
RNA-seq data	This paper	GEO: GSE190432
scRNA analysis	This paper	https://github.com/leeyoyohku/EPSC_COVID
Experimental models: Cell lines		
Monkey: Vero E6 cells	ATCC	CCL-81
Human embryonic stem cell (hESC) line: Man-1/M1	(Camarasa, 2010)	N/A
Caco-2 [Caco2]	ATCC	HTB-37
TSC-BST, Human Blastocyst derived hTSCs	(Okae et al., 2018)[35]	N/A
Oligonucleotides		
Primers used, see Table S5	This paper	N/A
Software and algorithms		
ImageJ Fiji (2.0.0)	NIH	https://imagej.net/Fiji
GraphPad Prism 8.0	GraphPad	https://www.graphpad.com/scientific- software/prism/
Microsoft	Microsoft	https://www.microsoft.com/de-at/microsoft- 365/excel
Synthego	N/A	https://ice.synthego.com/#/
BioRender	N/A	https://biorender.com/
Adobe Illustrator	Adobe	https://www.adobe.com/at/products/illustrator.html
FlowJo	BD Life Sciences	https://www.flowjo.com/
Zeiss Zen (Blue edition)	Zeiss	https://www.zeiss.com/microscopy/int/products/microscope-software/zen-lite.html
FeatureCounts v2.0.1	N/A	http://subread.sourceforge.net
SCANPY (v1.7.2, scRNA/integrative analysis)	N/A	https://scanpy-tutorials.readthedocs.io/en/latest/index.html

RESOURCE AVAILABILITY

Lead contact
Further information and requests for resources and reagents should be directed to and will be fulfilled by the Lead Contact, Pentao Liu (pliu88@hku.hk).

Materials availability
All unique/stable reagents generated in this study are available from the Lead contact with a completed Materials Transfer Agreement.

Data and code availability
- RNA-seq data generated in this study have been deposited at NCBI Gene Expression Omnibus (GEO): GEO: GSE190432.
- All original code has been deposited (https://github.com/leeyoyohku/EPSC_COVID) and is publicly available as of date of publication.
- Any additional information required to reanalyze the data reported in this work paper is available from the Lead contact upon request.
- Additional Supplemental Items are available from Mendeley Data: https://doi:10.17632/rnsbwdr7gw.2.

EXPERIMENTAL MODEL AND SUBJECT DETAILS

Human expanded potential stem cells (hEPSCs)
The primed human embryonic stem cells (hESCs) Man-1/M1 line (female, XX) was converted to hEPSCs (M1 hEPSCs). C5-hiEPSCs (female, XX) are derived from fetal neural stem cell line BRC1019 (NSCs, a gift from Dr. Colin Watts) and were established by episomal (integration-free) six-factor reprogramming.[24,87] The six factors were human complementary DNAs of OCT4, cMYC, KLF4, SOX2, RARG, and LRH1 linked by 2A peptides. Transfected cells (2×10^5; GM00013, Coriell Institute; Amaxa Nucleofector) were seeded on feeder cells (10-cm dish) in M15 (Knockout DMEM, 15% FBS, 1×Glutamine Penicillin-Streptomycin and 1×NEAA, 50 μM 2-mercaptoethanol) and supplemented with 50 μg mL−1 vitamin C and Dox (1.0 μg mL−1). Dox was removed at days 12–14 and the media was switched to hEPSCM. The survival colonies were picked at day 21 to hEPSCM and expanded to stable hiEPSC lines. The maintenance and expansion of hEPSCs were routinely performed on SNL feeder cells (SNL76/7). Gamma irradiation-inactivated SNL feeder cells were plated on 0.1% gelatinised plates 3–4 days before seeding hEPSCs at a density of ~3.125×10^4 cells/cm^2.

Culture of human trophoblast stem cells (hTSCs)
Human trophoblast stem cells (hTSCs) (the BST-TSC line provided from Dr. T. Arima[35]; EPSC-TSCs derived from M1 hEPSCs; naive TSCs derive from H1 PXGL naive stem cells) were cultured with the TSC medium in Matrigel/Geltrex-coated plates at 37°C and 5% CO$_2$ conditions. The medium was changed daily. Human TSCs were treated with TrypLE and then passaged onto new Matrigel/Geltrex-coated plates every 3–4 days. All cells were maintained in a 5% CO$_2$ incubator at 37°C and routinely tested negative for mycoplasma.

Cell lines
The SNL cell line is an immortalized subclone of the STO line created to stably express the neomycin resistance and leukemia inhibitory factor (LIF) genes. SNL feeder cells were maintained in regular M10 medium: Knockout DMEM, 10% FBS, 1×Glutamine Penicillin-Streptomycin and 1× NEAA. Human colon Caco-2 cells (epithelial cells isolated from colon tissue, ATCG, HTB-37) and monkey Vero E6 cells (kidney epithelial cells from female African green monkey, ATCC, CCL-81) were maintained in DMEM culture medium supplemented with 10% heat-inactivated FBS, 50 Uml−1 penicillin and 50 μgml−1 streptomycin. All cells were maintained in a 5% CO$_2$ incubator at 37°C and routinely tested negative for mycoplasma.

Culturing hEPSC-TSC derived trophoblast organoids
Dissociated hEPSC-TSCs were resuspended into single-cells in ice-cold trophoblast organoid medium (TOM) containing 80 ng/mL R-spondin-1, 1.5 μM CHIR99021, 500 nM A83-01, 50 ng/mL human EGF, 100 ng/mL FGF2, 50 ng/mL human HGF, 2.5 μM prostaglandin E2, and Y-27632 5.0 μM. A final concentration of 60% growth factor-reduced Matrigel (GFR-M, Corning) was added. 40 μL drops of cell/Matrigel mixture) with 1×10^5 EPSC-TSCs each were pipetted into the well centers of 24-well plates. After 15 min solidification at 37°C for the drops to form domes, 500 μL prewarmed TOM was added to overlay the domes. Trophoblast organoid formation require around 4–6 days at P0. They were passaged after reaching 200–300 μm in diameter.

Virus
The wildtype SARS-CoV-2 HKU-001a strain (GenBank accession number: MT230904) was isolated from the nasopharyngeal aspirate specimen of a patient who was laboratory-confirmed to have COVID-19 in Hong Kong. The SARS-CoV-2 Delta variant isolate

(B.1.617.2) (hCoV-19/Hong Kong/HKU-210804-001/2021; GISAID accession number EPI_ISL_3221329) has been described previously.[88] The Omicron variant strain was isolated from the nasopharyngeal throat swab of a COVID-19 patient in Hong Kong (hCoV-19/Hong Kong/HKU-344/2021; GISAID accession number EPI_ISL_7357684). The MERS-CoV strain (HCoV-EMC/2012) was a gift from R. Fouchier. All experiments involving live SARS-CoV-2 and MERS-CoV were performed following the approved standard operating procedures of the biosafety level 3 facility in Queen Mary Hospital at The University of Hong Kong.[89]

METHOD DETAILS

Culture of hEPSCs and naive stem cells

Human EPSC cells were maintained on SNL 76/7 feeder layers and enzymatically passaged (1:10) every 3–5 days by a brief PBS wash followed by treatment with TrypLE for 3 min. Cells were dissociated and centrifuged (300g for 3 min) in 10% fetal bovine serum (FBS)-containing medium (M10 medium). After removing the supernatant, human EPSCs were resuspended and seeded in hEPSC Medium (EPSCM) supplemented with 5.0 μM Y27632. The hEPSCM is a N2B27-based media supplement with 3 small molecules 5 μM XAV939, 1 μM CHIR99021 and 0.1 μM A-419259 as previously published.[24] N2B27 basal media [1:1 of DMEM/F12 (Thermo, Cat.21331020) and Neurobasal Medium (Thermo, Cat. 21103049); 200x N2 supplement and 100x B27 supplement, 100x ITS-X, 50.0 μM β-mercaptoethanol, 1% Penicillin-Streptomycin-Glutamine, 100x Non-essential amino acid solution, 50 μg/mL Vitamin C].

Naive stem cells were maintained on inactivated MEF (mouse embryonic fibroblasts) feeder layers in PXGL medium. The PXGL medium is prepared by supplementing N2B27 basal medium with PD0325901(1 μM), XAV-939(2 μM), Gö 6983 (2 μM), 0.45% BSA and human leukemia inhibitory factor (hLIF, 10 ng/mL) as previously reported.[32]

Differentiation of hEPSCs to trophoblast lineages by TGF-β inhibitor SB431542 treatment

Human EPSCs were dissociated with TrypLE and seeded in 100x Geltrex coated six-well plates at a density of 1×10^{5} cells per well. Cells were cultured (pre-treatment) in 20% KSR media supplemented with 10 μM Y27632 for one day. From the second day, 10 μM SB431542 was added into 20% KSR media to start the differentiation. Cells were collected at the indicated time points for analysis.

Derivation of human trophoblast stem cells (hTSCs) from hEPSCs and naive stem cells

Single cell-dissociated hEPSCs were plated on 6-well plates pre-coated with 100x Geltrex at a density of 2,000 cells per well and cultured in the published hTSC media with modifications.[35] DMEM/F12 supplemented with 50.0 μM β mercaptoethanol, 0.2% FBS, 0.5% Penicillin-Streptomycin-Glutamine, 0.3% BSA, 1.0% ITS-X supplement, 50.0 μg/mL Vc, 50.0 ng/mL EGF, 2.0 μM CHIR99021, 0.5 μM A83-01, 1.0 μM SB431542, 10.0 μM VPA and 5.0 μM Y27632. After 12–14 days of culture, the colonies with TSC-like morphologies were picked, dissociated in TrypLE, and replated on a plate pre-coated with 100x Geltrex. After 10 passages, the cells were collected for syncytiotrophoblast (STB) and extravillous trophoblast (EVT) differentiation.

Single cell-dissociated naive stem cells were plated on 6-well plates pre-coated with 100x Geltrex and cultured in PD0325901 (1 μM) + A83-01(1 μM) for 3 days then induced in hTSCM as described.[32]

Differentiation of EPSC-TSCs to STBs

Wells of a six-well plate were coated with 100× Matrigel for at least 1h. 2.0×10^{5} hTSCs were seeded per well in 2 mL STB medium [DMEM/F12 supplemented with 50 μM β-mercaptoethanol, 0.5% Penicillin-Streptomycin-Glutamine, 0.3% BSA, 1% ITS-X, 2.5 μM Y-27632, 2 μM Forskolin and 4% KnockOut Serum Replacement. Media was changed on day 3, and the cells were ready for downstream analysis on day6. The eSTBs correspond to day 2 cells differentiating in the STB medium.

Differentiation of EPSC-TSCs to EVTs

For EVT differentiation, wells of a 6-well plate were coated with 100× Matrigel for at least 1h. 2.0 ×10^{5} hTSCs were seeded per well in 3.0 mL EVT basal medium [DMEM/F12 supplemented with 50uM β-mercaptoethanol, Penicillin-Streptomycin-Glutamine, 0.3% BSA, 1%ITS-X, 7.5 μM A83-01, 10 μM Y27632] supplemented with 4% KSR, 100 ng/mL NRG1 and 2% Matrigel. On day 3, the media were replaced with 2 mL EVT basal medium supplemented with 4% KSR and 0.5% Matrigel. On day 6, they were dissociated with TrypLE for 10–15 min and passaged to a fresh matrigel-coated 6-well plate. The media were replaced with 2 mL EVT basal medium and 0.5% Matrigel. On day 8, the cells were ready for downstream analysis.

Generation of trophoblast organoids from EPSC-TSCs

EPSC-TSCs were digested with TrypLE and dissociated into single cells by pipetting. After centrifugation, growth factor-reduced Matrigel (GFR-M) was added to reach a final concentration of 60% and the remaining 40% was made up of trophoblast organoid medium (TOM). The Matrigel/TOM mixture (40 μL) containing 1.0 × 10^{5} hTSCs was seeded into the wells' center of a 24-well plates. After 3 min at 37°C in a CO$_2$ incubator, the plates were turned upside down to ensure equal spreading of the cells in the well. After 15 min at 37°C in an incubator, the solidifying GFR-M formed domes and were carefully overlaid with 500 μL TOM. Trophoblast organoids were allowed to form for 4–6 days at P0. After 20 days of culturing, trophoblast organoids were collected by dissolving the Matrigel with recovery solution and submitted to SARS-CoV-2 infection. TOM is composed of N2B27 basal media, recombinant human EGF 50 ng/mL, CHIR99021 1.5μM, recombinant human R-spondin-1 80 ng/mL, recombinant human

FGF-2 100 ng/mL, recombinant human HGF 50 ng/mL, A83-01 500 nM, Prostaglandin E2 2.5 μM, Y-27632 5 μM. All medium was stored at 4°C for up to 2 weeks.

SARS-CoV-2 infection and viral copy detection

SARS-CoV-2 stock was propagated using Vero E6 cells, and the titer of supernatant was assessed by plaque assay as previously described.[90]

For viral detection, the supernatant of the cultured cells challenged by SARS-CoV-2 was harvested at various time points. A total of 140 μL of culture supernatant was lysed with 560 μL of AVL buffer, which was subsequently extracted for total RNA with the QIAamp® Viral RNA Mini Kit. The extracted RNA was quantified with the one-step QuantiNova Probe RT-PCR kit. Each 20 μL reaction mixture contained 10 μL of 2× QuantiNova Probe RT-PCR Master Mix, 0.2 μL of QuantiNova Probe RT-Mix, 1.6 μL each of 10μM forward and reverse primer, 0.4 μL of 10 μM probe, 5 μL of extracted RNA as template, and 1.2 μL of RNase-free water. Reactions were incubated at 45°C for 10 min for reverse transcription, 95°C for 5 min for denaturation, 45 cycles of 95°C for 5 s and 55°C for 30 s, followed by a cooling step at 40°C for 30 s. The primers and probe sequences were against the RNA-dependent RNA polymerase/helicase (RdRP/Hel) gene region of SARS-CoV-2 were listed in Table S5.

Plaque assay

Plaque assay was performed as previously described.[91] Briefly, Vero E6 cells were seeded at 300,000 cells/well in 12-well tissue culture plates on the day before carrying out the assay. After 24 h of incubation, a serial dilution of supernatant was added to the cell monolayer and the plates were further incubated for 1 h at 37°C in 5% CO$_2$ before removal of unbound viral particles by aspiration of the media and washing once with DMEM. Monolayers were then overlaid with media containing 1% low melting agarose (Cambrex Corporation, East Rutherford, NJ, USA) in DMEM, inverted and incubated as above for another 72 h. The wells were then fixed with 10% formaldehyde (BDH, Merck, Darmstadt, Germany) overnight. After removal of the agarose plugs, the monolayers were stained with 0.7% crystal violet (BDH, Merck) and the plaques were counted. The plaque assay experiments were performed in triplicates.

Antiviral evaluation in eSTBs

The EPSC-TSCs were dissociated into single cells and rinsed with STB medium. Then cells were seeded into 96 well plate at the density of 10000 cells per well and cultured for two days (eSTBs). The eSTBs were infected with SARS-CoV-2 WT, Delta, Omicron variant or MERS-CoV with 0.1 MOI inoculum at 100 μL per well. After 1 h, the inoculum was removed, and the eSTBs were washed 3 times with PBS. The infected eSTBs were then cultured in 100ul of STB medium with remdesivir or GC376 at indicated concentrations. Supernatants were collected at 48 h after inoculation for downstream assays.

Guide RNA design and plasmid DNA preparation

The human ACE2 exon 2 sequence was analyzed by the online CRISPR tool for designing a pair of highly specific gRNAs. Chemically synthesized ssDNA oligos were incubated at 95°C for 10 min for annealing into dsDNA, which were then ligated into a linearized empty gRNA vector using the DNA Ligation Kit, Mighty Mix. The ligation product was transformed into Chemically Competent DH 5α Cell (KT Health) and spread onto an LB agar plate with ampicillin for selection. The next day, single colonies were picked and cultured in LB broth with ampicillin for plasmid miniprep using the TIANprep Rapid Mini Plasmid Kit. After confirmation of ligated gRNA sequences by Sanger Sequencing, gRNA plasmids with the correct target sequence were amplified and extracted by the Endo-free Plasmid Kit II to purify a large amount of endotoxin-free gRNA plasmid DNA for electroporation. Plasmid DNA of BSD-Cas9 was similarly prepared as described previously.[24]

Electroporation and selection

Electroporation of hEPSCs was performed when the cells reached 70–80% confluence. Plasmid DNA including Cas9 and double sgRNA at a ratio of 2:1:1 (4μg Cas9, 2μg sgRNA1, 2μg sgRNA2 per 1million cells as one group) were added into 300 μL Opti-MEM. hEPSCs were washed twice with PBS, then dissociated into single cells using 0.05% Trypsin-EDTA. M10 medium (DMEM with 10% FSB) was added to neutralize the trypsin. Single-cell hEPSCs were resuspended in an Opti-MEM medium containing the plasmid DNA mixture. Electroporation was performed using the Bio-Rad Gene Pulser Xcell Electroporation Systems in 0.4cm cuvettes at 230V, 500 μF. After electroporation, cells were seeded with a recovery medium (500 μL EPSCM + 10% KSR+10μM Y27632). After incubation overnight, cells were switched to a typical hEPSC medium. One day after electroporation, cells were selected by 10 μg/mL Blasticidin S HCl. Two days after electroporation, cells were selected by 10 μg/mL Blasticidin S HCl and 1 μg/mL Puromycin Dihydrochloride for another 2 days. After 7–10 days, single colonies were picked, expanded, and genotyped.

Genotyping and sanger sequencing

Single hEPSC colonies were picked and digested into single cells in a 96-well plate using 0.05% trypsin-EDTA for 3–5 min. Half of these cells were transferred into a 48-well plate with EPSCM medium and SNL feeders for culturing. The other half cells of the same colony were collected for genotyping using primers designed to amplify the targeted as well as the wildtype bands. The genotyping primer sequences for *ACE2* were as follows: Forward: 5′-GTGGCCTGGTCACTCTTAAC-3′; Reverse: 5′-CAAATAAAGGCAGC TGCTGTG-3′. The mutant PCR band was gel-purified and confirmed by Sanger sequencing for a 148-bp deletion.

Reverse transcription- quantitative polymerase chain reaction (RT-qPCR)

Total RNA extraction was performed using the RNeasy Mini Kit as per the manufacturer's instructions. The isolated RNA was reverse transcribed into complementary (cDNA) using the Fastking gDNA Dispelling RT Super-Mix on a thermal cycler. The PowerUp™ SYBR™ Green Master Mix was used for amplifying intracellular SARS-CoV-2 and gene cDNA. Primer sequences are listed in Table S5. All qPCR experiments were performed using The StepOnePlus™ Real-Time PCR System (Applied Biosystems). Gene expression levels were normalized to *GAPDH* using the ΔCt method. Data were analyzed using one/two-tailed Student's *t* test in Prism 8 (GraphPad).

Immunofluorescence staining

Samples were fixed in 4% paraformaldehyde at room temperature for 15 min, permeabilized with 0.3% Triton X-100 for 30 min, and blocked for 3h with 5% donkey serum as well as 1% BSA. This was followed by incubation with primary antibodies in a 4°C cold room overnight. After washing in PBS, fluorophore-conjugated secondary antibodies were incubated with the samples at room temperature for 1 h. After another 3 rounds of washing in PBS, samples were counterstained with 10 μg/mL DAPI for 10 min to mark nuclei and were imaged under a fluorescence microscope or confocal LSM900.

Western blotting

Proteins were separated in 7.5% polyacrylamide gels and transferred to PVDF membranes using the Bio-Rad transblot turbo system according to the manufacturer's guidance. The following primary antibodies were used for Western blot: rabbit ACE2 (1:500, Abclonal. Cat. A4612), rabbit β-actin (1:5000, Abmart. Cat. P30002M). Goat anti-rabbit IgG H&L (HRP) (1:10000, Abcam. Cat. ab205718) was used as the secondary antibody. Images were developed and analyzed by the ChemiDoc Imaging System.

Flow cytometry

Cells were digested with 0.25% trypsin/EDTA for 2–3 min at 37°C and dissociated to single cells by pipetting. The dissociated cells were filtered through a 40-μm nylon mesh to remove cell clumps. After centrifugation, the cells were fixed using Fixation Medium according to the manufacturer's protocol and the washed cells were stored at 4°C in PBS supplemented with 0.1% NaN3 and 5% FBS before analysis with flow cytometry. All the samples were assayed by the ACEA NovoCyte Quanteon. 488nm (530/30 bandpass filter) and 561nm (610/20 bandpass filter) channels were used to detect FITC and excluded autofluorescence. 405nm (445/45 bandpass filter) channel was used to detect DAPI positive cells. FACS data were analyzed by the Flowjo software.

Transwell invasion assay

The invasion ability of hTSCs-derived EVTs was determined by cell invasion according to manufacturers' instructions. Briefly, the invasion chambers were incubated with a warm DMEM base medium at 37°C for 1 h. After rehydration, the medium was removed. EPSC-EVTs (1×10^5 cells/well) was mixed with DMEM basal medium, and the mixture was added into an invasion chamber and placed into a 24 well culture plate, with the lower chamber filled with DMEM containing 10% FBS. The cells were allowed to pass through the chamber and attached to the lower bottom of the polycarbonate membrane for 22 h. After that, the medium from the top insert was aspirated, and non-invasive/-migratory cells on the upper surface were wiped away with a cotton bud. The invaded/migrated cells on the lower surface were stained with crystal violet for 15 min. The membrane was observed under a light microscope.

QUANTIFICATION AND STATISTICAL ANALYSIS

Statistical analysis and reproducibility

The statistical analysis was conducted with Microsoft Excel or Prism 8 (GraphPad). p values were calculated using (un)paired Student's *t* test and ANOVA for comparisons of multiple groups. The threshold for statistical significance was p < 0.05. The exact number of measurements, the number of independent experiments, and the statistical test used for each analysis performed were listed in the figure legends. Experiments were repeated independently with similar results obtained.

RNA-seq analysis

Cutadapt was used to remove adapter sequences and low-quality 3′ end sequences. Processed reads were mapped to the human hg38 genome assembly by hisat2. Gene annotation form Ensembl was used. FeatureCounts was used to quantify gene expression. Genes with mean count number <5 were filtered out. Transposable element annotations were from UCSC Genome Browser (RepeatMasker). SQuIRE with "total" mode was used to quantify TE expression. DESeq2 was used to analyze differentially expressed genes and TEs. Genes and TEs with expression fold change >1.5 and adjusted p-value < 0.05 were considered significant differential expressed. R package clusterprofiler was used for gene ontology (GO) and KEGG analysis. GSEA (Gene Set Enrichment Analysis) was performed by GSEApy, and the gene sets were downloaded directly from https://www.gsea-msigdb.org. Bigwig files for RNA-seq signal were generated by bamCoverage from Deeptools and IGV was used for visualization. For the RNA-seq signal on endogenous retrovirus, GenBank: AY101582.1, BC068585.1, JN675077.1 were used to inquire about the sequence of HERV-W, HERV-FRD, and HERV-K and the reads were mapped by hisat2. GenBank accession number MN985325 was used to inquire about

the sequence of SARS-CoV-2 genes, then the reads were mapped to sequences by hisat2 and quantified. For data deposited in E-MTAB-10429, the processed count table was used directly. For the comparison between E-MTAB-10429 and our data, we used ComBat-seq to remove the batch effect.

For the PCA analysis for hEPSC-TSCs, naive hPSC-hTSCs, primed-hTSCs and early/late AMEs, data processing were followed by another study[92]: the expression of genes are normalized by DESeq2 and the top 1000 most variable protein coding genes were used in the analysis.

scRNA preprocessing

scRNA preprocessing was performed according to the SCANPY pipelines.[93] Briefly, Transcripts Per Million (TPM) of pre-to post-implantation cells were extracted from Zhou's dataset[44] (GEO: GSE109555), and placenta cells were extracted from Liu's dataset[45](GEO: GSE89497). In the original studies, cells have been categorized by their stages and lineages into 7 coarse clusters (3 in pre-to post-implantation, 3 in the first-trimester placenta, and 1 in the second-trimester placenta; N.B., Zhou's dataset annotation was obtained from Castel. et al.).[33] Here, we performed pseudotime analysis on these two datasets jointly. First, we pre-processed the combined dataset by 1) log-transformation of the TPM counts, 2) scaling to 10 on each gene, and 3) regressing out on the sequencing depth. Then, we calculated the diffusion pseudotime by DPT using scanpy.tl.dpt with default parameters.[94] Cells with inconsistent stage-lineage annotations and pseudotime values have been removed, and 4041 and 952 cells were retained for downstream analysis, respectively. Based on log counts, Pearson correlations were computed for selected markers with ACE2, and visualized by scatterplots. Batch effects among bulk RNA-seq have also been regressed out before comparing *in vitro* cells to *in vivo* reference.

Integration of *in vitro* and *in vivo* extra-embryonic datasets

For integrative analysis, we mapped the *in vitro* bulk RNA-seq to the *in vivo* scRNA reference by using singular value decomposition (SVD) modeling,[95,96] based on the assumption that top components could capture cell identity and biological variations, regardless of sequencing types. First, the batch effects between the two scRNA datasets were regressed out to construct an extra-embryonic landscape containing peri-implantation to placenta stages. Then, we fitted the SVD model using the whole transcriptome of the combined *in vivo* scRNA reference and generated a 50-component decomposition result for the *in vivo* reference. Next, we applied the fitted model to project the *in vitro* cells (bulk RNA-seq) to the corresponding 50 components in the same space. After concatenating the bulk RNA and scRNA datasets as 50-component samples, UMAP visualization could be generated. As a proof of the effectivity of the SVD modeling in segregating cell types, for the *in vivo* sector, inter-cell type variations were captured by each cluster in the UMAP.

Whole-transcriptome correlation analysis between *in vitro* cell line bulk RNA-seq and *in vivo* scRNA-seq

With the assumption that bulk RNA-seq reflects additive effects of scRNA levels, we generated pseudo-bulk sets from the *in vivo* scRNA-seq. For each *in vivo* subtype, we randomly selected two sets of 50 cells as two "pseudo-bulk cells" and calculated an average to simulate two bulk samples for each subtype, hence we have 14 pseudo-bulk samples. After merging the 14 pseudo-bulk samples with *in vitro* cells (19 samples, 10 types), we calculated the pairwise Pearson coefficients across the whole transcriptome between every two samples. The coefficients were visualized in the cluster map to impute the corresponding *in vivo* stage of each *in vitro* cell line.

Integrative pseudotime analysis

First, diffusion pseudotime was computed for the whole *in vivo* reference using SCANPY (scanpy.tl.dpt, default parameters). We then extracted the PI-TB to PI-STB subsets as the pseudotime reference set for downstream analysis of *in vitro* ST differentiation cells. There are 2295 PI-TB cells and 1282 PI-STB cells, constituting a unidirectional differentiation trajectory. Similar to the process described in the integration of bulk RNA and scRNA datasets part, we fitted a 50-component SVD model using the scRNA reference to reduce the dimensions of both scRNA and bulk RNA to a common 50-component space. We hypothesized that these 50 components could predict the pseudotime calculated by SCANPY. The machine learning prediction process was achieved using sklearn.linear_model. LinearRegression. Briefly, the 50 components and the pseudotime of 1721 PI-TB cells and 961 PI-STB cells (75% of each subtype) were used to train the linear regression model, and the remaining 25% test set of each subtype was used to validate the model. The validation result was visualized by the density plot. After confirming the effectivity of the model, we applied the model to predict the pseudotime of *in vitro* differentiated cells. We also calculated the theoretical "observed pseudotime" for *in vitro* cells by the following linear equation between the predicted and observed pseudotime in the *in vivo* reference: Observed pseudotime = 1.022 * Predicted pseudotime - 0.0032. Then pseudotime of each dataset was then merged to visualize the relative differentiation stage of each cell.

Supplemental information

Human early syncytiotrophoblasts are highly
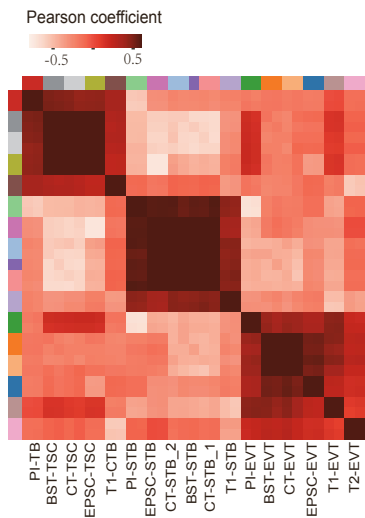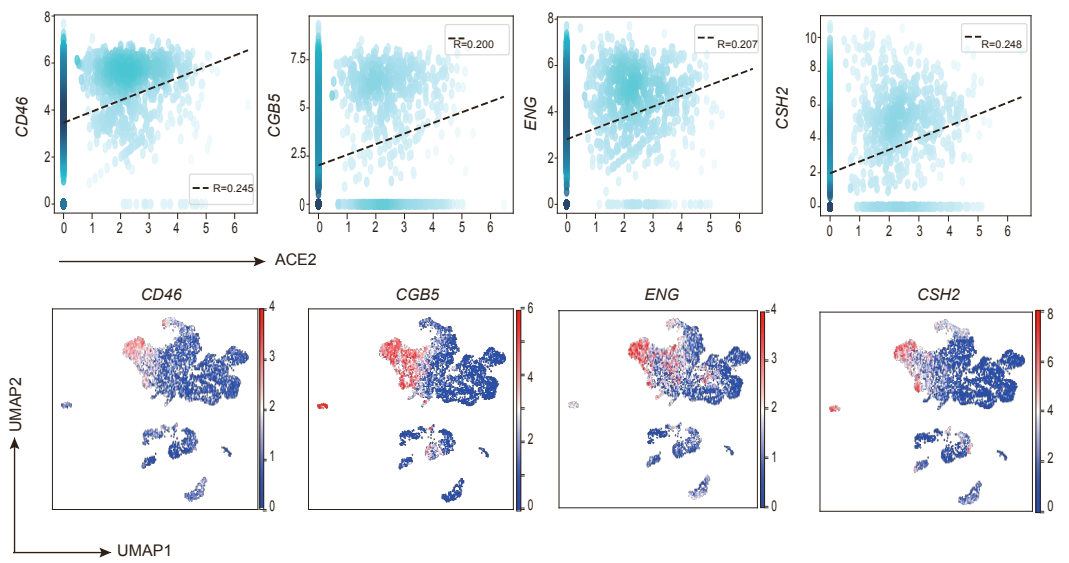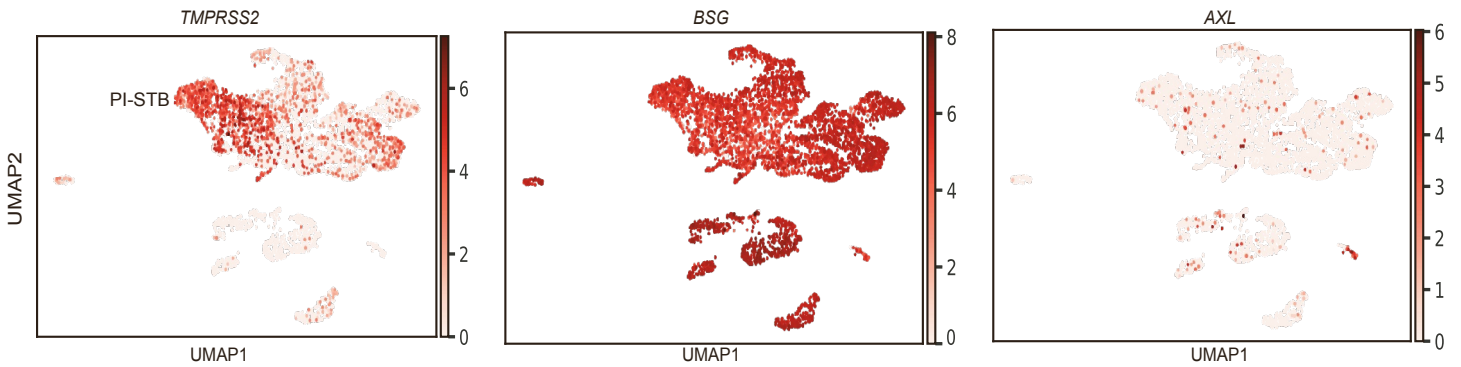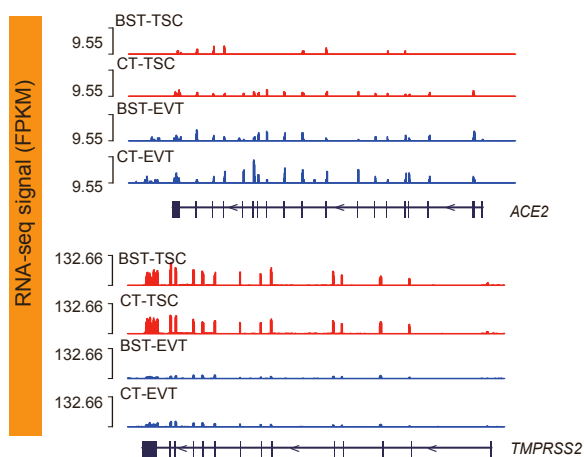
susceptible to SARS-CoV-2 infection

Degong Ruan, Zi-Wei Ye, Shuofeng Yuan, Zhuoxuan Li, Weiyu Zhang, Chon Phin Ong, Kaiming Tang, Timothy Theodore Ka Ki Tam, Jilong Guo, Yiyi Xuan, Yunying Huang, Qingqing Zhang, Cheuk-Lun Lee, Liming Lu, Philip C.N. Chiu, William S.B. Yeung, Fang Liu, Dong-Yan Jin, and Pentao Liu
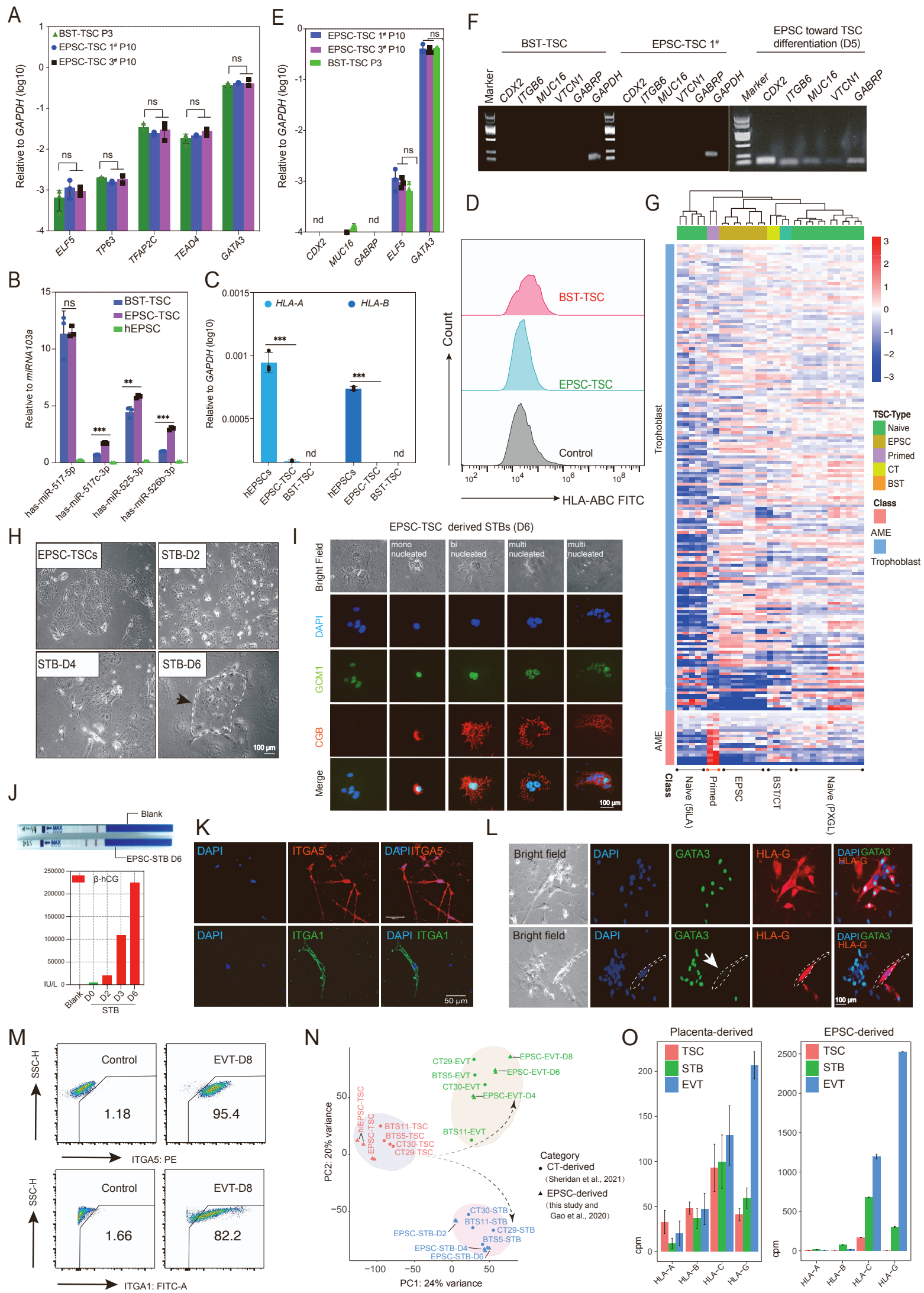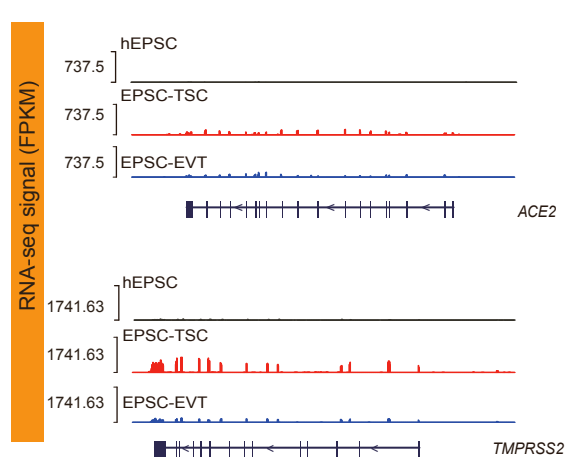
Figure S1. Generating trophoblast stem cells (TSCs) and subtype trophoblasts from hEPSCs. Related to Figure 1. RT-qPCR analysis of trophoblast genes (A) trophoblast-specific C19MC miRNAs (B), *HLA-A* and *-B* (C), and *CDX2* and putative AME genes (E) were performed in hEPSCs and/or EPSC-TSCs and BST-TSC. Results are normalized to levels of *GAPDH* for marker genes or *miR-103a* for miRNAs using the ΔCt method Data are mean ± sd, n=3 biological replicates. Student's *t*-test, nd: not detectable, ns: not significant, **P <0.01; *** $P < 0.001$; (D) Flow cytometry quantification of HLA-A, B, C on EPSC-TSCs and BST-TSCs. The antibody isotype is the control. (F) RT-PCR detection of *CDX2* and putative AME genes in EPSC-TSCs, BST-TSC, and in cells of hEPSCs differentiation toward hTSCs on day 5. (G) Heatmap for signature genes of trophoblast and AME (Table S1). Genes are ordered by expression in respective gene sets and samples are ordered by cluster result. Expression is normalized with mean and log2 transformed. (H) Representative bright field images of STBs generated from EPSC-TSCs on day 2, 4 and 6. The arrow points to a multinucleated STB circled by a dashed line. Scale bar: 100 μm (I) STBs generated from EPSC-TSCs have distinct morphologies (mono-, bi- or multinucleated) and express GCM1 and CGB. Scale bar: 100 μm (J) Upper panel: Representative results using a human pregnancy test strip on medium collected from day-6 EPSC-STBs and STB medium control (Blank). Lower panel: ELISA (IU/L) detection of β-hCG in supernatant from different STB differentiation timepoints as indicated. (K) Immunofluorescence staining (ITGA1 and ITGA5) of day8 EVTs generated from EPSC-TSCs. Scale bar: 100 or 50 μm as indicated (L) EVTs generated from EPSC-TSCs (day 8) are immunofluorescence stained for GATA3 and HLA-G. Arrow indicates that a mature EVT (spindle shape, circled by a dashed line) does not express high GATA3. Scale bar: 100 μm (M) Flow cytometry quantification of EVT marker ITGA5 and ITGA1 on EVTs differentiated from EPSC-TSCs (day 8). (N) PCA analysis for comparison of placenta-derived trophoblast cells (CT and BTS) and EPSC-derived trophoblast cells (EPSC-TSC; EPSC-TSC differentiating toward STB at day2, 4, 6, and toward EVT at day4, 6 and 8, respectively). (O) Expression of HLA genes in human placenta-derived trophoblasts and EPSC-TSCs and their derivative trophoblasts. Error bars: standard errors.

A

TP63 PI-TB PI-STB PI-EVT T1-CTB T1-STB T1-EVT T2-EVT

TEAD4 PI-TB PI-STB PI-EVT T1-CTB T1-STB T1-EVT T2-EVT

CGB5 PI-TB PI-STB PI-EVT T1-CTB T1-STB T1-EVT T2-EVT

CSH2 PI-TB PI-STB PI-EVT T1-CTB T1-STB T1-EVT T2-EVT

HLA-G PI-TB PI-STB PI-EVT T1-CTB T1-STB T1-EVT T2-EVT

MMP2 PI-TB PI-STB PI-EVT T1-CTB T1-STB T1-EVT T2-EVT

B

MUC16 PI-TB PI-STB PI-EVT T1-CTB T1-STB T1-EVT T2-EVT

ITGB6 PI-TB PI-STB PI-EVT T1-CTB T1-STB T1-EVT T2-EVT

GABRP PI-TB PI-STB PI-EVT T1-CTB T1-STB T1-EVT T2-EVT

ISL1 PI-TB PI-STB PI-EVT T1-CTB T1-STB T1-EVT T2-EVT

VTCN1 PI-TB PI-STB PI-EVT T1-CTB T1-STB T1-EVT T2-EVT

CDX2 PI-TB PI-STB PI-EVT T1-CTB T1-STB T1-EVT T2-EVT

D

Cell-line
- BST-EVT
- BST-STB
- BST-TSC

TPM: VTCN1 ITGB6 ISL1 GABRP MUC16 CDX2 GATA3

Cell-line
- EPSC-EVT
- EPSC-STB
- EPSC-TSC

TPM: VTCN1 ITGB6 ISL1 GABRP MUC16 CDX2 GATA3

C

Pearson coefficient

E

R=0.245 *CD46* ACE2

R=0.200 *CGB5* ACE2

R=0.207 *ENG* ACE2

R=0.248 *CSH2* ACE2

UMAP2 / UMAP1 — *CD46* *CGB5* *ENG* *CSH2*

F

TMPRSS2 PI-STB   *BSG*   *AXL*

G

In vivo derived hTSCs and trophoblast subtypes

RNA-seq signal (FPKM)

9.55 BST-TSC
9.55 CT-TSC
9.55 BST-EVT
9.55 CT-EVT
ACE2

132.66 BST-TSC
132.66 CT-TSC
132.66 BST-EVT
132.66 CT-EVT
TMPRSS2

H

hEPSC and hEPSC derived hTSCs and trophoblast subtypes

RNA-seq signal (FPKM)

737.5 hEPSC
737.5 EPSC-TSC
737.5 EPSC-EVT
ACE2

1741.63 hEPSC
1741.63 EPSC-TSC
1741.63 EPSC-EVT
TMPRSS2

Figure S2. Trophoblasts derived from hEPSCs resemble those in human peri-implantation embryos and the placenta. Related to Figure 2. Violin plots showing log-transformed TPM of trophoblast genes (A) and putative AME genes (B) in human peri-implantation embryos and placenta trophoblasts. (C) Heatmap of Pearson correlation coefficients among transcriptomics of peri-implantation embryo and placenta (pseudo-bulk RNAseq), and the *in vitro* cultured trophoblasts (bulk RNAseq). Batch effects were regressed out in transcriptomic expression. *In vitro* trophoblast samples include blastocyst- and placenta-derived TSCs (BST-TSC, CT-TSC) and the trophoblast subtypes STBs (BST-STB, CT-STB) and EVTs (BST-EVT, CT-EVT), and EPSC-TSC and their trophoblast subtypes STBs and EVTs (EPSC-STB, EPSC-EVT). (D) Potential amnion marker expression (in TPM) in hTSC derived from the blastocyst (BST, Upper panel) and hEPSC (Bottom panel) and their derivatives. *GATA3* is a non-amnion marker for comparison. (E) Upper panel: Scatter plots showing the positive Pearson correlations of *CD46*, *CGB5*, *ENG* and *CSH2* with *ACE2* expression. Linear regression is drawn in black dashed line. The darkness of blue indicates cell density. Lower panel: Scaled expression of STB genes in human peri-implantation embryo and placenta trophoblasts. (F) Scaled expression of *TMPRSS2*, *BSG* and *AXL* in human peri-implantation embryo and placenta trophoblasts. (G-H) RNA-seq signal of *ACE2* and *TMPRSS2* in *in vivo* derived trophoblasts (G) and in hEPSCs and hEPSC derivatives (H). *ACE2* and *TMPRSS2* genomic regions are plotted at the bottom, where each vertical bar represents an exon.
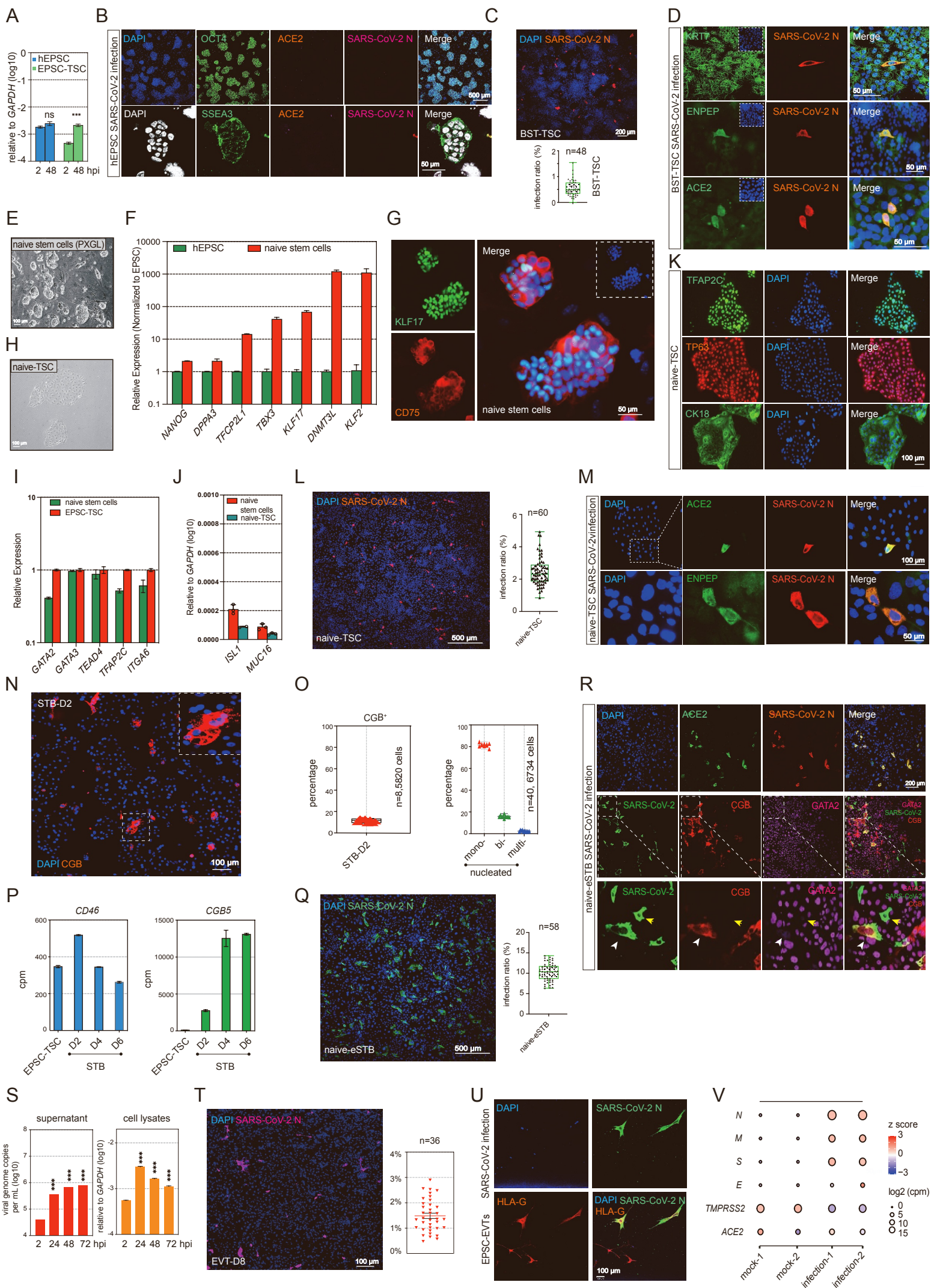
Figure S3. *In vitro* generated human trophoblasts are susceptible to SARS-CoV-2 infection. Related to Figure 3. (A) RT-qPCR detection of SARS-CoV-2 genome copy number in cell lysates of 2 h.p.i. and 48 h.p.i hEPSCs and EPSC-TSCs. (B) Immunofluorescence staining of 48 h.p.i. hEPSCs for pluripotent markers OCT4 or SSEA3 and ACE2, SARS-CoV-2 N protein. Scale bar: 100 μm. (C) Immunofluorescence-stained 24 h.p.i. BST-TSCs for SARS-CoV-2 N protein. Scale bar: 100 μm. Lower panel: Percentages of SARS-CoV-2 N protein positive BST-TSCs. n=48 random immunofluorescence staining images. (D) Immunofluorescence-stained SARS-CoV-2 N protein, ACE2, ENPEP, and KRT7 in 24 h.p.i. BST-TSC. Scale bar: 50 μm (E) Phase-contrast image of human naïve stem cells (H1) cultured on MEFs in PXGL condition. Scale bar: 100 μm (F) RT-qPCR quantification of naïve marker gene expression in naïve stem cells compared to hEPSCs (mean ± s.d. n=3). (G) Immunofluorescence staining of naïve pluripotency markers KLF17 and CD75 in naïve stem cells. Scale bar: 50 μm. (H) Phase-contrast image of naïve stem cell-derived hTSCs (naïve-TSCs). Scale bar: 100 μm (I) RT-qPCR quantification of hTSC marker gene expression in naïve-TSC compared to EPSC-TSC (mean ± s.d. n=3). (J) RT-qPCR quantification of *ISL1* and *MUC16* gene expression in naïve stem cells and naive-TSCs (mean ± s.d. n=3). (K) Immunofluorescence staining of hTSC markers in naïve-TSCs. Scale bar: 50 μm. (L) Immunofluorescence staining of SARS-CoV-2 N protein in 24 h.p.i. naïve-TSCs. Scale bar: 500 μm. Right panel: Percentages of SARS-CoV-2 N protein positive naïve-TSCs, respectively. n=60 random images. (M) Immunofluorescence staining of ENPEP and ACE2, SARS-CoV-2 N protein and in 24 h.p.i. naïve-TSCs. Scale bar: 100 μm and 50 μm as indicated. (N) Immunofluorescence staining for CGB in STB-D2. Dotted box showed a multinucleated CGB⁺ cells. Scale bar: 100 μm. (O) Quantification of the percentages of CGB⁺ in STB-D2. Error bar, mean and standard error (SEM). n=8 random images, total 5820 cells. Right panel: Quantification of percentages of mono-, bi- and multi-nucleated cells in STB-D2. Error bar, mean and standard error (SEM). n=40 random images, total 6734 cells. (P) RNAseq analysis of expression of *CD46* and *CGB5* in EPSC-TSCs and different STB differentiation timepoints. (Q) Representative immunofluorescence staining of 24 h.p.i. naïve-eSTB for SARS-CoV-2 N protein. Scale bar: 500 μm. Right panel: Percentages of SARS-CoV-2 N protein positive naïve-eSTBs, respectively. n=58 random images. (R) Immunofluorescence staining of 24 h.p.i. naïve-eSTB for ACE2, SARS-CoV-2 N protein, GATA2 and CGB. Dotted box showed mononucleated and binucleated infected naïve-eSTBs, some of them (white arrows) start to express CGB. Scale bar: 200 μm. (S) RT-qPCR analysis of SARS-CoV-2 genome copy number in supernatants and cell lysates of 2, 24, 48 and 72 h.p.i. EVTs (day8). Data are mean ± s.d. n=3 biological replicates. Student's *t*-test, *** *P* < 0.001 (T) Immunofluorescence staining of 48 h.p.i. EVTs for SARS-CoV-2 N protein. Scale bar: 100 μm. Right panel: Percentages of SARS-CoV-2 N protein positive EVTs. n=36 random images. (U) Immunofluorescence-stained SARS-CoV-2 infected EVTs for N protein and HLA-G. Scale bar: 100 μm (V) Bubble plot for *ACE2*, *TMPRSS2* and genes of SARS-CoV-2 expression in 48 h.p.i. mock and infected EVTs. Label color is according to z-score and bubble sizes are proportional to expression levels.
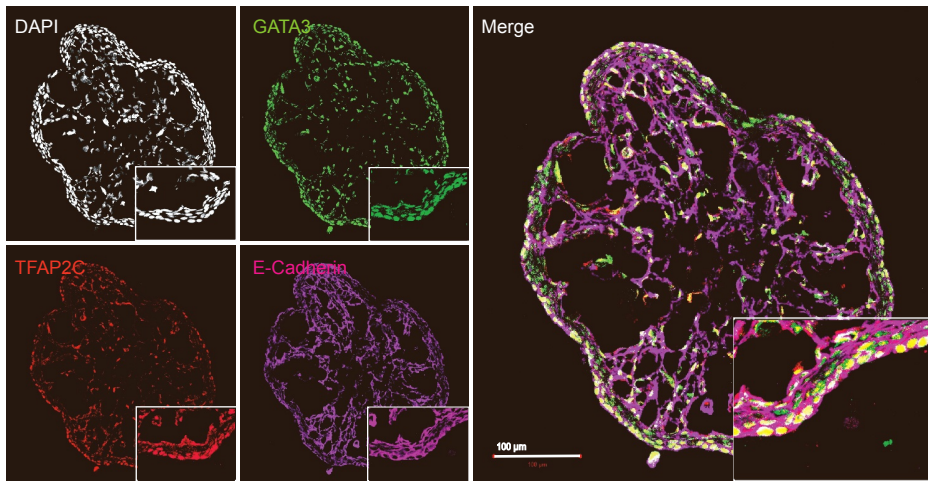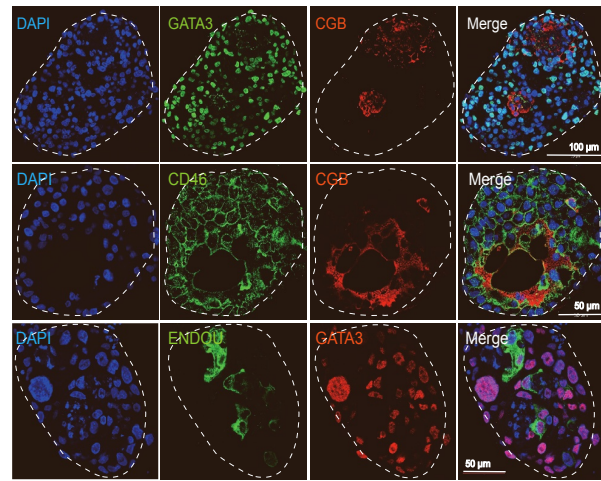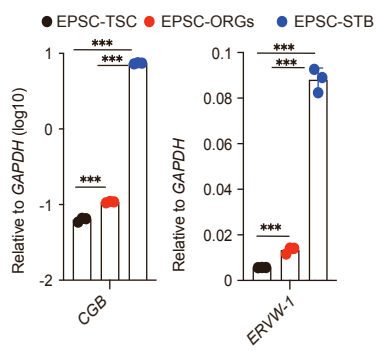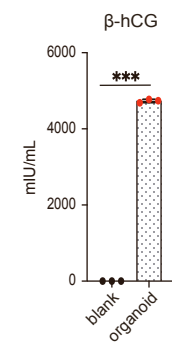
A Vero E6

WT (0.001MOI) Delta (0.001MOI) Omicron (0.001MOI)

EPSC-eSTB

WT (0.001MOI) Delta (0.001MOI) Omoicron (0.001MOI)

hiEPSC-eSTB

WT (0.001MOI) Delta (0.001MOI) Omoicron (0.001MOI)

B

WT (0.1MOI) Delta (0.1MOI) Omicron (0.1MOI)

C Pearson correlation coefficient

D

E KEGG-cell cycle (D3) KEGG-cell cycle (D4) KEGG-cell cycle

Cell cycle-G2/M (D3) Cell cycle-G2/M (D4) Cell cycle-G2/M

KEGG-Apoptosis (D3) KEGG-Apoptosis (D4) KEGG-Apoptosis

F

G

H Up regulation Down regulation

I Vero E6 SARS-CoV-2 infection
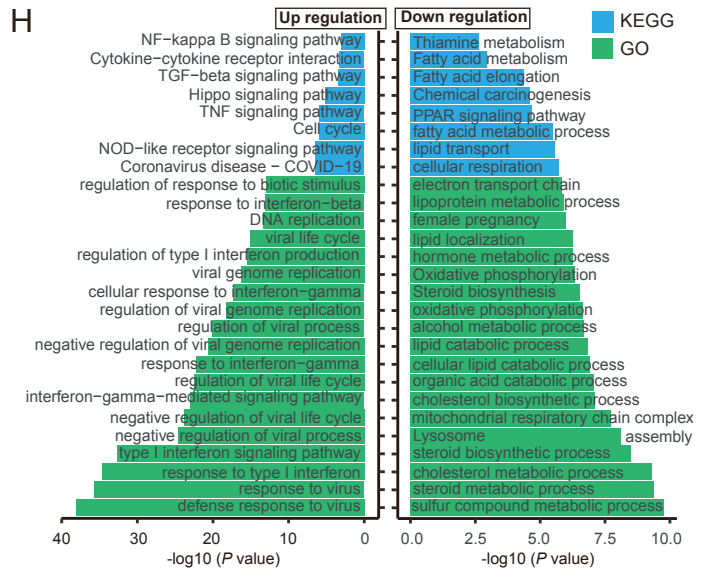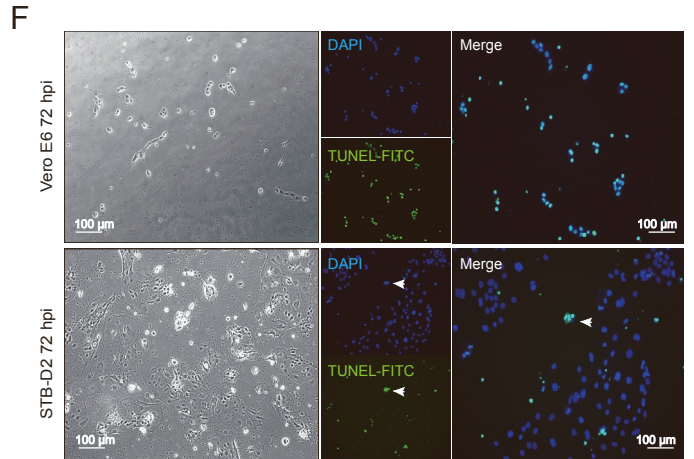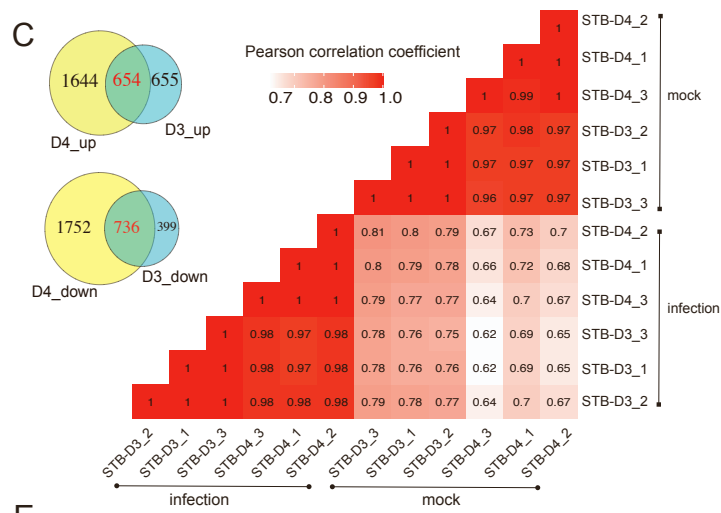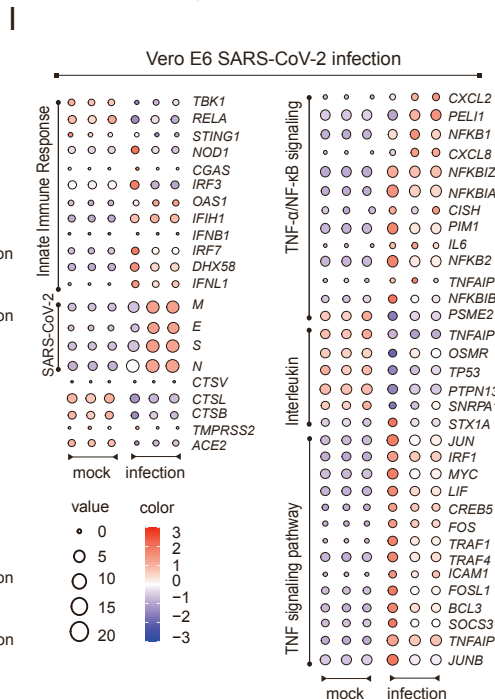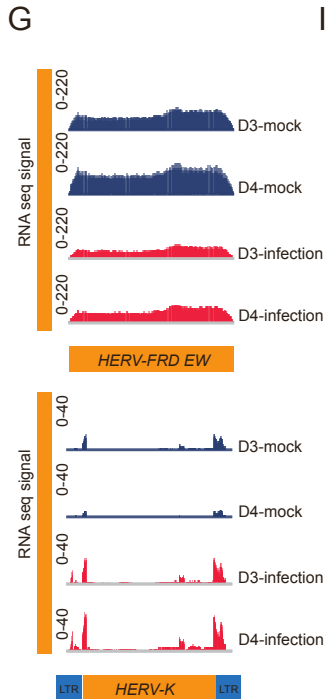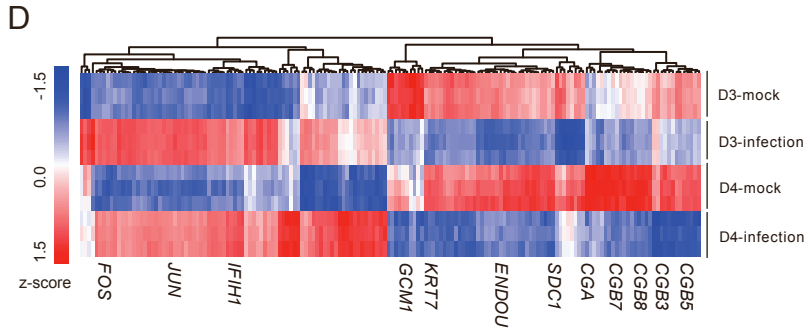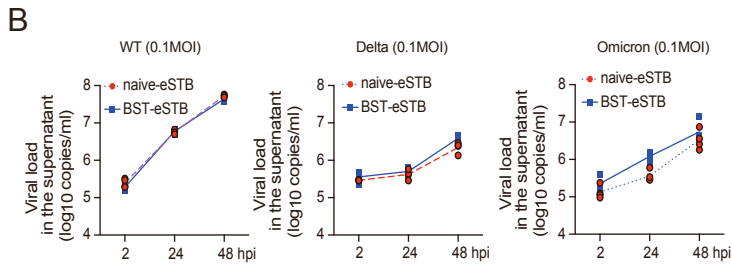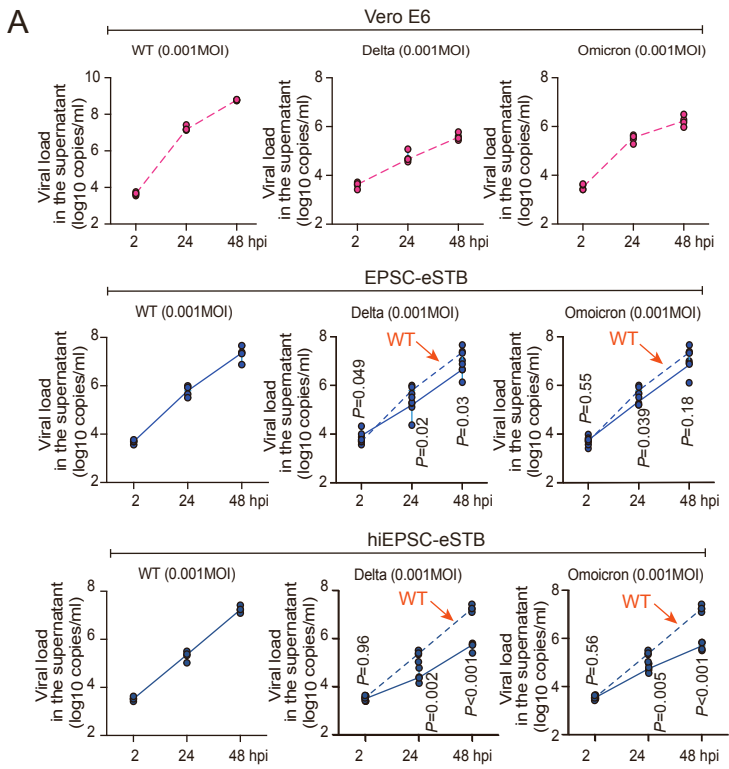
Figure S4. eSTB's susceptibility to SARS-CoV-2 variants and their differentiation impairment. Related to Figure 4. (A) Comparison of SARS-CoV-2 replication kinetics among Vero E6, EPSC-eSTB and hiEPSC-eSTB cells. Cells were infected with WT, the Delta variant or Omicron variant at 0.001MOI. Cell culture supernatant were collected at the indicated time-points and subject to viral load detection using RT-qPCR method. Data are mean ± s.d. n=3. Student's *t*-test, exact *P* values are presented. (B) Comparison of SARS-CoV-2 replication kinetics in naïve-eSTB and BST-eSTB cells. (C) Left panel: Venn plots for differential genes after SARS-CoV-2 WT infection in STB-D3 and STB-D4. Right panel: Heatmap for correlation between infected STBs and mock infection STBs. (D) The top 50 up or down-regulated genes in STB after virus infection. Genes are sorted by -log10 (p value). Z-score of log2 transformed cpm was used. Red, upregulated genes; blue, downregulated genes. (E) Gene set enrichment analysis (GSEA) for cell cycle and apoptosis pathways in STB-D3, STB-D4 and Vero E6 cells after SARS-CoV-2 WT infection. (F) Images of SARS-CoV-2 infected Vero E6 cells and eSTBs and representative immunofluorescence staining images of TUNEL cell apoptosis detection assay. White arrows point to apoptotic cells. (G) RNAseq signal of *HERV-K* and *HERV-FRD* in SARS-CoV-2 infected STB-D3 and STB-D4 and the mock controls. Library size is used to normalize the reads. (H) GO and KEGG analysis for shared upregulated and downregulated genes in SARS-CoV-2 infected STB-D3 and STB-D4. (I) Bubble plot for genes of SARS-CoV-2, monkey host factors *ACE2*, *TMPRSS2*, *CTSV*, *CTSL*, *CTSB*, innate immune response, TNF signaling pathway, interleukin signaling pathway and TNF-α/NF-κB signaling in Vero E6 after SARS-CoV-2 infection. Label color is according to z-score and bubble sizes are proportional to expression levels.
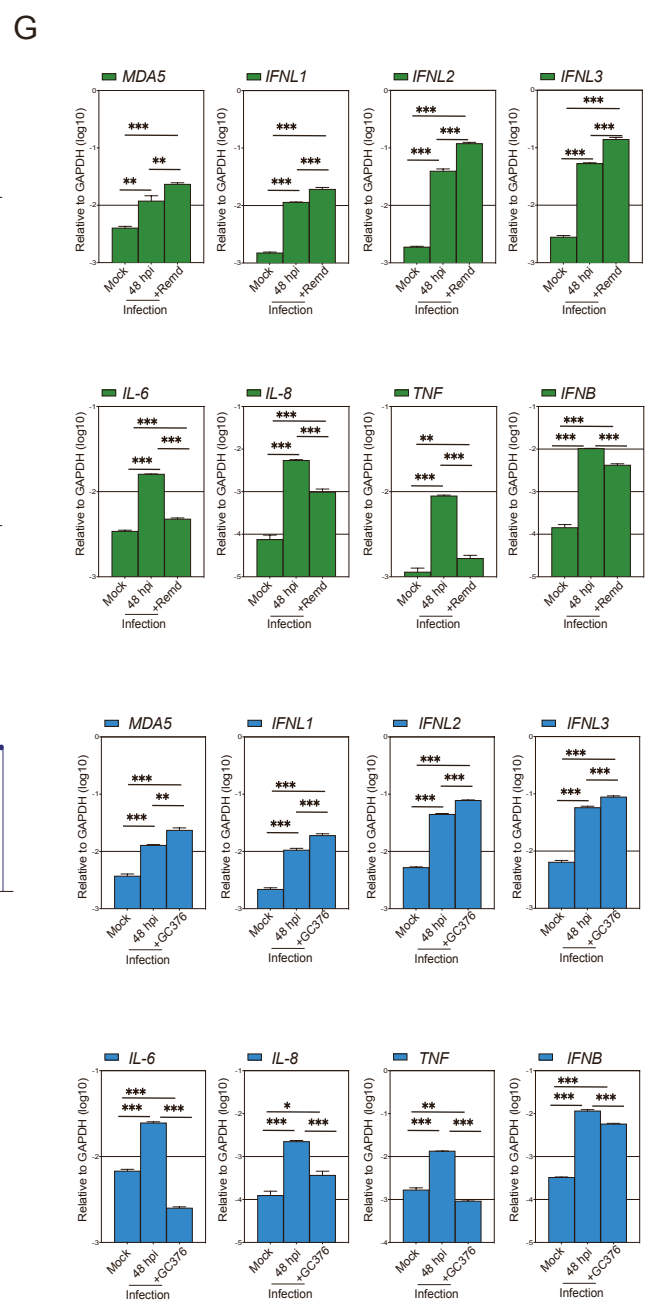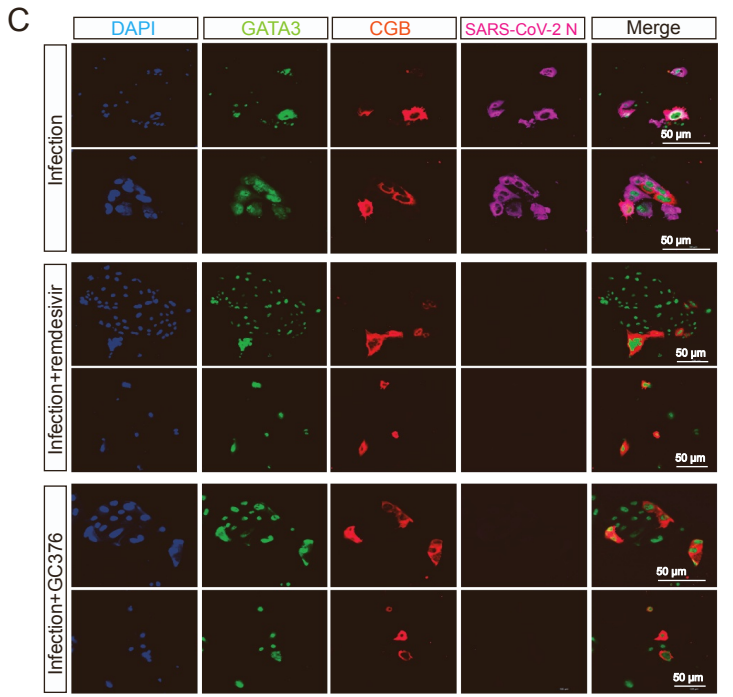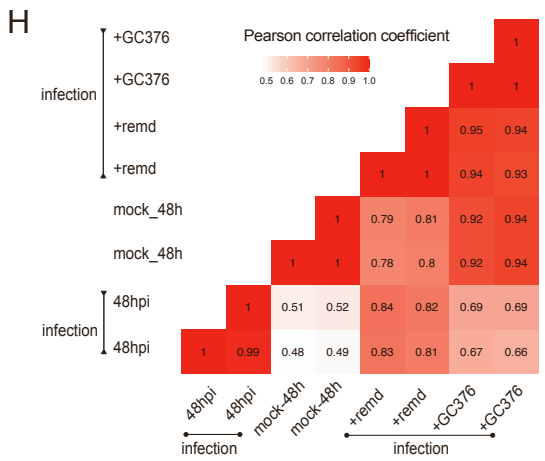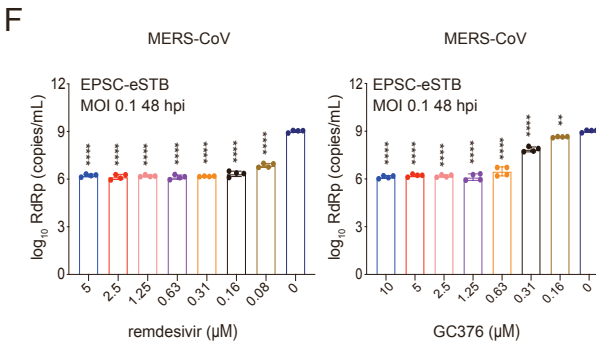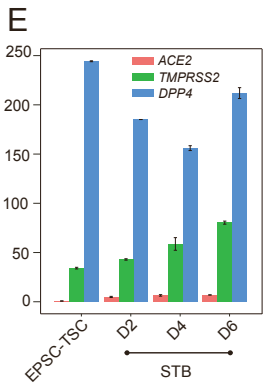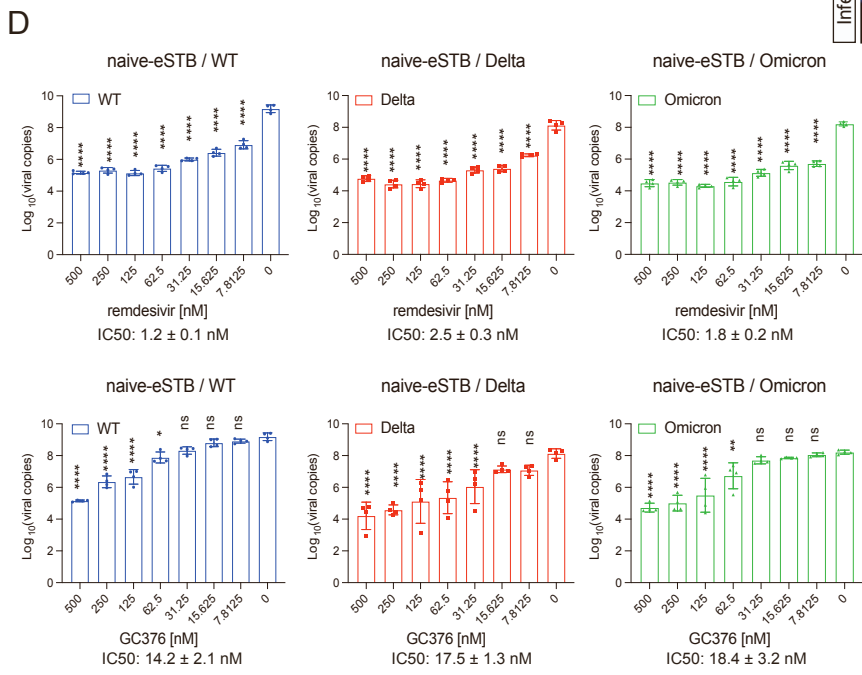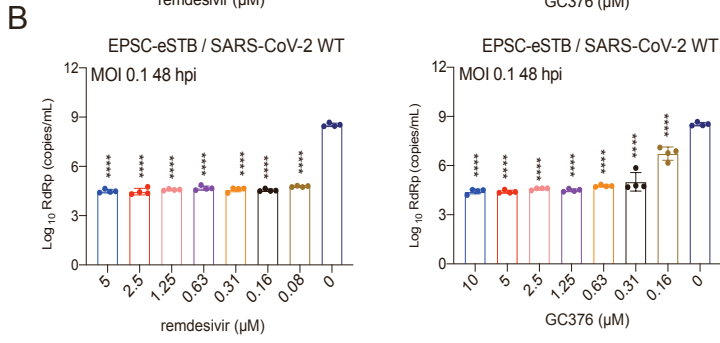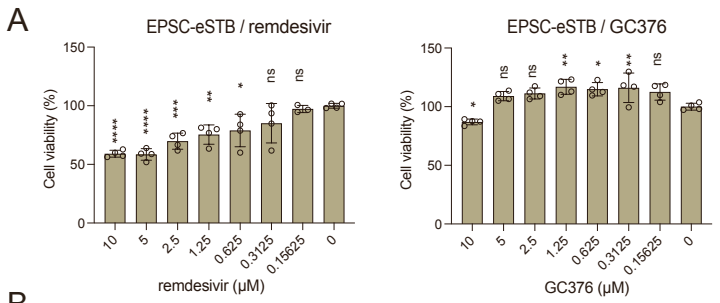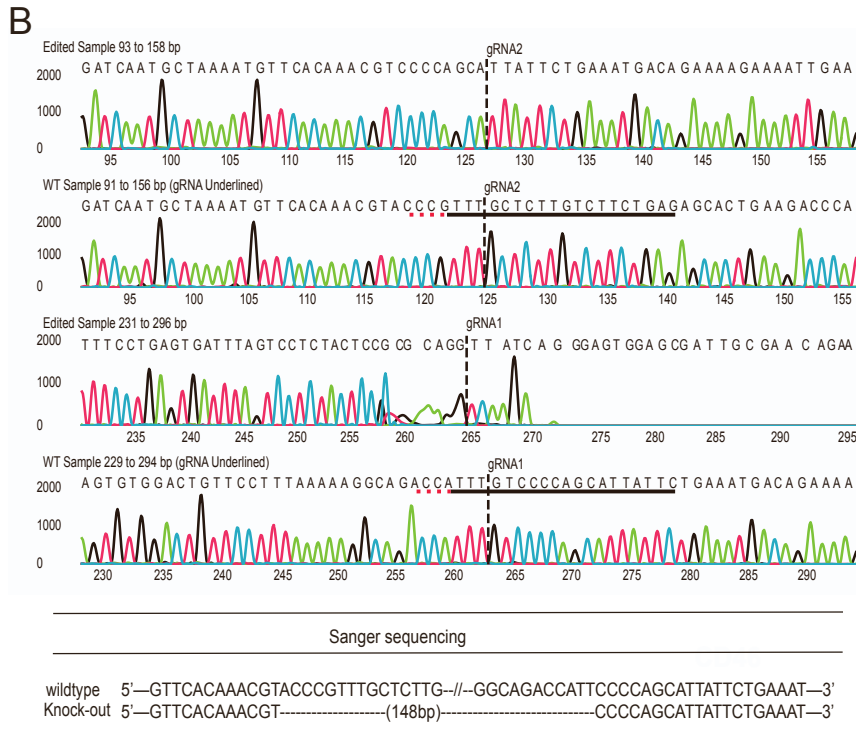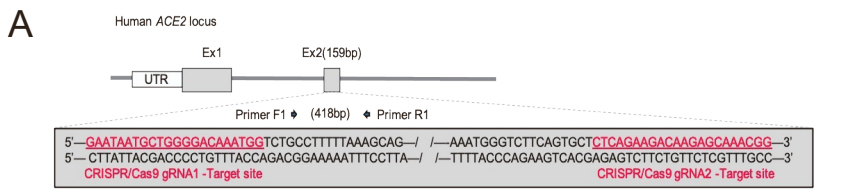
Figure S5. eSTBs for evaluating antiviral drugs in SARS-CoV-2 and MERS-CoV infection. Related to Figure 5. (A) Measurement of eSTB cell viability by a CellTiter-Glo assay kit upon remdesivir or GC376 treatment for 48 hours. The results are shown as % of the non-treated cells (mean ± SEM). Statistics analysis by two-tailed unpaired Student's *t*-test. (B) Viral load reduction assay was performed to evaluate the inhibitory effect of remdesivir and GC376 against SARS-CoV-2 WT infection in EPSC-eSTBs. Data are mean ± SEM, One-way ANOVA. (**** *P*<0.0001) (C) Immunofluorescence-stained eSTB for nucleus (Blue), GATA3 (Green), CGB (Red), and SARS-CoV-2 N protein (purple). eSTB infected by SARS-CoV-2 with or without remdesivir (10μM) /GC376 (10μM) treatment, respectively. (Scale bar, 50 μm). (D) Viral load reduction assay for evaluating the inhibitory effect of the indicated drugs against SARS-CoV-2 WT and Delta and Omicron variants infection in naïve-eSTB cells. (E) Barplot for expression (cpm) of *ACE2*, *TMPRSS2* and *DPP4* in EPSC-TSC and EPSC-TSC differentiation toward STB. (F) Viral load reduction assay for evaluating the inhibitory effect of the indicated drugs against MERS-CoV infection in EPSC-eSTBs. (G) RT-qPCR detection of *MDA5*, *IFNLs*, *IL6*, *IL8*, *TNF* and *IFNB* in SARS-CoV-2 infected EPSC-eSTBs, in the presence or absence of remdesivir or GC376. Data are normalized to *GAPDH* using ΔCt, mean ± s.d. n=3. Student's *t*-test, *** *P*<0.001, ** *P*<0.01,* *P*<0.05 (H) Heatmap for correlation between infected and mock infection EPSC-eSTBs. Non-expressed genes were filtered out and cpm was used to calculate the Pearson correlation coefficient.

A

DAPI   GATA3   Merge

TFAP2C   E-Cadherin

100 μm

B

DAPI   GATA3   CGB   Merge
100 μm

DAPI   CD46   CGB   Merge
50 μm

DAPI   ENDOU   GATA3   Merge
50 μm

C

EPSC-TSC   EPSC-ORGs   EPSC-STB

*** ***
*** ***

*** ***

CGB   ERVW-1

D

β-hCG

***

blank   organoid

E

EPSC-TSC   EPSC-ORGs

*** * *** ns

has-miR-517a   has-miR-517b   has-miR-525-3p   has-miR-526-3p

F

Organoid-EVTs

100 μm

Bright field   DAPI

HLA-G   DAPI HLA-G

Bright field
DAPI
KRT7
ITGA5

100 μm

Bright field   DAPI

KRT7   ITGA5

G

EPSC-ORG   EPSC-ORG-EVT (D8)

*** *** *** ***

HLA-G   IGTA5   MMP2   ITGA1

H

GATA3   CD46   DAPI SARS-CoV-2 N   GATA3   CD46   SARS-CoV-2 N
100 μm   100 μm

GATA3 SARS-CoV-2 N   CD46 SARS-CoV2 N   GATA3 SARS-CoV-2 N CD46   GATA3 SARS-CoV-2 N   CD46 SARS-CoV-2 N   DAPI SARS-CoV-2 N
100μm   100 μm

Figure S6. Infection of EPSC-TSC-derived trophoblast organoids by SARS-CoV-2. Related to Figure 6. (A) Immunofluorescence-stained trophoblast organoid cryosections for TFAP2C, GATA3 and E-cadherin. Scale bar: 100 μm (B) Immunofluorescence-stained trophoblast organoid paraffin sections for CD46, GATA3, ENDOU and CGB. (C) Expression of STB genes in STBs, EPSC-TSCs and trophoblast organoids by RT-qPCR (mean ± s.d. n=3). Student's *t*-test. *** $P<0.001$ (D) ELISA (mIU/mL) detection of hCG-β secreted by trophoblast organoids in the supernatant. Fresh TOM was used as the blank control. n=3 independent replicates. *** $P < 0.001$ (Student's *t*-test). (E) Expression changes (RT-qPCR) of Trophoblast-specific C19MC miRNAs in EPSC-TSCs and trophoblast organoids. *miRNA103a* expression is used as the control. Data are mean ± s.d., n=3. (F) Representative phase-contrast image of cells migrating out of a trophoblast organoid seeded in EVT medium for 8 days. EVTs were stained for HLA-G, ITGA5 and KRT7. Nuclei were counterstained with DAPI. (G) EVT genes expression (RT-qPCR) in trophoblast organoids and trophoblast organoid-derived EVTs. Data are mean ± s.d. n=3. Student's *t*-test, *** $P < 0.001$ (H) Additional immunofluorescence-stained SARS-CoV-2-infected trophoblast organoid paraffin sections for GATA3, CD46 and SARS-CoV-2-N. Arrows indicate an infected cell that is co-stained for GATA3, CD46 and SARS-CoV-2-N. Scale bar: 100 μm

A Human *ACE2* locus

B Sanger sequencing

wildtype 5'—GTTCACAAACGTACCCGTTTGCTCTTG--//--GGCAGACCATTCCCCAGCATTATTCTGAAAT—3'
Knock-out 5'—GTTCACAAACGT------------------(148bp)------------------CCCCAGCATTATTCTGAAAT—3'

D summary of *ACE2* Knock-out in EPSCs

cell line	no.of picked single clones	no. of genotyped	no. of heterozygote	no. of homozygote
M1 EPSCs	24	24	4	5
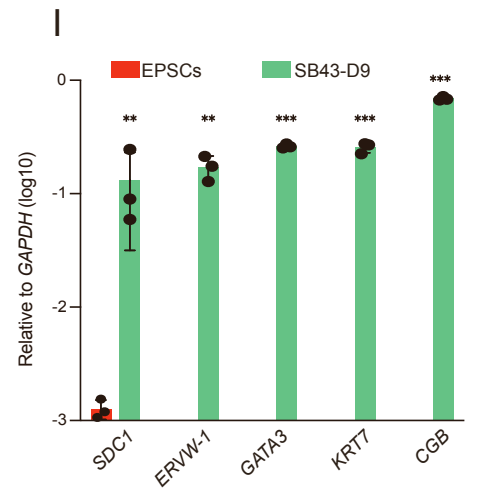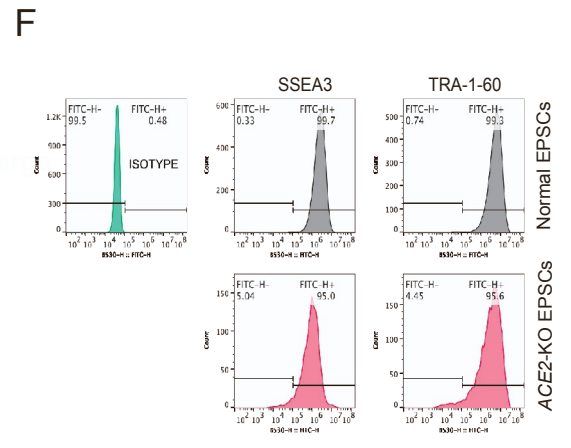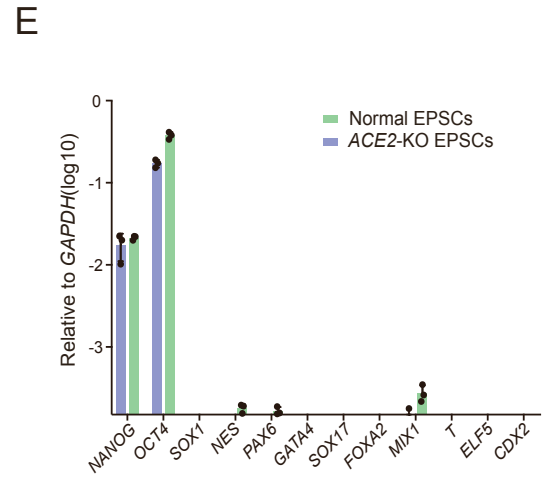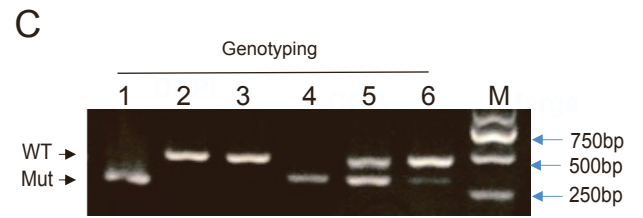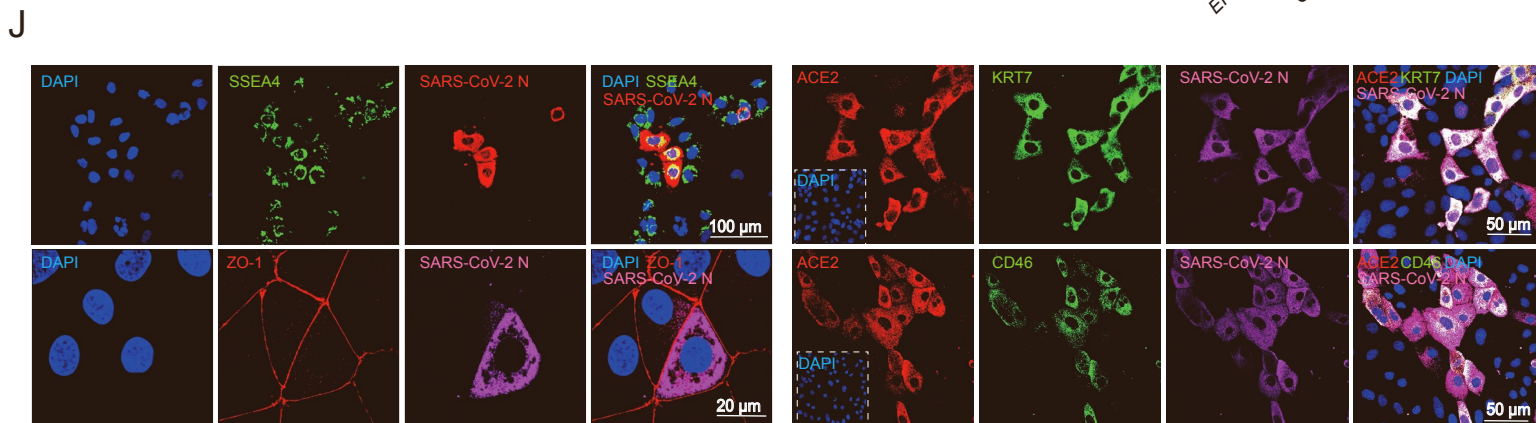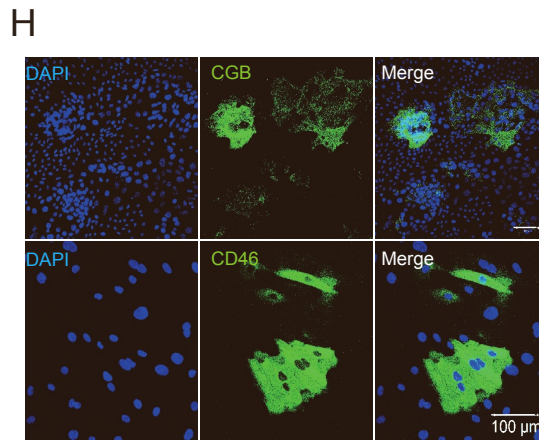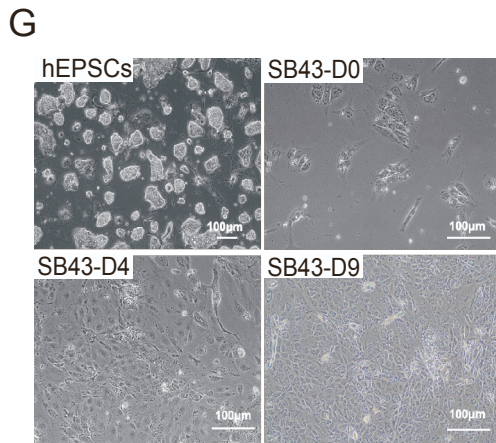
Figure S7. ACE2 is required for SARS-CoV-2 infection of human trophoblasts differentiated from hEPSCs. Related to Figure 7. (A) CRISPR/Cas9-mediated knockout of the human *ACE2* gene. A pair of gRNAs targeting exon 2 of *ACE2* are listed in red. (B) Sanger sequencing of the mutant PCR fragment reveals a 148 bp deletion between the two CRISPR gRNAs in exon 2 as expected. (C) Genotyping of *ACE2*-KO hEPSC colonies by genomic DNA PCR. Colonies 1 and 4 are homozygous KO mutants. (D) Genome editing efficiency at the *ACE2* locus in hEPSCs. (E) Expression of pluripotency and various cell lineage genes in normal and *ACE2*-KO hEPSCs. (F) Flow cytometry quantification of pluripotency markers SSEA3 and TRA-1-60 on normal and *ACE2*-KO hEPSCs. (G) Morphology of hEPSCs and SB43-treated cells on days 0, 4 and 9. Scale bars: 100 μm (H) Immunofluorescence staining images of STB markers CGB and CD46 in SB43-treated hEPSC on day 9. Scale bars: 100 μm (I) Expression of trophoblast genes in SB43-treated hEPSCs on day 9 by RT-qPCR. Data are mean ± s.d. n=3. Student's *t*-test. (J) Immunofluorescence images of SARS-CoV-2 infection in SB43-treated hEPSCs (day 4). More mono- and bi-nucleated cells were infected. Scale bar: 50 μm and 100 μm as indicated.

Table S2. Culture conditions for hTSCs from different reports, Related to Figure 1.

Cell Type	CO2 and O2	ECM	TSCM modification 1	TSCM modification 2	TSCM modification 3	TSCM modification 4	Reference
TSC-BST/ct	5% CO2	Collagen IV	0.5 uM A83-01	1uM SB431542	1.5 ug/ml L-ascorbic acid	0.8 mM VPA	Okae, H., et al. (2018)
Primed-TSC	5% CO2	Matrigel	0.5 uM A83-01	1uM SB431542	1.5 ug/ml L-ascorbic acid	0.8 mM VPA	Wei, Y., et al. (2021)
Naïve-TSC (PXGL)	7% CO2 and 5% O2	Collagen IV/ MEF	1.0 uM A83-01	Without SB431542	1.5 mg/ml L-ascorbic acid	0.8 mM VPA	Guo, G., et al. (2021)
Naïve-TSC (5iLA)	5% CO2 and 20% O2	Collagen IV	0.5 uM A83-01	1uM SB431542	1.5 ug/ml L-ascorbic acid	0.8 mM VPA	Dong, C., et al. (2020)
EPSC-TSC	5% CO2	Geltrex	0.5 uM A83-01	1uM SB431542	50 ug/ml	10 uM VPA	This study

Table S3. Correlation index between ACE2 and Trophoblast markers, Related to Figure 2.

Gene	coefficient	*P* value
CDX2	0.04266543	0.00256635
CD46	0.24451753	7.03E-69
TFRC	-0.0493468	0.00048636
GCM1	-0.0636706	6.72E-06
CGB3	0.10253989	3.79E-13
CGB5	0.19950932	5.37E-46
SDC1	0.10222731	4.46E-13
GATA2	-0.0356747	0.01170267
GATA3	-0.0968373	7.03E-12
TP63	-0.0269452	0.05692952
TEAD4	-0.1328758	4.15E-21
ACE2	1	0
ENG	0.20688926	2.11E-49
ITGA5	0.10266201	3.55E-13
ITGA6	-0.0676585	1.71E-06
CSH1	0.18957838	1.27E-41
CSH2	0.24808141	6.54E-71
HLA-G	0.0706351	5.85E-07
MMP2	0.03941273	0.00534726

Table S5. List of PCR primers, Related to Figure 1, 4, 6, 7, S1, S3, S5-7.

Gene Name	Forward (5'-3')	Reverse (5'-3')
SARS-CoV-2	CGCATACAGTCTTRCAGGCT	GTGTGATGTTGAWATGACATGGTC
ACE2 (Exon9-10)	TCCATTGGTCTTCTGTCACCCG	AGACCATCCACCTCCACTTCTC
TMPRSS2	CTCTACGGACCAAACTTCATC	CCACTATTCCTTGGCTAGAGTA
CD147	GGCTGTGAAGTCGTCAGAACAC	ACCTGCTCTCGGAGCCGTTCA
NANOG	TGAACCTCAGCTACAAACAG	TGGTGGTAGGAAGAGTAAAG
Oct-04	CCTCACTTCACTGCACTGTA	CAGGTTTTCTTTCCCTAGCT
SOX2	TTCACATGTCCCAGCACTACCAGA	TCACATGTGTGAGAGGGGCAGTGTGC
CDX2	TTCACTACAGTCGCTACATCACC	TTGATTTTCCTCTCCTTTGCTC
GATA3	ACATCTCGCCCTTCAGCCAC	CATGGCGGTGACCATGCTGGA
KRT7	AGGATGTGGATGCTGCCTAC	CACCACAGATGTGTCGGAGA
TEAD4	CAGGTGGTGGAGAAAGTTGAGA	GTGCTTGAGCTTGTGGATGAAG
TFAP2C	ACAGGATCCATGTTGTGGAAAATAACCGAT	ATACTCGAGTTTCCTGTGTTTCTCCATTTT
TP63	AGAAACGAAGATCCCCAGATGA	CTGTTGCTGTTGCCTGTACGTT
CGB	ACCCTGGCTGTGGAGAAGG	ATGGACTCGAAGCGCACA
ERVW-1	GTTAATGACATCAAAGGCACCC	CCCCATCTCAACAGGAAAACC
SDC1	GCTGACCTTCACACTCCCCA	CAAAGGTGAAGTCCTGCTCCC
HLA-G	CAGATACCTGGAGAACGGGA	CAGTATGATCTCCGCAGGGT
MMP2	TGGCACCCATTTACACCTACAC	ATGTCAGGAGAGGCCCCATAGA
ITGB6	CTCAACACAATAAAGGAGCTGGG	AAAGGGGATACAGGTTTTTCCAC
GABRP	TTTCTCAGGCCCAATTTTGGT	GCTGTCGGAGGTATATGGTGG
MUC16	GGAGCACACGCTAGTTCAGAA	GGTCTCTATTGAGGGGAAGGT
VTCN1	TCTGGGCATCCCAAGTTGAC	TCCGCCTTTTGATCTCCGATT
cGAS	TAACCCTGGCTTTGGAATCAAAA	TGGGTACAAGGTAAAATGGCTTT
ZBP1	TGGTCATCGCCCAAGCACTG	GGCGGTAAATCGTCCATGCT
MDA5	GAGCAACTTCTTTCAACCACAG	CACTTCCTTCTGCCAAACTTG

STING1	AGCATTACAACAACCTGCTACG	GTTGGGGTCAGCCATACTCAG
IFNA2	CTTGAAGGACAGACATGACTTTGGA	GGATGGTTTCAGCCTTTTGGA
IFNB1	AAACTCATGAGCAGTCTGCA	AGGAGATCTTCAGTTTCGGAGG
IFNG	TGGCTTTTCAGCTCTGCATC	CCGCTACATCTGAATGACCTG
IFNL1	CGCCTTGGAAGAGTCACTCA	GAAGCCTCAGGTCCCAATTC
IFNL2	AGTTCCGGGCCTGTATCCAG	GAGCCGGTACAGCCAATGGT
IFNL3	TCGCTTCTGCTGAAGGACTGCA	CCTCCAGAACCTTCAGCGTCAG
IFNL4	ATGCGGCCGAGTGTCTGG	GCTCCAGCGAGCGGTAGTG
IL6	GTCAGGGGTGGTTATTGCAT	AGTGAGGAACAAGCCAGAGC
IL28A	TCCAGTCACGGTCAGCA	CAGCCTCAGAGTGTTTCTTCT
TNF	CTCTTCTGCCTGCTGCACTTTG	ATGGGCTACAGGCTTGTCACTC
HLA-A	CGAGGATGGCCGTCATGGCG	CACATTCCGTGTCTCCTGGTCCC
HLA-B	CAGTTCGTGAGGTTCGACAG	CAGCCGTACATGCTCTGGA
ITGA1	CTGGACATAGTCATAGTGCTGGA	ACCTGTGTCTGTTTAGGACCA
ITGA5	GTCGGGGGCTTCAACTTAGAC	CCTGGCTGGCTGGTATTAGC
ITGA6	CACATCTCCTCCCTGAGCAC	TATCTTGCCACCCATCCTTG
CDX2	TTCACTACAGTCGCTACATCACC	TTGATTTTCCTCTCCTTTGCTC
ELF5	TGCCCTCACGGTAATGTTGGA	TGATGCTCAAAGGCAGGGTAG
GAPDH	CAAATTCCATGGCACCGTCA	ATCGCCCCACTTGATTTTGG
human miR-103a	GTAGCAGCATTGTACAGGG	
human miR-526b-3p	GTTTGGGAAAGTGCTTCCTTTT	
human miR-517a	GTTTGGATCGTGCATCCTTTTA	
human miR-517b	GTGCCTCTAGATGGAAGCA	
human miR-525-3p	GTTGAAGGCGCTTCCCTTT	